EUROPEAN ORGANISATION FOR NUCLEAR RESEARCH (CERN)

Submitted to: JHEP

CERN-EP-2025-208
28th October 2025

Constraints on effective field theories via quadruple-differential angular decay rates from t-channel single-top-quark production at $\sqrt{s} = 13$ TeV with the ATLAS detector

The ATLAS Collaboration

Events with t-channel single top quarks are used to probe effective field theory operators in $\sqrt{s} = 13$ TeV proton–proton collision data corresponding to 140 fb^{-1} recorded by the ATLAS detector at the Large Hadron Collider. An analysis method leveraging Fourier techniques applied to quadruple-differential decay rates based on observables containing angular information about the decays of the top quarks is used to achieve high sensitivity. The relevant effective field theory operators are those sensitive to top-quark decay and t-channel production vertices. Their Wilson coefficients are tightly constrained, with results compatible with Standard Model predictions.

Contents

1 Introduction

An interesting avenue in searching for possible interactions beyond the Standard Model (BSM) is looking for non-zero Wilson coefficients (WCs) of effective field theories (EFTs), and in particular those that couple to the top quark. Owing to its heavy mass, $m_t \approx 172.5$ GeV [1], and short lifetime, $1/\Gamma_t \sim O(10^{-25})$ s [2], the top quark decays before hadronising, mainly through the weak process $t \to Wb$ [2]. This makes the measurement of its production and decay kinematics a unique probe of BSM physics.

In the bottom-up approach, an effective theory is an approximation to physics at a higher energy scale. A prominent example is the Standard Model effective field theory (SMEFT) [3]. In the SMEFT, the Standard Model (SM) is treated as the EFT of an unknown BSM theory at a higher scale, where the scale of the SM is characterised by the electroweak (EW) scale given by the vacuum expectation value v. Even though the BSM theory is unknown, its effects can still be parameterised by higher-dimensional operators in a power expansion. Therefore, the effective SM Lagrangian can be written as an expansion

$$\mathcal{L}_{\mathrm{eff}} = \mathcal{L}_{\mathrm{SM}}^{(4)} + \frac{1}{\Lambda}\sum_i c_i^{(5)} O_i^{(5)} + \frac{1}{\Lambda^2}\sum_i c_i^{(6)} O_i^{(6)} + O\left(\frac{1}{\Lambda^3}\right) + \ldots,$$

where the c_i are the Wilson coefficients (WC) [4] of the operators O_i, containing all degrees of freedom below the scale Λ, which is the energy scale of the BSM physics. The scale Λ is the cut-off scale at which the power expansion breaks down and the BSM theory cannot be explained by the effective theory anymore. At this energy scale, the heavy particles that were parameterised out in the EFT approach can instead be produced directly (‘on-shell’), and their dynamics must be explicitly included in the theory. The number in parentheses is the energy dimension of the respective operators. Usually, $O^{(5)}$ terms are not considered because they violate baryon-number conservation.

Because the top quark is much heavier than other SM fermions, BSM physics at higher scales could manifest itself at lower energies through its effective interactions, leading to detectable deviations from SM predictions [5]. There are a large number of top-quark-related dimension-six operators that can be constructed from the SM degrees of freedom [6]. A complete, non-redundant basis expressed in the Warsaw basis was given in Ref. [7] and consists of 59 independent operators, not counting flavour indices and Hermitian conjugates. Among the 59 operators, this analysis focuses solely on the five operators contributing to the t-channel single-top-quark production process or the $t \rightarrow Wb$ decay, out of which three have complex WCs.

In proton–proton (pp) collisions at the Large Hadron Collider (LHC) [8], the t-channel has the largest rate among all single-top-quark production channels [9, 10]. Moreover, it is the only channel that produces a polarised top quark, providing unique access to the imaginary sector of the Lagrangian through analyses of differential angular decay rates. Figure 1 shows a representative Feynman diagram for t-channel single-top-quark production, occurring at leading order (LO) in the four-flavour factorisation scheme (4FS), but at next-to-leading order (NLO) in the five-flavour scheme (5FS) [11–13]. In this diagram, a light-flavour quark q (i.e. u-, c-, $\bar{d}$-, or $\bar{s}$-quark) from one of the colliding protons interacts with a gluon (splitting into a $b\bar{b}$ pair) by exchanging a space-like virtual W boson, producing a top quark t and a recoiling light-flavour quark q', the so-called spectator quark. The second b-quark from gluon scattering is expected to have a softer transverse momentum (p_{T}) spectrum and a broader pseudorapidity (η) distribution than the b-quark produced in the top-quark decay. It is generally either not detected in the experiment or does not pass the event selection. The final state includes one light-flavour spectator jet, one b-jet, one lepton and missing transverse momentum from the neutrino.

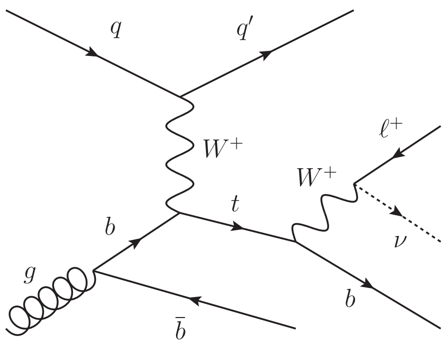

Figure 1: Representative LO Feynman diagram for t-channel single-top-quark production and decay in the 4FS. Here q represents a u/c or $\bar{d}/\bar{s}$ quark, and q' represents a d/s or $\bar{u}/\bar{c}$ quark. The initial b-quark typically arises from a gluon splitting into a $b\bar{b}$ pair.

The differential distribution of the top-quark decay, $t \rightarrow Wb \rightarrow \ell\nu b$, can be fully determined by four angles [14]. The first two angles (θ, ϕ) are the spherical coordinates of the outgoing W-boson momentum direction in the top-quark rest frame, defined in a Cartesian coordinate system (x, y, z). The frame is chosen by first selecting the proton beam whose p_z matches that of the outgoing spectator jet, aligned with the incoming proton beam. Then, following Ref. [15], three orthogonal directions are defined. The $\hat{z}$ direction is the direction of the momentum of the spectator jet, $\vec{p}_s$, in the top-quark rest frame. The $\hat{y}$ direction is taken to lie along $\hat{z} \times \hat{p}_q$, where $\vec{p}_q$ is the direction of the incoming proton, in the top-quark reference frame. The $\hat{x}$-direction is then chosen so as to make a right-handed coordinate system. The remaining two angles (θ^*, ϕ^*) are the spherical coordinates of the charged lepton's momentum in the W-boson rest frame, in the coordinate system (x', y', z') obtained by a 'standard' boost from the previous frame, such that the $\hat{z}'$ axis is the direction (θ, ϕ) of the W-boson momentum and the $\hat{y}' = \hat{z}' \times \hat{p}_s$ axis lies in the x–y plane. In this system, ϕ is the angle between the production plane and the top-quark decay frame, while ϕ^* is the angle between the top-quark decay plane and the W-boson decay frame. The four angles are illustrated in Figure 2.

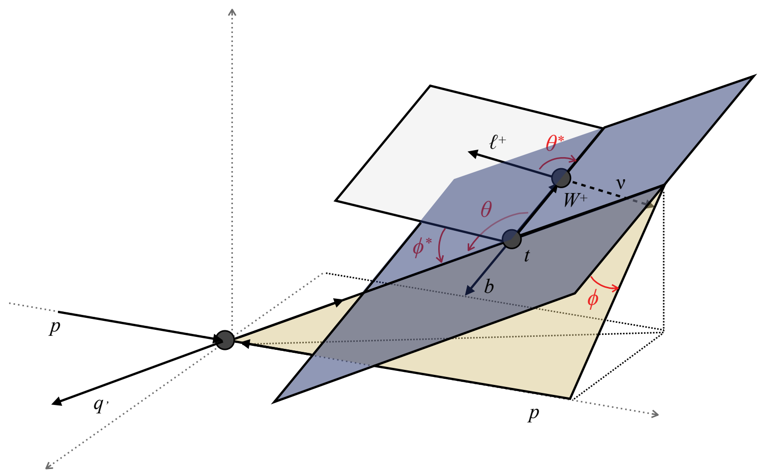

Figure 2: Illustration of the definition of the four angles $(\theta, \phi, \theta^*, \phi^*)$ in the $t \to Wb \to \ell\nu b$ decay chain. The incoming protons, the spectator, top and b quarks, the W boson, and the lepton and neutrino are denoted by p, q', t, b, W, ℓ, and ν, respectively. The angles θ and ϕ specify the direction of the W-boson (or spectator-quark) momentum in the top-quark rest frame, while θ^* and ϕ^* specify the direction of the charged lepton momentum in the W-boson rest frame.

Many previous measurements by ATLAS [10, 16–18] and CMS [19–23] provide constraints on the WCs examined in this paper. In addition, other measurements [24–26] by ATLAS constrain BSM contributions to the tWb vertex, albeit in the language of anomalous couplings rather than EFT coefficients. Constraints on the real parts of the three complex WCs examined in this paper have also been obtained from an ATLAS measurement of W-boson helicity in top-quark decay [27], although there were not enough independent observables available to constrain all of the WCs simultaneously.

This paper is structured as follows. The WCs chosen for study in this analysis are introduced in Section 2. A brief description of the ATLAS detector is given in Section 3. Details about the data samples, the Monte Carlo (MC) simulation event samples, and the background estimation are provided in Section 4. Then the object definitions, reconstruction, and the event selection are discussed in Section 5 and Section 6, respectively. Section 7 describes the systematic uncertainties arising in this analysis. Section 8 presents the analysis strategy, including the Fourier techniques employed to extract observables from the dataset, the manner in which they are related to the Wilson coefficients, and the construction of the profile-likelihood. Finally, the results are discussed in Section 9 and the conclusions are given in Section 10.

2 Choice of Wilson coefficients

Written in the physical basis, where the Higgs field of the Warsaw basis is set to its vacuum expectation value [28], four of the operators contribute to the tWb Lagrangian as

$$\begin{aligned} O^3_{\varphi Q} &\supset -\frac{gv^2}{\sqrt{2}} \bar{b}_\mathrm{L} \gamma^\mu t_\mathrm{L} W^-_\mu, \\ O_{\varphi tb} &\supset \left[\frac{gv^2}{2\sqrt{2}} \bar{b}_\mathrm{R} \gamma^\mu t_\mathrm{R} W^-_\mu \right]^\dagger, \\ O_{tW} &\supset 2v \bar{b}_\mathrm{L} i\sigma^{\mu\nu} q_\nu t_\mathrm{R} W^-_\mu, \\ O_{bW} &\supset \left[2v \bar{b}_\mathrm{R} i\sigma^{\mu\nu} q_\nu t_\mathrm{L} W^-_\mu \right]^\dagger, \end{aligned}$$

where γ denotes the Dirac matrices, σ the generators of the Clifford basis, and q_ν the four-momentum transferred in the t-channel process.

Each of the operators contributes to the tWb vertex with a different Lorentz structure: $O^3_{\varphi Q}$ has a Lorentz structure similar to the SM and therefore modifies the left-handed vector coupling (V_L) present in the SM, while $O_{\varphi tb}$ induces a right-handed vector coupling and O_{bW} and O_{tW} contribute as left-handed and right-handed tensor couplings, respectively. Furthermore, $O_{\varphi tb}$, O_{bW}, and O_{tW} are non-Hermitian operators and therefore their Wilson coefficients are complex. A non-vanishing imaginary part can then lead to CP violation [29].

The remaining two operators contributing to the top-quark physics studied in this analysis are two four-quark operators, with LL and RR chiral structure

$$\begin{aligned} O^{3,1}_{Qq} &= \left(\bar{Q} \gamma_\mu \tau^I Q \right) \left(\bar{q}_i \gamma^\mu \tau^I q_i \right), \\ O^{3,8}_{Qq} &= \left(\bar{Q} \gamma_\mu T^A \tau^I Q \right) \left(\bar{q}_i \gamma^\mu T^A \tau^I q_i \right), \end{aligned}$$

where $Q = (t_\mathrm{L}, b_\mathrm{L})$, while q refers to left-handed doublets in the first two generations. The first operator is an SU(2) triplet and colour singlet and the second one is an SU(2) triplet and colour octet. From these two, only the first operator interferes with the SM amplitude, since W-boson exchange is also a colour singlet. The colour-octet operator has already been constrained quite tightly using processes where it does interfere with the SM amplitude [17, 20, 30, 31]. Therefore, it is assumed that the colour-singlet operator dominates, and this analysis is restricted to studying the operator $O^{3,1}_{Qq}$. For convenience, the WC of $O^{3,1}_{Qq}$, $c^{3,1}_{Qq}$, is referred to as c_{Qq} in this paper.

As seen above, the dimension-six operators contributing to the top-quark interactions considered in this analysis are

$$O^3_{\varphi Q}, \qquad O_{\varphi tb}, \qquad O_{bW}, \qquad O_{tW}, \qquad O^{3,1}_{Qq}.$$

The corresponding EFT coefficients $c_{\varphi Q}$ and c_{Qq} are real, while $c_{\varphi tb}$, c_{bW}, and c_{tW} are complex, giving a total of eight free parameters. However, the measurement of the angular distributions can only constrain a subspace of the eight-dimensional complex parameter space. At LO, there are four distinct amplitudes for top-quark decay. Two of them correspond to decays to a left-handed b-quark and for $m_b = 0$, only receive contributions from the SM, $c_{\varphi Q}$ and c_{tW}. The others correspond to decays to a right-handed b-quark and only receive contributions from $c_{\varphi tb}$ and c_{bW}. Thus, one can in principle determine the relative phase between $c_{\varphi tb}$ and c_{bW}, but one cannot determine the phase relative to the SM for either. For convenience, the analysis takes $c_{\varphi tb}$ to be real and positive, and interprets $\mathrm{Arg}\left(c_{bW}\right)$ as implying a phase relative to that of $c_{\varphi tb}$. This leaves two imaginary parameters that, in principle, can be constrained by analysing the angular variables. In total, seven free parameters [14] remain to be measured: $C_{\varphi Q}$, C_{tW}, C^{I}_{tW}, C_{bW}, C^{I}_{bW}, $C_{\varphi tb}$, and C_{Qq}, with: [1]

$$\begin{aligned} V_{\mathrm{L}} &= V_{tb}\left(1 + \frac{v^2}{\Lambda^2}C_{\varphi Q}\right), \\ c_{tW} &= C_{tW} + iC^{I}_{tW}, \\ c_{bW} &= C_{bW} + iC^{I}_{bW}, \\ c_{\varphi tb} &= C_{\varphi tb}, \\ c_{Q,q} &= C_{Qq}. \end{aligned}$$

Fixing $c_{\varphi tb}$ to be real and positive is done purely for practical purposes and does not constrain $c_{\varphi tb}$ to have positive or even real values. Multiplying $c_{\varphi tb}$ by an arbitrary phase does not change the posterior probability distributions of the fit as long as c_{bW} is multiplied by the same phase.

Finally, it is noted that $O^{3}_{\varphi Q}$ has the same Lorentz structure as the SM top-quark decay, and therefore only affects the overall cross-section, and has no effect on the angular distributions. Thus, measuring normalised angular distributions only constrains the ratios of coefficients C_{tW}/V_{L}, $C^{I}_{tW}/V_{\mathrm{L}}$, etc., while measuring the total rate allows one to set constraints on the absolute values of the coefficients. In this analysis, the strength of measuring both the normalised angular distribution and the cross-section is used to obtain the best sensitivity among all the targeted WCs.

3 ATLAS detector

The ATLAS experiment [32] at the LHC is a multipurpose particle detector with a forward–backward symmetric cylindrical geometry and nearly 4π coverage in solid angle.[2] It consists of an inner tracking detector surrounded by a thin superconducting solenoid providing a 2 T axial magnetic field, electromagnetic and hadronic calorimeters, and a muon spectrometer. The inner tracking detector covers the pseudorapidity range $|\eta| < 2.5$. It consists of silicon pixel and microstrip detectors, and a transition radiation tracker (TRT). Lead/liquid-argon (LAr) sampling calorimeters provide electromagnetic (EM) energy measurements with high granularity within the region $|\eta| < 3.2$. A steel/scintillator-tile hadronic calorimeter covers the central pseudorapidity range ($|\eta| < 1.7$). The endcap and forward regions are instrumented with LAr calorimeters for EM and hadronic energy measurements up to $|\eta| = 4.9$. The muon spectrometer surrounds the calorimeters and is based on three large superconducting air-core toroidal magnets with eight coils each. The field integral of the toroids ranges between 2.0 and 6.0 T m across most of the detector. The

[1] In this work, lowercase c is used for complex-valued Wilson coefficients, while uppercase C is reserved for parameters that are strictly real.

[2] ATLAS uses a right-handed coordinate system with its origin at the nominal interaction point (IP) in the centre of the detector and the z-axis along the beam pipe. The x-axis points from the IP to the centre of the LHC ring, and the y-axis points upwards. Polar coordinates (r, ϕ) are used in the transverse plane, ϕ being the azimuthal angle around the z-axis. The pseudorapidity is defined in terms of the polar angle θ as $\eta = -\ln\tan(\theta/2)$ and is equal to the rapidity $y = (1/2)\ln[(E + p_z)/(E - p_z)]$ in the relativistic limit. Angular distance is measured in units of $\Delta R \equiv \sqrt{(\Delta y)^2 + (\Delta\phi)^2}$.

muon spectrometer includes a system of precision tracking chambers up to $|\eta| = 2.7$ and fast detectors for triggering up to $|\eta| = 2.4$. The luminosity is measured mainly by the LUCID-2 [33] detector, which is located close to the beam pipe. A two-level trigger system is used to select events [34]. The first-level trigger is implemented in hardware and uses a subset of the detector information to accept events at a rate below 100 kHz. This is followed by a software-based trigger that reduces the accepted event rate to about 1.25 kHz on average depending on the data-taking conditions. A software suite [35] is used in data simulation, in the reconstruction and analysis of real and simulated data, in detector operations, and in the trigger and data acquisition systems of the experiment.

4 Data and simulated event samples

This analysis uses data from pp collisions at $\sqrt{s} = 13$ TeV collected with the ATLAS detector at the LHC during 2015–2018. Stringent detector and data quality requirements were applied [36], resulting in a data sample corresponding to a total integrated luminosity of 140 fb^{-1} [33]. The events were selected by single-lepton (electron or muon) triggers [37, 38], imposing low thresholds on the transverse energy (E_{T}) of electrons and the p_{T} of muons, in addition to isolation requirements, or imposing a looser identification criterion and higher thresholds with no isolation requirement. The lowest thresholds were varied from 20 to 26 GeV depending on the lepton flavour and the data-taking period.

Samples of simulated events were produced using different MC event generators, including parton shower (PS) and hadronisation models for both the signal and background processes. The effect of multiple interactions in the same and neighbouring bunch crossings (pile-up) was modelled by overlaying the hard-scattering event with simulated inelastic pp collisions generated with Pythia 8.186 [39] using the NNPDF2.3lo set of parton distribution functions (PDFs) [40] and the A3 set of parameters (tune) [41]. Events were reweighted such that the distribution of the average number of interactions per bunch crossing matches that observed in data. Table 1 presents a summary of all configurations used to generate events for signal (t-channel) and background processes.

The effects of variations associated with different sources of modelling systematic uncertainty were evaluated by comparing alternative simulation samples with the nominal ones. These alternative samples were generated either through internal reweighting or with dedicated event generators. Each variation was introduced independently unless explicitly stated otherwise, ensuring a consistent assessment of its individual impact on the analysis. Further details about these samples are provided in Section 7.

Single-top-quark production in the t-channel was modelled using the Powheg Box v2 [44–47] generator, which provides matrix-element (ME) calculations at NLO accuracy in the strong coupling constant α_{s} in the 4FS with the corresponding NNPDF3.0nlo [48] set of PDFs. The functional form of the renormalisation and factorisation scales was set to $\sqrt{m_b^2 + p_{\mathrm{T},b}^2}$ following the recommendations of Refs. [44, 49]. Top quarks were decayed at LO using MadSpin [50, 51] to preserve all spin correlations. For PS and hadronisation, the events were interfaced with Pythia 8.230 [52], which used the A14 tune [53] and the NNPDF2.3lo PDF set [40].

The predicted cross-sections for single-top-quark and single-top-antiquark production in the t-channel in pp collisions at a centre-of-mass energy of 13 TeV are $\sigma(tq) = 134.2^{+2.6}_{-1.7}$ pb and $\sigma(\bar{t}q) = 80.0^{+1.8}_{-1.4}$ pb, respectively. The cross-sections were calculated with the MCFM program [54] at next-to-next-to-leading order (NNLO) in quantum chromodynamics (QCD). The quoted uncertainties include the uncertainties due to choosing renormalisation scale (μ_{r}) and factorisation scale (μ_{f}) values, the uncertainty in the PDFs,

Table 1: The configurations used to generate events for signal (t-channel) and background processes. 'ME order' refers to the order of the matrix-element calculation. The EFT simulation samples are shown in grey.

Process	Generator	ME order	Parton shower	PDF set	Tune
t-channel	Powheg Box	NLO	Pythia 8	NNPDF3.0nlo	A14
	MadGraph	LO	Pythia 8	NNPDF3.0nlo	A14
$t\bar{t}$	Powheg Box	NLO	Pythia 8	NNPDF3.0nlo	A14
	MadGraph	LO	Pythia 8	NNPDF3.0nlo	A14
V + jets	Sherpa 2.2.11	MEPS@NLO	Sherpa	NNPDF3.0nnlo	default
Associated tW	Powheg Box	NLO	Pythia 8	NNPDF3.0nlo	A14
s-channel	Powheg Box	NLO	Pythia 8	NNPDF3.0nlo	A14
VV, $qqVV$	Sherpa 2.2.2	MEPS@NLO	Sherpa	NNPDF3.0nnlo	default
VVV	Sherpa 2.2.2	MEPS@NLO	Sherpa	NNPDF3.0nnlo	default
$t\bar{t}H$	Powheg Box	NLO	Pythia 8	NNPDF3.0nlo	A14
$t\bar{t}W$	Sherpa 2.2.10	NLO QCD+EW	Sherpa	NNPDF3.0nnlo	default
$t\bar{t}Z$	MadGraph5_aMC@NLO	NLO	Pythia 8	NNPDF3.0nlo	A14
tZ	MadGraph5_aMC@NLO	NLO	Pythia 8	NNPDF3.1nlo	A14
tWZ	MadGraph5_aMC@NLO	NLO DR1	Pythia 8	NNPDF2.3lo	A14
$t\bar{t}t$, $t\bar{t}t\bar{t}$	MadGraph5_aMC@NLO	QCD NLO	Pythia 8	NNPDF3.1nlo	A14
ggH, qqH	Powheg Box	QCD NLO	Pythia 8	CTEQ6L1 [42]	AZNLO [43]
WH, ZH	Pythia 8	QCD NLO	Pythia 8	NNPDF2.3lo	A14

and the uncertainty in the value of the strong coupling constant α_s. The uncertainty due to the scales was determined by raising and lowering μ_r and μ_f independently by a factor of two, whilst never allowing them to differ by more than a factor of two. The combined PDF and α_s uncertainties were determined at the 68% confidence level (CL) according to the Hessian representation of the PDF4LHC21 PDF set [55].

The production of $t\bar{t}$ events was modelled at NLO in QCD in the 5FS using Powheg Box v2 [45–47, 56] with the NNPDF3.0nlo PDF set. The `Powheg:hdamp` parameter was set to $1.5 \times m_t$ [57].[3] Events were interfaced with Pythia 8.230, which used the A14 tune and the NNPDF2.3lo PDF set [40]. The simulation samples were normalised to the cross-section of 834^{+29}_{-37} pb predicted at NNLO in QCD, including the resummation of next-to-next-to-leading logarithmic (NNLL) soft-gluon terms calculated using Top++ 2.0 [58–64]. The combined PDF and α_s uncertainties were determined at the 68% CL according to the Hessian representation of the PDF4LHC21 PDF set.

To model the EFT effects, LO SM events were produced with MadGraph 2.8.1 [65] interfaced with Pythia 8.244, and then LO reweighting was applied to scale each event by the ratio of EFT to SM MEs, using the `dim6top` UFO model [66]. A six-dimensional grid, formed by C_{tW}, C^I_{tW}, C_{bW}, C^I_{bW}, $C_{\varphi tb}$, and C_{Qq}, was generated for both the t-channel signal sample and the $t\bar{t}$ background sample. Here, $C_{\varphi Q}$ is not included in the grids, since it only changes the overall cross-section, which can be parameterised by a scale factor, as introduced in Section 2. The points of this grid were designed to cover the 95% confidence intervals of the previous analysis results [16, 67]. An analytically derived top-quark width correction was incorporated into the reweighting to account for variations in the top-quark's width Γ_t induced by changes in the WCs [68], since this correction cannot be handled by the MadGraph 2.8.1 reweighting function.

[3] The `Powheg:hdamp` parameter controls the p_T of the first additional emission beyond LO in the PS and therefore regulates the high-p_T emission against which the $t\bar{t}$ system recoils.

The production of single-boson (V + jets) events was simulated using Sherpa 2.2.11 [69]. The virtual QCD corrections were provided by the OpenLoops library [70–72]. The ME calculations were matched and merged with the default Sherpa PS [73], which was based on Catani–Seymour dipole factorisation and the cluster hadronisation model [74]. The NNPDF3.0nnlo PDF set was used together with a dedicated set of Sherpa-tuned PS parameters. The MEs were generated at NLO (LO) accuracy in QCD for up to two (for three or four) partons (0,1,2j@NLO + 3,4j@LO) using the Comix library [75], and the simulation samples were normalised to NNLO cross-section predictions [76].

Single top quarks from s-channel and tW associated production were generated with Powheg Box v2 in the 5FS at NLO in QCD with the NNPDF3.0nlo PDF set, with μ_f and μ_r set to $\sqrt{m_b^2 + p_{T,b}^2}$, following the recommendation of Refs. [49, 77], respectively. For the latter process, the Diagram Removal 1 (DR1) scheme was employed to handle the interference between tW and $t\bar{t}$ [57].

The VV and VVV processes were simulated by Sherpa 2.2.2 [69] with off-shell effects and Higgs contributions at NLO (LO accurate for up to three additional parton emissions). The MEs were matched to parton showers with MEPS@NLO [78–81] with the set of tuned parameters developed by the Sherpa authors. The samples include events from loop-induced and EW production.

Top-quark associated and Higgs-boson backgrounds were simulated at NLO in QCD using various generators with matched parton showers. They include $t\bar{t}H$, $t\bar{t}W$, $t\bar{t}Z$, tZq, tWZ, ttt, $t\bar{t}t\bar{t}$, and Higgs-related processes (ggH, qqH, WH, ZH).

In all simulated signal and background samples, the top-quark mass was set to m_t = 172.5 GeV. The strong coupling constant was set to $\alpha_s = 0.118$. These values were also used in the computation of production cross-sections for processes involving the top quark. The bottom and charm hadron decays were simulated with EvtGen [82] for non-Sherpa-generated event samples.

5 Object definitions

Interaction vertices from the pp collisions are reconstructed from at least two tracks with $p_T > 500$ MeV that are consistent with originating from the beam collision region in the $x-y$ plane. If more than one primary vertex candidate is found in the event, the candidate for which the associated tracks form the largest sum of squared p_T is selected as the hard-scatter primary vertex [83].

Electron candidates are reconstructed from energy clusters in the electromagnetic calorimeter matched to a track in the inner tracking detector (ID) [84]. They are required to satisfy $p_T > 10$ GeV and $|\eta_{\mathrm{cluster}}| < 2.47$, excluding the transition region between the barrel and endcap calorimeters ($1.37 < |\eta_{\mathrm{cluster}}| < 1.52$). The `loose` and `tight` electron identification working points are used to identify Loose and Tight electrons respectively, based on a likelihood discriminant employing calorimeter, tracking, and combined variables that provide separation between electrons and jets, and electrons and photons.

Muon candidates are reconstructed from tracks measured in the ID matched to tracks measured in the muon spectrometer [85, 86]. The resulting muon candidates are re-fitted using the complete track information from both detector systems. They are required to satisfy $p_T > 10$ GeV and $|\eta| < 2.5$. The `medium` muon identification working point [86] is used.

Electron (muon) candidates are matched to the primary vertex by requiring that the significance of their transverse impact parameter, d_0, satisfies $|d_0/\sigma(d_0)| < 5.0$ (3.0), where $\sigma(d_0)$ is the measured uncertainty in d_0, and by requiring that their longitudinal impact parameter, z_0, satisfies $|z_0 \sin(\theta)| < 0.5$ mm [84, 85].[4] Furthermore, lepton isolation is required for both the electron and muon candidates [87]. Tight electrons with incorrect charge assignment are suppressed by a BDT discriminant based on calorimeter and tracking quantities [84]. Most electrons originating from photon conversions, whether from internal conversions or conversions in detector material, are rejected by the standard electron identification criteria [84].

Table 2 summarises the definitions of the reconstructed electron and muon candidates.

Table 2: Summary of the electron and muon object definitions. The selection requirements for Tight electrons/muons are applied in addition to the preselected (Loose) objects used for the overlap removal.

	Loose electron	**Loose muon**
Identification	`loose`	`medium`
Acceptance	$p_T > 10$ GeV, $\|\eta^{\text{cluster}}\| < 2.47$ except $1.37 < \|\eta^{\text{cluster}}\| < 1.52$	$p_T > 10$ GeV, $\|\eta\| < 2.5$
Impact parameter	$\|d_0/\sigma(d_0)\| < 5.0$ $\|z_0 \sin(\theta)\| < 0.5$ mm	$\|d_0/\sigma(d_0)\| < 3.0$ $\|z_0 \sin(\theta)\| < 0.5$ mm
	Tight electron	**Tight muon**
Identification	`tight`	`medium`
Isolation	required	required
Extra selections	Electron charge-misassignment veto Electron conversion candidate veto	

The constituents for jet reconstruction are identified by combining measurements from both the ID and the calorimeter using a particle flow (PFlow) algorithm [88]. Jet candidates are reconstructed from these PFlow objects using the anti-k_t algorithm [89, 90] with a radius parameter of $R = 0.4$. They are calibrated using simulation with corrections obtained by using in situ techniques in data [91]. Only jet candidates with $p_T > 30$ GeV and within $|\eta| < 4.5$ are selected. To reduce the effect of pile-up, each jet with $p_T < 60$ GeV and $|\eta| < 2.4$ must satisfy the `Tight` working point of the jet vertex tagger (JVT) [92] criteria. Moreover, jets with $2.5 < |\eta| < 4.5$ (hereafter called 'forward jets') and $p_T < 120$ GeV must satisfy the `Tight` working point of the forward jet vertex tagger (fJVT) [93] criteria. A set of quality criteria is also applied to reject events containing at least one jet arising from non-collision sources or detector noise [94].

Jets containing b-hadrons are identified (b-tagged) via the `DL1r` [95] algorithm. It uses a deep feed-forward neural network based on the distinctive features of b-hadron decays, primarily the impact parameters of tracks and the displaced vertices reconstructed in the ID. Additional input to this network is provided by discriminating variables constructed by a recurrent neural network (RNN) [95], which exploits the spatial and kinematic correlations between tracks originating from the same b-hadron. A multivariate b-tagging discriminant value is calculated for each jet. In this measurement, a jet is considered b-tagged if it passes the working point corresponding to 60% average expected efficiency to tag a b-quark jet, with a light-flavour-jet rejection factor of about 2500, and a charm-jet rejection factor of about 40. Correction factors, derived from dedicated calibration samples enriched in b-jets, c-jets, or light-flavour jets, are applied to the simulated event samples [96–98].

[4] The transverse impact parameter, d_0, is defined in the x–y plane as the distance of closest approach of the track to the beamline. The longitudinal impact parameter, z_0, is defined as the distance in z between the primary vertex and the point on the track used to evaluate d_0.

The reconstruction of hadronically decaying τ-lepton candidates (τ_{had}) is seeded by jets reconstructed via the anti-k_t algorithm, using calibrated energy clusters as inputs, with a radius parameter of $R = 0.4$ [99, 100]. Jets seeding τ_{had} candidates are additionally required to have $p_{\text{T}} > 10\,\text{GeV}$ and $|\eta| < 2.5$. To separate the τ_{had} candidates initiated by hadronic τ-lepton decays from jets initiated by quarks or gluons, an RNN [100] identification method was trained on information from reconstructed charged-particle tracks and clusters of energy in the calorimeter matched to τ_{had} candidates, as well as on high-level discriminating variables. A separate multivariate discriminant based on a BDT [99, 101] is also used to reject backgrounds arising from electrons mimicking a τ_{had}. This discriminant (`eBDT`) is built using information from the calorimeter and the ID. Transition radiation information from the TRT system plays a key role in the performance of this discriminant. Baseline τ_{had} are required to have one or three associated tracks, electric charge of ± 1, $p_{\text{T}} > 20\,\text{GeV}$ and $|\eta| < 2.5$, excluding the barrel–endcap transition region. Each τ_{had} must satisfy the `Medium` RNN identification requirement, with efficiencies of 75% for 1-prong decays and 60% for 3-prong decays, and the `Loose` `eBDT` requirement, with an efficiency of 95% [99, 101].

Ambiguities between independently reconstructed electrons, muons, jets and τ_{had} can arise. A sequential 'overlap removal' procedure is performed to resolve these ambiguities and thus avoid double counting of candidates. This procedure is applied to leptons satisfying the Loose criteria described in Table 2. If two electrons are separated by $\Delta R < 0.1$, only the one with the higher p_{T} is kept. If an electron and a muon overlap within $\Delta R < 0.1$, the muon is removed if it is reconstructed only from an ID track and calorimeter energy deposits consistent with a minimum-ionising particle, otherwise the electron is removed. If an electron and a selected jet are found within $\Delta R < 0.2$, the jet is removed. Any electron subsequently found less than $\Delta R = 0.4$ from a jet is removed. Muons ghost-associated [89] with a regular $R = 0.4$ jet must satisfy a jet–muon separation of $\Delta R < 0.4$. If the overlapping jet contains less than three tracks with $p_{\text{T}} > 500\,\text{MeV}$, the jet is removed, otherwise the muon is rejected. Any τ_{had} found less than $\Delta R = 0.2$ from an electron is removed. Any τ_{had} found less than $\Delta R = 0.2$ from any type of muon with $p_{\text{T}} > 2\,\text{GeV}$ is removed, except those with $p_{\text{T}} > 50\,\text{GeV}$ which are only removed if overlapping with a combined-type muon. Finally, if a jet is found less than $\Delta R = 0.2$ from a τ_{had}, the jet is removed.

The missing transverse momentum $\vec{p}_{\text{T}}^{\text{ miss}}$ (with magnitude $E_{\text{T}}^{\text{miss}}$) is defined as the negative vector sum of the transverse momenta of all identified and calibrated objects and remaining unclustered energy, the latter (composing the 'soft term') being estimated from low-p_{T} tracks associated with the primary vertex but not with any lepton or jet candidate [102]. The $E_{\text{T}}^{\text{miss}}$ is taken as a measurement of the undetectable particles, and is affected by energy losses due to detector inefficiencies and acceptance, and by energy resolution.

6 Reconstruction and event selection

The on-shell W boson originating from the decay of the top quark is reconstructed from the momenta of the lepton and the neutrino by imposing four-momentum conservation. Since the neutrino escapes undetected, the x and y components of the reconstructed $\vec{p}_{\text{T}}^{\text{ miss}}$ are assumed to correspond to the p_{T} of the neutrino. The unmeasured longitudinal component of the neutrino momentum, p_z^{ν}, is computed by imposing a W-boson mass constraint on the lepton–neutrino system. A quadratic expression is found for p_z^{ν}, and the solution closer to zero is taken. If the solutions are complex, the reconstructed $\vec{p}_{\text{T}}^{\text{ miss}}$ is rescaled, preserving its direction, in order to have a unique real solution for p_z^{ν}. The top-quark candidate is then reconstructed by combining the four-momenta of the reconstructed W boson and the selected b-tagged jet.

To enhance the sensitivity to the relevant WCs, it is crucial to maximise the selected yield of t-channel single-top-quark events while minimising background contributions from other processes. To achieve this, one signal-enriched region (SR) and two control regions (CRs) are defined. These regions facilitate the simultaneous extraction of the WC values and the data-driven normalisation factors of the $t\bar{t}$ and $W+$jets backgrounds. In the analysis, both the SR and CRs are divided into four channels based on the lepton charge and the p_{T} of the reconstructed top quark, where channels with reconstructed top-quark p_{T} greater than 80 GeV are labelled as high-p_{T}, and those with lower p_{T} are labelled as low-p_{T}. Partitioning the data by lepton charge takes advantage of the charge asymmetry present in $W+$jets and t-channel single-top-quark production, in contrast to the charge-symmetric $t\bar{t}$ background. Likewise, separating events by top-quark p_{T} (above and below 80 GeV) improves the sensitivity, because certain EFT operators, most notably C_{Qq}, impact the high- and low-energy regions differently, with a stronger impact in the high-p_{T} region than in the low-p_{T} region.

Events are first required to satisfy a set of preselection criteria, primarily designed to suppress backgrounds from jets misidentified as other objects. The preselection is defined as follows:

- Exactly one Tight charged lepton ℓ (electron or muon as defined in Table 2) with $p_{\mathrm{T}} > 30$ GeV, matched to the single-lepton trigger.
- Veto on any additional Loose charged leptons (defined in Table 2); events containing reconstructed hadronically decaying τ-leptons (τ_{had}) are also vetoed to further suppress processes involving a τ_{had}.
- Exactly two jets; for jets within the calorimeter's endcap–forward transition region ($2.75 < |\eta_j| < 3.5$, where η_j denotes the η of the jets), the threshold is increased to 35 GeV.
- At least one of the jets must be b-tagged.
- $E_{\mathrm{T}}^{\mathrm{miss}} > 35$ GeV.

Two additional multijet background rejection criteria are applied [16]:

- Transverse mass of the lepton–$\vec{p}_{\mathrm{T}}^{\,\mathrm{miss}}$system must fulfill $m_{\mathrm{T}}(\ell\vec{p}_{\mathrm{T}}^{\,\mathrm{miss}}) > 60$ GeV.
- The lepton transverse momentum $p_{\mathrm{T}}(\ell)$ must satisfy $p_{\mathrm{T}}(\ell) > 50\left[1 - (\pi - |\Delta\phi(j_1, \ell)|)/(\pi - 1)\right]$ GeV, where j_1 refers to the jet with leading p_{T} and $\Delta\phi$ is the azimuthal angle between the jet and lepton. This requirement rejects backgrounds, especially the QCD multijet process where two jets are produced back-to-back in the azimuthal plane and one of those is misreconstructed as a lepton.

Events that pass the single-lepton trigger but fail the preselection are enriched in non-prompt lepton ('fake') background contributions and are therefore used to validate the fake-lepton background estimation. These backgrounds arise from processes that produce either a jet misidentified as an electron, or a muon or electron originating from the semileptonic decay of a heavy-flavour quark. In this analysis, a matrix method [87] is employed to estimate such backgrounds in a data-driven way. The parameterised efficiencies of lepton misidentification are derived from a multijet-enriched control region requiring a single Loose lepton. The real- and fake-lepton efficiencies, parameterised in lepton p_{T} and $|\eta|$, are then applied event by event to data events with a Loose, but not Tight, lepton.

Events that satisfy the preselection criteria are classified into three mutually exclusive regions: an SR, a $W+$jets-enriched CR (CR-W), and a $t\bar{t}$-enriched CR (CR-$t\bar{t}$). Events in the SR and CR-W are required to have exactly one b-tagged jet, with the second jet failing the b-tagging working point. The CR-W region is defined by events that match this b-tagging configuration but fail at least one of the additional SR selection requirements. Events in CR-$t\bar{t}$ are required to contain two jets that both satisfy the b-tagging criteria.

An event is classified as being in the SR if it satisfies the preselection and the following additional requirements:

- Invariant mass of the lepton and b-jet: $m_{\ell b} < 153$ GeV; top-quark mass proxy reconstructed from the lepton, missing transverse momentum $\vec{p}_{\mathrm{T}}^{\,\mathrm{miss}}$ and b-jet four-vectors: $m_t^{\mathrm{reco}} = m_{\ell \vec{p}_{\mathrm{T}}^{\,\mathrm{miss}} b} \in [120.6, 234.6]$ GeV. These criteria help to select events consistent with a top-quark mass around 172.5 GeV.
- Trapezoidal requirement defined as:

$$\left(\eta_j < a_1 \eta_{\ell \vec{p}_{\mathrm{T}}^{\,\mathrm{miss}} b} + b_1\right) \cap \left(\eta_j > a_1 \eta_{\ell \vec{p}_{\mathrm{T}}^{\,\mathrm{miss}} b} - b_1\right) \cap \left[\left(\eta_j > a_2 \eta_{\ell \vec{p}_{\mathrm{T}}^{\,\mathrm{miss}} b} + b_2\right) \cup \left(\eta_j < a_2 \eta_{\ell \vec{p}_{\mathrm{T}}^{\,\mathrm{miss}} b} - b_2\right)\right],$$

  where the parameters $a_{1,2}$ and $b_{1,2}$ are optimised by applying the $m_{\ell b}$ requirement and finding the maximum signal-to-background ratio, S/B. The chosen values are $a_1 = 3$, $b_1 = 10.5$, $a_2 = 0.25$, and $b_2 = 2.5$. This requirement helps to distinguish the signal process from the W+jets background.
- Invariant mass of the full system: $m_{j\ell \vec{p}_{\mathrm{T}}^{\,\mathrm{miss}} b} > 320$ GeV. In t-channel single-top-quark events, the angles between these objects are typically large, leading to a high invariant mass, whereas the backgrounds peak at a lower mass value.
- Scalar sum of the p_{T} of all the reconstructed objects in the final state (lepton, jets and $\vec{p}_{\mathrm{T}}^{\,\mathrm{miss}}$): $H_{\mathrm{T}} > 190$ GeV. This ensures the presence of significant hadronic activity.
- Well-measured events are selected by performing a kinematic fit with the reconstructed masses of the W boson and the top quark constrained to their measured values [2] in the kinematic likelihood (KL) fit framework [103], and selecting those events with a computed KL above a threshold of −36.[5]

Table 3 summarises the yields for each channel in the SR, detailing contributions from different MC process components as well as the data.

7 Sources of systematic uncertainty

Various sources of systematic uncertainty are evaluated for their effect on the signal and background rates and the shape of the angular distributions. In the following, the procedures used to evaluate these sources of systematic uncertainty are discussed. The systematic uncertainties considered are of two main types: experimental uncertainties and theory modelling uncertainties. The effect due to the limited size of the simulated event samples is also taken into account when evaluating the total uncertainty.

The uncertainty in the integrated luminosity is ±0.83% [104] and is applied to the signal and all simulated background processes that are scaled by the luminosity as one overall rate uncertainty in the fit. To account for the difference between the pile-up distributions in data and MC simulations, an uncertainty related to

[5] Breit–Wigner distributions are used to construct the kinematic likelihood function. For the W boson, the Breit–Wigner distribution of the $\ell\nu$ system has a mean value of $m_W = 80.4$ GeV and a width of $\Gamma_W = 2.1$ GeV. For the top quark, the Breit–Wigner distribution of the $W b$ system has a mean value of $m_t = 172.5$ GeV and a width of $\Gamma_t = 1.5$ GeV.

Table 3: The pre-fit event yields in the four SRs: t low-p_{T}, t high-p_{T}, $\bar{t}$ low-p_{T}, and $\bar{t}$ high-p_{T}. The event yield predictions are obtained from simulated samples normalised to theoretical cross-sections, except for the multijet contribution which is derived from a data-driven method. Uncertainties quoted include both statistical and systematic components. Individual predictions are rounded to integers, with the 'Total expected' obtained from the sum of the full-precision individual predictions and subsequently rounded. The last two rows show the signal-to-background (S/B) and the data-to-prediction ratios in each region, computed using full-precision individual predictions.

Process	**SR t low-p_{T}**	**SR t high-p_{T}**	**SR $\bar{t}$ low-p_{T}**	**SR $\bar{t}$ high-p_{T}**
t-channel	$23\,900 \pm 1400$	$15\,400 \pm 1300$	$13\,900 \pm 800$	7260 ± 600
s-channel	80 ± 7	20 ± 2	80 ± 5	30 ± 2
tW	570 ± 20	210 ± 10	570 ± 20	198 ± 10
$t\bar{t}$	3350 ± 450	1730 ± 240	3380 ± 540	1780 ± 230
W+jets	6500 ± 700	1680 ± 200	5300 ± 800	1150 ± 150
Z+jets, VV	600 ± 130	170 ± 32	550 ± 120	160 ± 35
Others	300 ± 110	80 ± 40	400 ± 160	110 ± 40
Total expected	$35\,300 \pm 1600$	$19\,300 \pm 1300$	$24\,100 \pm 1200$	$10\,690 \pm 700$
Data	35 817	18 573	24 639	10 536
$\boldsymbol{S/B}$	2.10 ± 0.20	3.95 ± 0.50	1.36 ± 0.15	2.12 ± 0.25
Data / Prediction	1.02 ± 0.05	0.96 ± 0.07	1.02 ± 0.05	0.99 ± 0.06

the scale factor used to adjust the MC pile-up to the data pile-up profile is applied. This uncertainty is obtained by scaling the value of average number of interactions per bunch-crossing $\langle\mu\rangle$ in data by factors of $1/0.99$ and $1/1.07$ instead of the nominal scale factor of $1/1.03$ [105].

To determine the jet energy scale (JES) and its associated uncertainty, information from test-beam data, LHC collision data and simulation are used as described in Ref. [91]. The JES uncertainty is decomposed into a set of 31 uncorrelated components, with contributions from pile-up, jet flavour composition, single-particle response, effects of jets not contained within the calorimeter, theory modelling, and statistical uncertainties. The jet energy resolution (JER) is measured separately for data and MC simulation, using in situ techniques [91]. Its uncertainty is represented by 13 components accounting for jet-p_{T}- and jet-η-dependent differences between simulation and data. The uncertainty associated with the JVT is obtained by increasing and decreasing the scale factor used to correct the JVT efficiency in simulation within its uncertainties [93]. The uncertainties associated with the fJVT are related to data–MC efficiency scale factors in the same manner as the JVT uncertainty.

The efficiency of the b-tagging algorithm is measured for each jet flavour using control samples in data and in simulation. From these measurements, correction factors are derived to correct the tagging rates in the simulation. For b-jets, the correction factors and their uncertainties are estimated from data using dileptonic $t\bar{t}$ events [95, 96]. For c-jets, they are derived from jets arising from W boson decays in $t\bar{t}$ events [97]. For light-flavour jets, the correction factors are derived from Z + jets events [98]. Uncertainties from sources affecting the b-tagging efficiencies of b-jets, c-jets and light-jets are evaluated as a function of jet p_{T}, including bin-to-bin correlations.

For electrons and muons, the reconstruction, identification, isolation, and trigger performance can differ slightly between data and MC simulation. Scale factors, estimated using the tag-and-probe method [84–86], are applied to simulated events to correct for these differences. The lepton momentum scales and resolutions are assessed using leptonic decays of Z bosons and J/ψ mesons. Corrections to the lepton momentum scale and resolution are applied to data and simulation respectively, and include uncertainties in the lepton trigger efficiencies. The associated systematic uncertainties are then propagated to the distributions used in this analysis. Since events containing reconstructed hadronically decaying τ-leptons are vetoed, a τ_{had} energy scale systematic uncertainty [99] is also included.

The systematic uncertainties related to the modelling of the $E_{\text{T}}^{\text{miss}}$ in the simulation are estimated by propagating the uncertainties in the energy and momentum scales of electrons, muons and jets, as well as the uncertainties in the resolution and scale of the soft term [106]. For the data-driven fake-lepton background estimate, real-lepton and fake-lepton efficiency differences between the MC-driven and data-driven methods are taken as an additional source of systematic uncertainty.[6] Systematic uncertainties associated with the signal and background MC modelling are estimated by comparing event samples from different generators and by varying parameter values in the event generation.

The uncertainty due to the choice of hadronisation model and the other non-perturbative aspects of the PS is evaluated by comparing samples generated with different hadronisation models or set-ups. The uncertainty in the PS is estimated for all top-quark processes by comparing samples from Powheg Box interfaced to Pythia 8 with samples from Powheg Box interfaced to Herwig 7.1.3. To estimate the matching scheme uncertainties in $t\bar{t}$ and t-channel single-top-quark production, a sample was produced with Powheg Box v2 and Pythia using a `POWHEG:pThard` setting of 1, instead of 0 as in the nominal sample. This setting regulates the definition of the vetoed region of the Pythia 8 showering [107]. The effect of choosing a different `Powheg:hdamp` parameter value in $t\bar{t}$ simulation is assessed with alternative samples generated with $h_{\text{damp}} = 3.0 \times m_t$. The effect of the top-quark mass uncertainty is estimated as the difference resulting from samples with a 0.5 GeV top-quark mass variation. For associated tW production, an additional sample using the diagram subtraction (DS) scheme was produced to evaluate the $t\bar{t}$ interference uncertainties.

The uncertainty due to missing higher-order QCD corrections in the ME computation is estimated for all top-quark processes by independently varying the renormalisation and factorisation scales by factors of 0.5 and 2.0 from their chosen value. Additionally, uncertainties due to initial-state radiation from the PS are assessed by varying the corresponding parameter of the A14 PS tune, `Var3c` [108]. PDF uncertainties are evaluated using the PDF4LHC15 uncertainty set which consists of 30 eigenvector variations from multiple NLO PDF sets [109].

The event yields associated with the simulated signal and background processes are estimated using the selection acceptances and the theoretically predicted cross-sections reported in Section 4. The uncertainties in these cross-sections are taken into account. However, for those processes whose normalisation is extracted from the data-driven fits, the effect is negligible. To evaluate the impact of the flavour composition uncertainty in the W+ jets simulation templates, an upward and downward variation of 10% is applied to the relative rate of $W + b$-jets vs $W + c$-jets. No variation is considered for W + light-flavour jets production since its contribution is negligible. An uncertainty of 20% is assigned to the Z + jets cross-section. For $t\bar{t}$ events, an additional uncertainty in the modelling of the top-quark p_{T} distribution is evaluated by taking the full difference between applying and not applying the correction needed to match the predictions accurate to NNLO in QCD and NLO in EW theory [110].

Statistical fluctuations in the MC-simulated event samples contribute to the overall systematic uncertainty. These uncertainties arise from the finite number of simulated background and signal events.

[6] The MC-driven method employs the same matrix method as the data-driven method but replaces the data with simulated samples and recomputes the fake-lepton efficiency. The real-lepton efficiency remains the same for both methods.

8 EFT analysis strategy

A standard method for modelling EFT effects in differential distributions involves the use of templates; however, this becomes impractical for a fourfold distribution. The method used here instead performs a Fourier analysis of the quadruple-differential angular decay rate of t-channel single-top-quark production at detector level, using a set of orthogonal basis functions. The resulting Fourier coefficients provide a complete characterisation of the shape of the quadruple-differential angular decay distribution. They are computed through a simple averaging procedure, which simultaneously provides their uncertainties and correlations. Along with the event yields, these coefficients, their uncertainties, and their correlations serve as inputs to a χ^2 fit to the WCs. An advantage of this approach lies in its ability to simultaneously capture many features of the shape and normalisation of the differential cross-section, including those that are more frequently studied in dedicated analyses, such as cross-section or polarisation analyses.

This analysis procedure is more completely described in the following sections. Section 8.1 explains the procedure used to transform the quadruple-differential angular decay rates into a limited number of M-function coefficients. Section 8.2 describes how to obtain the EFT dependency of the M-function coefficients. Section 8.3 introduces the statistical tool used to obtain the final limits.

8.1 Choice of basis functions

The orthogonal functions employed in this analysis are called M-functions and are defined as

$$M^{j_1 j_2}_{m' m}(\cos\theta, \phi, \cos\theta^*, \phi^*) = \frac{1}{4\pi}(2j_1+1)^{1/2}(2j_2+1)^{1/2} D^{j_1}_{m' m}(\cos\theta, \phi, 0) D^{j_2}_{m,0}(\cos\theta^*, \phi^*, 0) \quad (1)$$

where $D^{j_1}_{m' m}$ and $D^{j_2}_{m,0}$ are the Wigner D-functions [111].

$$D^{j}_{m' m}(\alpha, \beta, \gamma) \equiv \langle jm' | e^{-i\alpha J_z} e^{-i\beta J_y} e^{-i\gamma J_z} | jm \rangle \, .$$

The M-function obeys the orthonormality condition

$$\iint M^{j_1 j_2}_{m_1 m_2}(\cos\theta, \phi, \cos\theta^*, \phi^*)^* M^{j_1' j_2'}_{m_1' m_2'}(\cos\theta, \phi, \cos\theta^*, \phi^*) \mathrm{d}\Omega \mathrm{d}\Omega^* = \delta_{j_1, j_1'} \delta_{j_2, j_2'} \delta_{m_1, m_1'} \delta_{m_2, m_2'} \, .$$

This choice of basis functions is motivated by the form of the quadruple-differential top-quark decay distribution [112]. Using the helicity formalism of Ref. [113], the amplitude for the top-quark decay $t \to Wb \to \ell\nu b$ can be written, in the narrow-width approximation, as

$$A_{\mu\lambda_2\lambda_3\lambda_4} = \sum_{\lambda_1} a_{\lambda_1\lambda_2} b_{\lambda_3\lambda_4} D^{1/2\,*}_{\mu\nu}(\cos\theta, \phi, 0)\, D^{1\,*}_{\lambda_1\lambda}(\cos\theta^*, \phi^*, 0) \, ,$$

where λ_1, λ_2, λ_3 and λ_4 are defined to be the helicities of the W boson, b-quark, charged lepton and neutrino, respectively, μ is the third spin component of the top quark, $\nu = \lambda_1 - \lambda_2$, $\lambda = \lambda_3 - \lambda_4$, and $a_{\lambda_1\lambda_2}$ and $b_{\lambda_3\lambda_4}$ are constants. For the top-quark decay, angular momentum conservation implies that there are only four non-zero reduced amplitudes (or just 'amplitudes' for short): $a_{1,\frac{1}{2}}$, $a_{0,\frac{1}{2}}$, $a_{0,-\frac{1}{2}}$ and $a_{-1,-\frac{1}{2}}$. The SM interaction of the W boson with charged leptons implies $\lambda_3 = \pm 1/2$ and $\lambda_4 = \mp 1/2$ for $W^{\pm}$ decays, assuming massless charged leptons. Therefore, $\lambda = 1$ for top quarks, $\lambda = -1$ for top anti-quarks, and in each case there is only one non-zero b constant, which can be factored out and plays no further role in the distributions. With this choice of basis functions, only 23 coefficients fully describe the top-quark decay.

Thus, the differential cross-section at parton level can be fully determined by 23 coefficients $c^{j_1 j_2}_{m' m}$ defined in Eq. (2), having $j_1 < 1$ and $j_2 < 2$ [112]:

$$\frac{1}{\Gamma}\frac{\mathrm{d}\Gamma}{\mathrm{d}\Omega\mathrm{d}\Omega^*} = \sum_{j_1 j_2 m' m} c^{j_1 j_2}_{m' m} M^{j_1 j_2}_{m' m}(\cos\theta, \phi, \cos\theta^*, \phi^*)\,, \tag{2}$$

where Γ is the decay rate.

Through a Fourier transform, the M-function coefficients can be determined by projecting the differential distribution $\rho(\cos\theta, \phi, \cos\theta^*, \phi^*) \equiv (1/\Gamma)\mathrm{d}\Gamma/\mathrm{d}\Omega\mathrm{d}\Omega^*$ onto the M-function basis:

$$c^{j_1 j_2}_{m' m} = \int \mathrm{d}\Omega\mathrm{d}\Omega^* \rho(\cos\theta, \phi, \cos\theta^*, \phi^*) M^{j_1 j_2}_{m' m}(\cos\theta, \phi, \cos\theta^*, \phi^*)^*\,.$$

The right-hand side of this equation is not only interpreted as a coefficient, but also represents the average of the quantity $M^{j_1 j_2}_{m' m}(\cos\theta, \phi, \cos\theta^*, \phi^*)^*$ over a dataset distributed according to $\rho(\cos\theta, \phi, \cos\theta^*, \phi^*)$. Therefore, the practical approach to determining $c^{j_1 j_2}_{m' m}$ for any given dataset is to first substitute $(\cos\theta_i, \phi_i, \cos\theta^*_i, \phi^*_i)$ into Eq. (1) for each individual event i, and then take the average over the entire dataset. This averaging procedure serves as the foundation of this analysis. Hence, the procedure used to obtain these coefficients for both data and MC simulation is to calculate

$$c^{j_1 j_2}_{m' m} = \frac{\sum_{i=1}^{N} w_i M^{j_1 j_2}_{m' m}\left(\cos\theta_i, \phi_i, \cos\theta^*_i, \phi^*_i\right)}{\sum_{i=1}^{N} w_i}\,, \tag{3}$$

where the sum is over the event sample, and w_i is the MC weight of the i^{th} event, and for data events $w_i = 1$. By averaging squares and products of M-function coefficients, the statistical covariance matrix for the full set of coefficients is obtained.

However, detector effects, including resolution, acceptance, and efficiency, strongly affect the angular distributions and hence the M-function coefficients. As well as modifying the 23 M-function coefficients, these effects introduce coefficients with $j_1 > 1$ and/or $j_2 > 2$[7]. This analysis is restricted to considering angular components with $j_1 < 1$ and $j_2 < 2$, at reconstruction level, since the coefficients with $j_1 > 1$ and/or $j_2 > 2$ are mainly shaped by the detector effects, whereas the chosen M-function coefficients are mainly shaped by the EFT operators. The dependence of these M-function coefficients on the WCs is computed at reconstruction level using MadGraph+Pythia MC events as described in Section 4. Both the signal and $t\bar{t}$ background are affected by the WCs and these effects are modelled by the MC simulation. However, the $t\bar{t}$ background is suppressed by the event selection as defined in Section 6.

[7] Angular momentum conservation ensures that, at the generator level, the M-function coefficients vanish whenever $j_1 > 1$ and $j_2 > 2$.

8.2 Morphing

To model the response of the M-function coefficients to variations of the Wilson coefficients, a morphing technique is used. The numerator of the right-hand expression in Eq. (3) is taken to give the unnormalised M-function coefficients. They are proportional to the cross-section of the process, and are each a polynomial function of the Wilson coefficients. For the Wilson coefficients C_{tW}, C^{I}_{tW}, C_{bW}, C^{I}_{bW} and $C_{\varphi tb}$, the corresponding operators contribute to both the t-channel production of a single top quark and its decay. Therefore, the observables that are proportional to the cross-section will depend on these WCs to at most fourth-order. On the other hand, their dependence on C_{Qq}, which only affects the production of single-top-quark events, will be at most second-order.

The unnormalised M-function coefficients, for different EFT assumptions, are computed from reconstructed LO MadGraph+Pythia events. For C_{Qq}, a three-point Lagrange interpolation is used to parameterise the M-function; for the other Wilson coefficients, a five-point Lagrange interpolation is employed. The correlations among all the WCs are incorporated in the results via the interference terms when using this procedure. Consequently, the final morphing function for each M-function coefficient is expressed as a 203-term polynomial in C_{tW}, C^{I}_{tW}, C_{bW}, C^{I}_{bW}, $C_{\varphi tb}$, and C_{Qq}.

An overall LO-to-NLO correction term for the M-function coefficients is calculated by determining the difference between the LO MadGraph+Pythia SM event sample and the NLO Powheg Box+Pythia SM event sample:

$$\vec{c}_{O}^{\,\mathrm{NLO}}(\vec{C}) = \vec{c}_{O}^{\,\mathrm{LO}}(\vec{C}) + \left[\vec{c}_{O}^{\,\mathrm{NLO}}(\vec{C}_{\mathrm{SM}}) - \vec{c}_{O}^{\,\mathrm{LO}}(\vec{C}_{\mathrm{SM}})\right].$$

The LO-to-NLO event-count correction is obtained as a scale factor equal to the ratio of the two event counts.

Finally, $C_{\varphi Q}$ is not morphed; instead, the dependency of $C_{\varphi Q}$ could be obtained from the t-channel scale factor $S_{t\text{-channel}}$ as described in Eq. (4):

$$S_{t\text{-channel}} = |V_{\mathrm{L}}|^2 = \left(1 + \frac{v^2}{\Lambda^2} C_{\varphi Q}\right)^2. \tag{4}$$

8.3 Fit strategy

Data used in the statistical analysis consist of 23 M-function coefficients $\vec{c}^{\,(s)}$ for each of the four channels $s = 1, \ldots, 4$, distinguished by top-quark p_{T} and lepton charge as defined in Section 6, which results in a total of 92 coefficients. In addition, the event counts in each channel's SR, W+jets CR and $t\bar{t}$ CR are used, which gives 12 additional inputs. A statistical covariance matrix in the coefficients is determined by the M-function analysis along with their values as described in Section 8.1. Because of the manner in which the M-functions are obtained, i.e. Eq. (1), the central limit theorem guarantees Gaussian uncertainties, and a simple χ^2 fit is used. Parameters of the fit include the Wilson coefficients C_{tW}, C^{I}_{tW}, $C_{\varphi tb}$, C_{bW}, C^{I}_{bW}, and C_{Qq}, collectively referred to as the parameter of interest (POI) vector $\vec{C}$, as well as normalisation factors for the t-channel single-top-quark process (namely $C_{\varphi Q}$ as defined in Eq. (4)) and the W+jets and $t\bar{t}$ processes, collectively denoted by the vector $\vec{S}$.

The systematic uncertainty is taken into account by computing a covariance matrix for the systematic uncertainty sources:

$$\mathbb{C}^{\text{syst.}} = \sum_{\text{syst. sources}} \Delta\vec{v} \otimes \Delta\vec{v}^{T}, \tag{5}$$

where $\Delta\vec{v}$ is the vector of the expected 1σ uncertainties from the sources of systematic uncertainty described in Section 7. Due to the central limit theorem, the likelihood function combining the M-function coefficients and the event counts is a multivariable Gaussian function. The $\chi^2 = -2\ln\mathcal{L}$ is given by

$$\chi^2(\vec{C},\vec{S}) = \sum_{(s)} \left\{ \left(\vec{c}^{(s)} - \vec{c}^{(s),\text{model}}(\vec{C},\vec{S})\right)^{T} \mathbb{C}^{(s)\,-1} \left(\vec{c}^{(s)} - \vec{c}^{(s),\text{model}}(\vec{C},\vec{S})\right) + \sum_{j\in\{\text{SR},\text{CR-}W,\text{CR-}t\bar{t}\}} \frac{\left(N^{(s,j),\text{model}}(\vec{C},\vec{S}) - N^{(s,j)}\right)^2}{N^{(s,j)}} \right\},$$

where $\vec{c}^{(s)}$ is the vector of 23 M-function coefficients in channel s, $N^{(s,j)}$ is the event count in channel s and SR or CR j, and the covariance matrix $\mathbb{C}^{(s)}$ is a linear sum of statistical covariance $\mathbb{C}^{\text{stat.}}_{\text{data}}$ from the data, statistical covariance $\mathbb{C}^{\text{stat.}}_{\text{MC}}$ from the MC events, and systematic covariance $\mathbb{C}^{\text{syst.}}$ as defined in Eq. (5). The superscript 'model' indicates values predicted from the fitting model. The fit has 92 + 12 inputs − 9 parameters = 95 degrees of freedom. The fit is tested with pseudoexperiments over a wide range of input physics and nuisance parameters consistent with the expected precision of the measurement.

Table 4: Summary of the expected systematic and statistical uncertainty breakdown for the 1σ confidence interval of each Wilson coefficient from the one-dimensional likelihood scans. The limited data and MC sample sizes are sources of statistical uncertainty. The symbol '–' indicates that the uncertainty is negligible.

Source of uncertainty	C_{tW}	C^{I}_{tW}	$C_{\varphi tb}$	C_{bW}	C^{I}_{bW}	C_{Qq}	$C_{\varphi Q}$
Jet energy scale	−0.03, +0.03	−0.01, +0.01	−0.6, +0.4	−0.3, +0.3	−0.3, +0.3	−0.02, +0.05	−0.10, +0.09
Pile-up	−0.01, –	–	−0.1, +0.2	–, +0.1	−0.1, –	–, +0.01	−0.08, +0.06
b-tagging	−0.02, +0.03	−0.01, +0.01	−0.6, +0.6	−0.1, +0.2	−0.1, +0.1	−0.02, +0.02	−0.13, +0.13
Jet energy resolution	−0.02, +0.02	−0.01, +0.01	−0.8, +0.7	−0.1, +0.1	−0.1, +0.1	−0.02, +0.03	−0.08, +0.09
PDF	−0.02, +0.02	−0.01, +0.01	−0.7, +0.6	−0.1, +0.1	−0.1, +0.1	−0.03, +0.04	−0.08, +0.09
Muon	−0.03, +0.02	–	−0.4, +0.3	−0.1, +0.1	−0.1, +0.1	−0.01, +0.03	−0.07, +0.06
$E_{\text{T}}^{\text{miss}}$	−0.02, +0.02	–	−0.5, +0.4	−0.1, +0.1	−0.2, +0.2	−0.01, +0.02	−0.06, +0.05
e/γ	−0.01, +0.01	–	−0.2, +0.1	−0.1, +0.1	−0.1, +0.1	–, +0.01	−0.06, +0.07
Jet vertex tagging	−0.01, +0.01	–	−0.1, +0.2	–, +0.1	–	−0.02, +0.03	−0.17, +0.18
Lumi. & cross-section	−0.01, –	–	−0.1, +0.1	−0.1, +0.1	−0.1, +0.1	−0.01, –	−0.07, +0.07
τ_{had} energy scale	–	–	–	–	–	–	–
Non-prompt leptons	−0.01, –	–	–, +0.2	–, +0.1	−0.1, +0.1	−0.01, –	−0.01, +0.01
t-channel modelling	−0.01, +0.01	–	−0.3, +0.1	–	–	−0.04, +0.04	−0.15, +0.15
$t\bar{t}$ modelling	−0.03, +0.02	−0.01, –	−0.5, +0.4	−0.1, +0.1	−0.1, +0.1	−0.01, +0.03	−0.04, +0.08
W+jets modelling	−0.01, +0.02	−0.01, +0.01	−0.8, +0.6	−0.1, +0.1	–, +0.1	−0.01, +0.02	−0.06, +0.08
MC sample sizes	−0.03, +0.03	−0.03, +0.03	−0.9, +0.8	−0.2, +0.2	−0.2, +0.2	−0.03, +0.05	−0.14, +0.14
Data sample size	−0.06, +0.05	−0.04, +0.04	−3.1, +1.7	−0.5, +0.7	−0.5, +0.5	−0.05, +0.08	−0.13, +0.15
Total	−0.10, +0.09	−0.06, +0.06	−3.9, +2.6	−0.8, +0.9	−0.7, +0.7	−0.09, +0.14	−0.41, +0.43

The effect of each systematic uncertainty on the WCs is evaluated by removing that systematic uncertainty from Eq. (5) and comparing the $-\ln\mathcal{L}$ scan with that for the nominal fit. Similarly, the impact of the MC statistical uncertainty is obtained by comparing the $-\ln\mathcal{L}$ scans with and without inclusion of $\mathbb{C}^{\text{stat.}}_{\text{MC}}$. Table 4 summarises the sources of both the systematic and statistical uncertainties for the 1σ confidence interval for each of the POIs. Although the total systematic uncertainty is comparable to the statistical uncertainty of the data except for $C_{\varphi Q}$, no single source of systematic uncertainty significantly outweighs the overall MC statistical uncertainty.

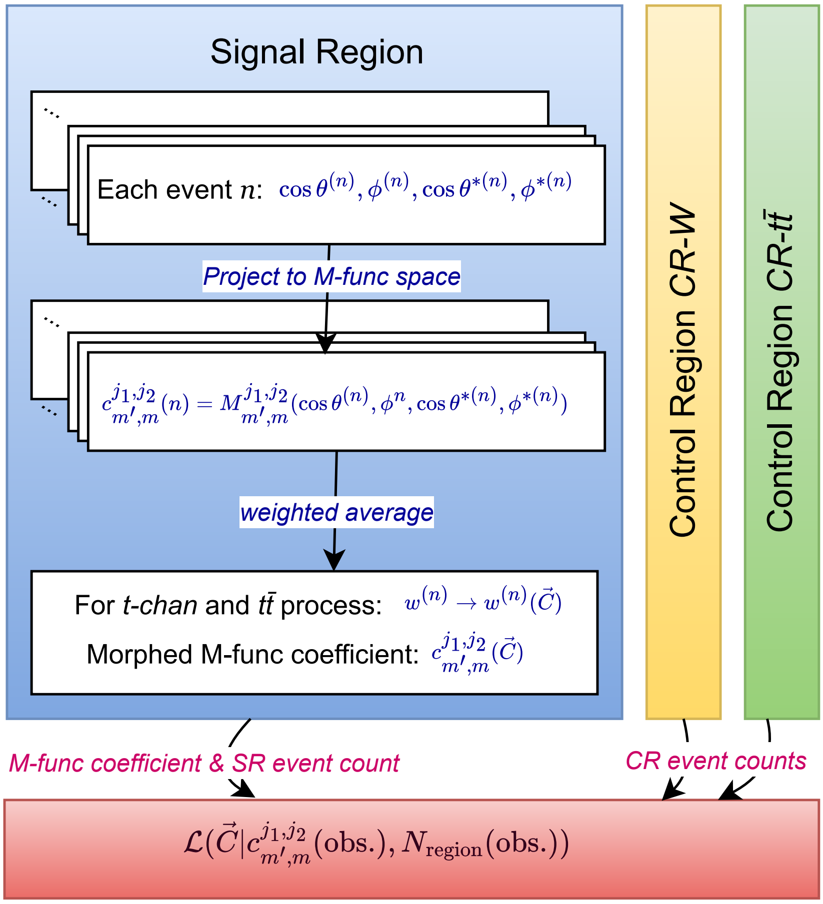

Figure 3: Overview of the analysis workflow. Events passing the preselection are separated into two CRs (CR-W, CR-$t\bar{t}$) and an SR. In the SR, the four decay angles are reconstructed for each event and projected onto the orthonormal M-function basis, providing event-by-event coefficients that are then averaged as defined in Eq. (3). The dependence of these coefficients on the WC vector, $\vec{C}$, in both the t-channel single-top-quark and $t\bar{t}$ processes is modelled using morphing. Final observables consist of the M-function coefficients in the SR and the event yields in both the SR and CRs.

Finally, the overall analysis workflow is illustrated in Figure 3. For the SR, the four decay angles are reconstructed event by event and inserted into Eq. (1) to compute the coefficients of the orthonormal M-function basis. These per-event coefficients are then combined via a (weighted) average over all SR events (as defined in Eq. (1)) to form the final M-function observables. The dependence of the (averaged) coefficients on the WC vector, $\vec{C}$, in both the t-channel single-top-quark and $t\bar{t}$ processes is obtained from MC simulation and modelled using the morphing technique described in Section 8.2. This approach fully captures the impact of the WCs on the quadruple-differential phase space without the need to bin a four-dimensional distribution. A Gaussian likelihood $\mathcal{L}$, built from the averaged M-function coefficients and the event counts in the SR and CRs, is then maximised to extract the best-fit WC values.

9 Results

The post-fit SR distributions of the four angles $\cos\theta$, $\cos\theta^*$, ϕ, and ϕ^* are shown in Figure 4. They are all in good agreement with the data, with χ^2 values ranging from 5 to 18 for 20 bins.

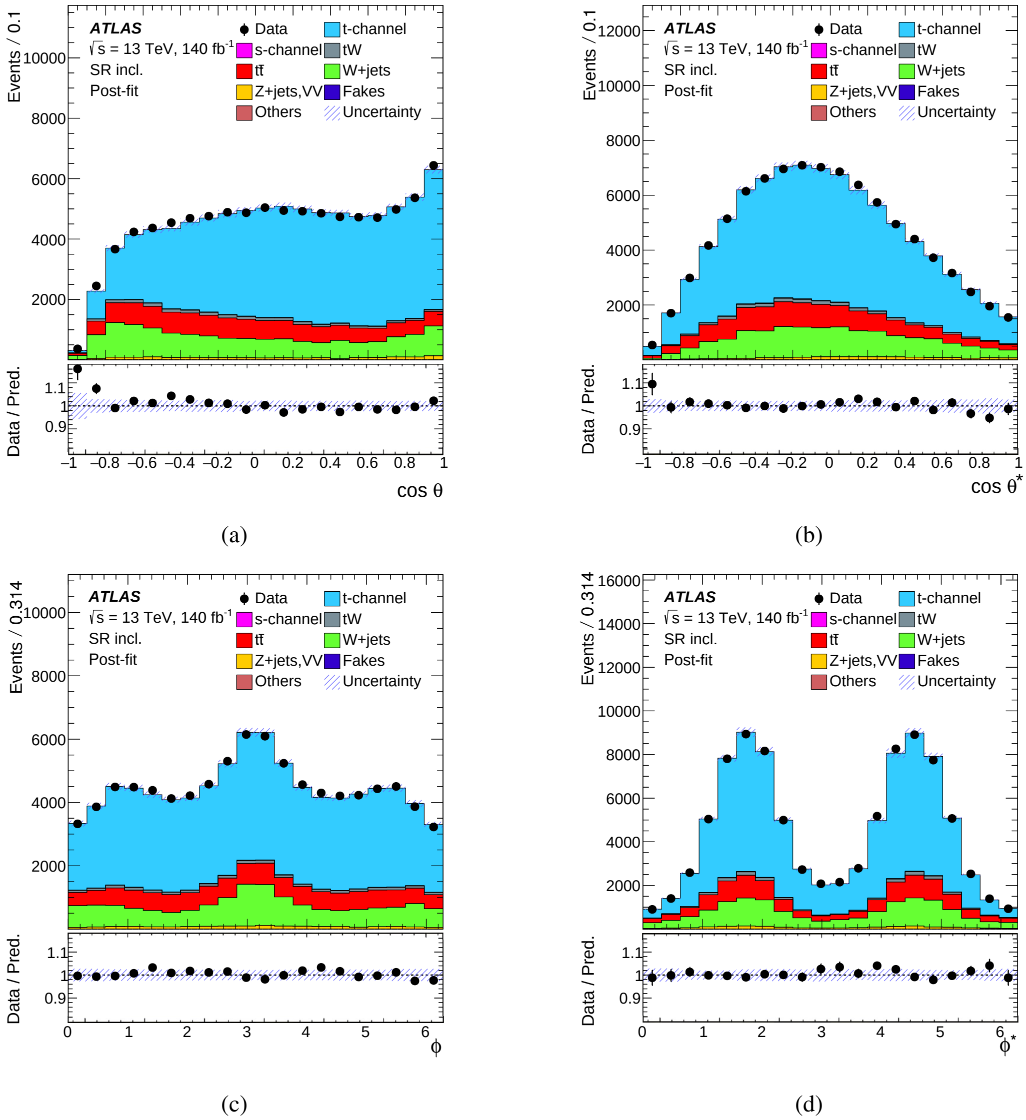

Figure 4: Post-fit distributions of the four angles, namely (a) $\cos\theta$, (b) $\cos\theta^*$, (c) ϕ, and (d) ϕ^* in the inclusive SR. The fitted predicted distributions are compared with the observed data, depicted as black points with statistical uncertainties. The uncertainty bands reflect the statistical and systematic uncertainties, taking into account the post-fit constraints from the profile likelihood fit. Correlations among all parameters obtained from the fit are accounted for in the calculation of the uncertainty bands. The lower plot for each angular distribution shows the ratio of the observed data to the fitted prediction in each bin, offering a quantitative measure of how well the two agree.

Summing over the four channels, the final observables are the 3×4 event counts in the SR and two CRs, along with the 23×4 M-function coefficients in the SR. Figure 5 shows the relative differences between the observed event counts and the SM predictions. Figure 6 shows the absolute deviations of the M-function coefficients from the SM prediction, for both the observed data and the fitted EFT model in each channel's SR. The black points represent the data, while the scattered markers correspond to the expected values when making various WC assumptions. The grey band, centred at zero, represents the SM expectation; its width indicates the pre-fit systematic uncertainties. The centre of each red box is determined by the best-fit value from the EFT fit; its height is set by the post-fit uncertainties, which include the effect of correlations. The plots demonstrate the effect of the data upon the fitted model.

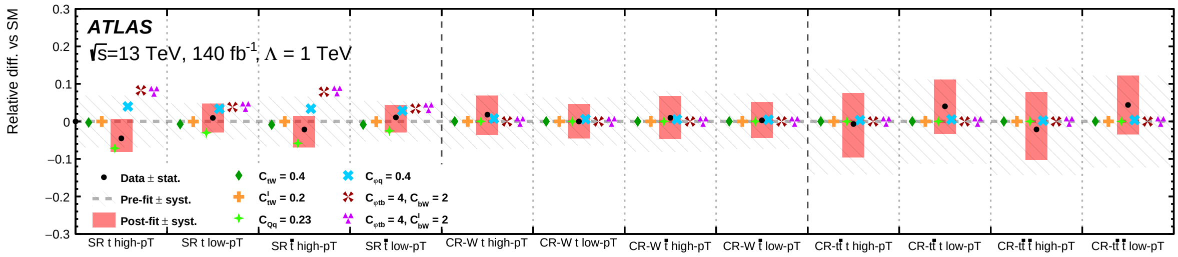

Figure 5: The relative differences between the observed and SM predicted event counts in the SRs and CRs, for both the observed data and the fitted EFT model. The black points represent observed data, with the data statistical uncertainties as error bars. The grey dashed area indicates the total systematic uncertainties, while the red boxes are centred at positions determined by the best-fit values of the Wilson coefficients, with heights determined by systematic uncertainties constrained by the fit. The coloured scattered markers correspond to expected values when making various WC assumptions.

As expected, due to the large number of observables compared to the number of unconstrained parameters, the uncertainties of the observables are reduced by the fit.

The SM prediction is in reasonable overall agreement with the 104 observables, with a $\chi^2 = -2 \ln \mathcal{L} = 105.2$, indicating a 45% confidence level (CL), although agreement is poorer for some high-p_{T} SR observables. At the best-fit point of the EFT fit with 9 parameters, the likelihood has a $\chi^2 = 87.4$ for 95 degrees of freedom (70% CL). Both hypotheses are consistent with the data.

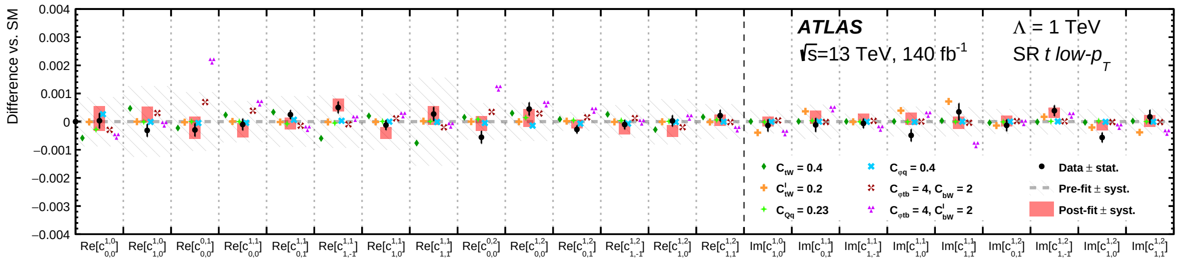

(a)

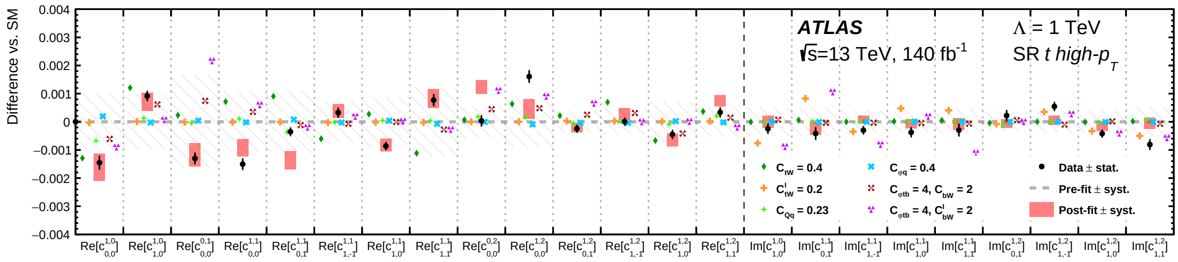

(b)

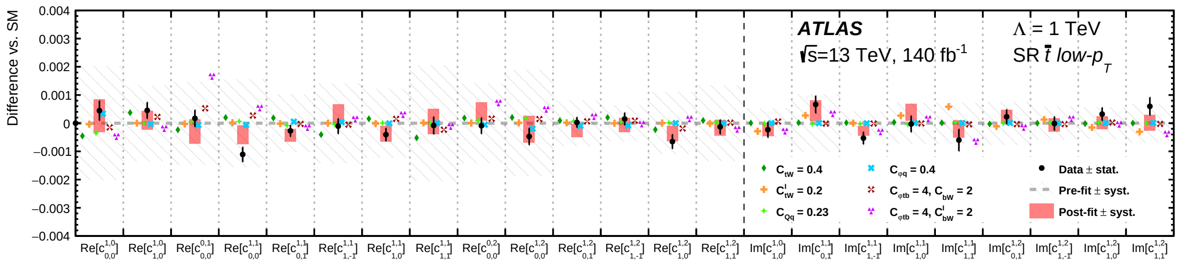

(c)

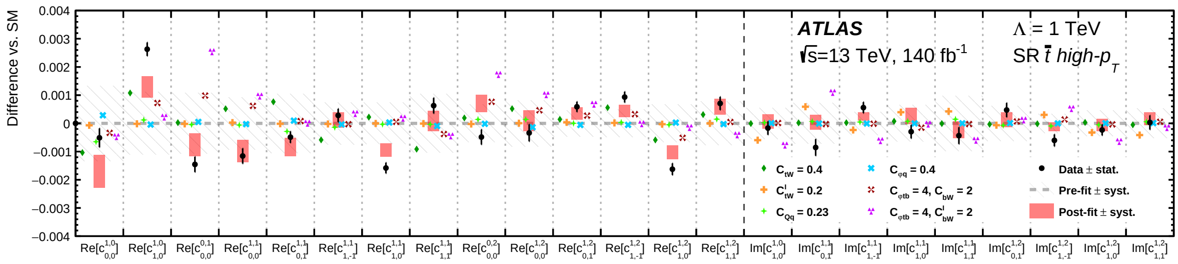

(d)

Figure 6: The absolute deviations of the M-function coefficients, as defined in Eq. (3), from the SM prediction, for both the observed data and the fitted EFT model, in the SR of the (a) low-p_{T} (< 80 GeV) top-quark channel, (b) high-p_{T} (≥ 80 GeV) top-quark channel, (c) low-p_{T} top-antiquark channel, and (d) high-p_{T} top-antiquark channel, respectively. The black points represent observed data, with the data statistical uncertainties as error bars. The grey dashed area indicates the total systematic uncertainties, while the red boxes are centred at positions determined by the best-fit values of the Wilson coefficients, with heights determined by systematic uncertainties constrained by the fit. The coloured scattered markers correspond to expected values when making various WC assumptions.

Three different fitting schemes are considered for a one-dimensional likelihood scan:

- **Fully profiled fit**: each POI is scanned while profiling the other six POIs.
- **Reduced fit**: WCs that are dominated by quadratic dependencies ($C_{\varphi tb}$, C_{bW}, C_{bW}^{I}) are fixed at SM values in this scheme. This fit allows one to obtain well-defined point estimates and a covariance matrix for the remaining parameters.
- **Individual fit**: all other POIs fixed at the SM values when scanning a POI.

The fitted scale factors of the two major background processes $t\bar{t}$ and $W+$jets are summarised in Table 5.

Table 5: The best-fit results for the scale-factor vector $\vec{S}$ with the corresponding 68% CL intervals.

Scale factor	Fully profiled fit		Reduced fit	
	Best-fit value	**68% CL interval**	**Best-fit value**	**68% CL interval**
$S^{W+\text{jets}}$	0.92	±0.07	0.91	±0.06
$S^{t\bar{t}}$	1.09	±0.08	1.10	±0.08

One-dimensional likelihood scans for these fitting schemes are shown in Figure 7 for the EFT coefficients that have a linear effect on the M-function coefficients, and in Figure 8 for those that have a quadratic effect. The non-zero value of the b-quark mass used in the generation of the EFT grid points used for the morphing leads to a slight linear dependence, so the resulting likelihood scans are not expected to be completely symmetric about the SM point.

The limits on each WC for each fitting scheme introduced above are summarised in Table 6 and Table 7. For the reduced fit, the covariance matrix of the four WCs C_{tW}, C_{tW}^{I}, C_{Qq} and $C_{\varphi Q}$ is given in Figure 9.

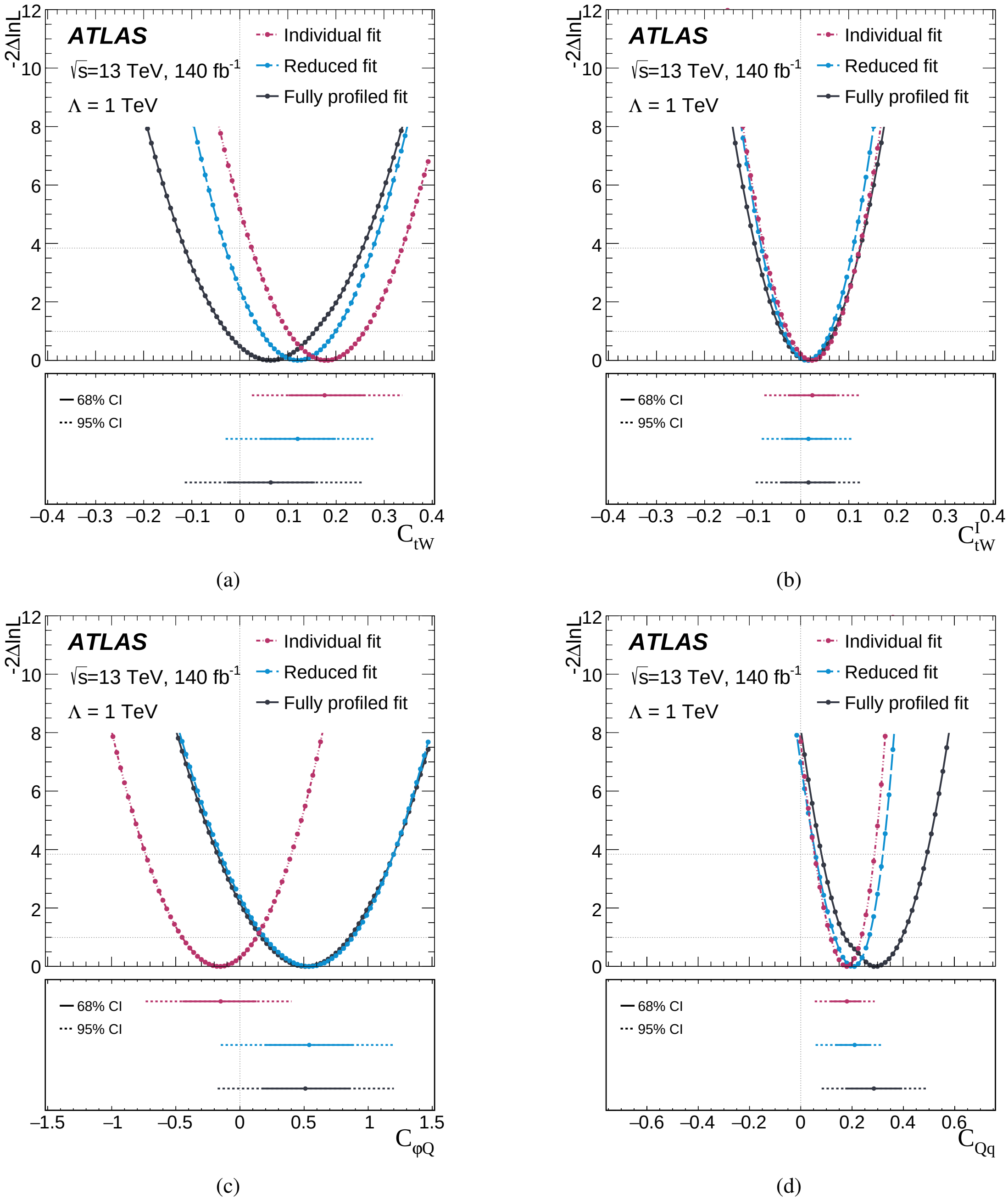

Figure 7: The likelihood scans for the parameters (a) C_{tW}, (b) C^{I}_{tW}, (c) $C_{\varphi Q}$, and (d) C_{Qq}, comparing the fully profiled fit scheme (black curve), the reduced fit scheme (dashed blue curve) and the individual fit scheme (dash-dotted red curve). The 68% and 95% CL intervals (CI) for each parameter in each scheme are shown in the bottom plots.

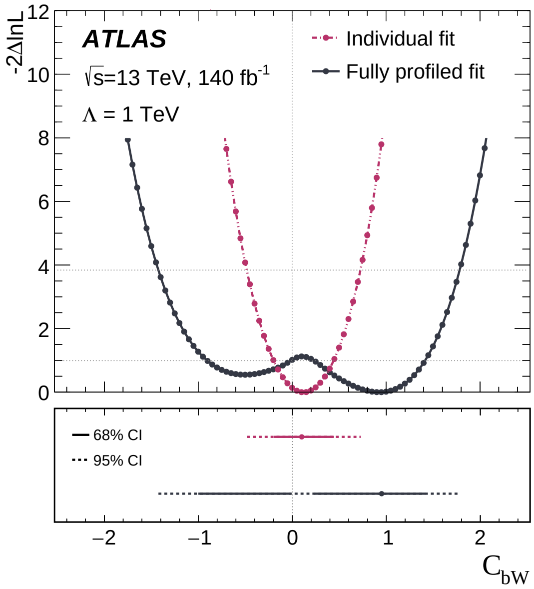

(a)

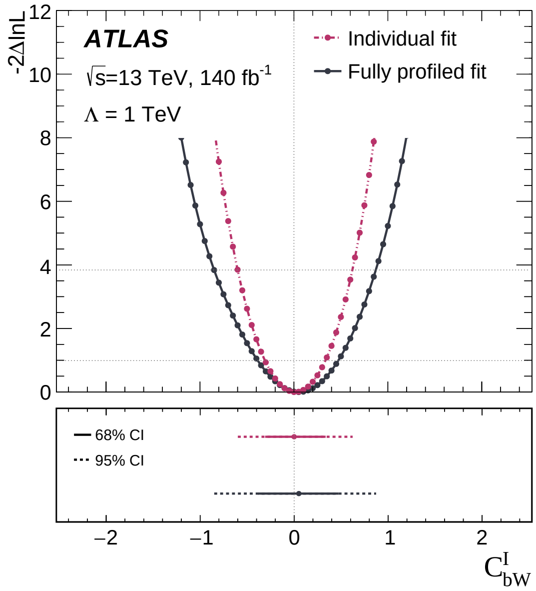

(b)

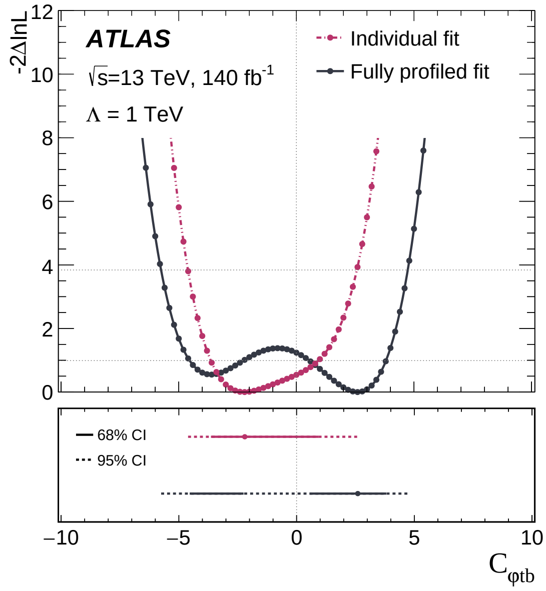

(c)

Figure 8: The likelihood scans for the parameters (a) C_{bW}, (b) C^{I}_{bW} and (c) $C_{\varphi tb}$, comparing the fully profiled fit scheme (black curve) with the individual fit scheme (dash-dotted red curve). The 68% and 95% CL intervals (CI) for each parameter in each scheme are shown in the bottom plots.

Table 6: The best-fit values obtained by the reduced fit scheme, and the 68% and 95% CL intervals. In this fitting scheme, only the WCs C_{tW}, C^{I}_{tW}, C_{Qq} and $C_{\varphi Q}$ that have a linear effect on the M-function coefficients are free floating.

Wilson coefficient [TeV^{-2}]	**Reduced fit** Central value	68% CL interval	95% CL interval
C_{tW}/Λ^2	0.12	[+0.04, +0.20]	[−0.03, +0.28]
C^{I}_{tW}/Λ^2	0.02	[−0.03, +0.06]	[−0.08, +0.11]
C_{Qq}/Λ^2	0.21	[+0.13, +0.27]	[+0.05, +0.32]
$C_{\varphi Q}/\Lambda^2$	0.54	[+0.19, +0.88]	[−0.16, +1.21]

Table 7: The WC intervals at 68% and 95% CL, obtained by a one-dimensional likelihood scan. The table compares two scenarios: a fully profiled fit in which all non-scanned WCs are profiled simultaneously, and an individual fit in which all other coefficients are kept fixed at their SM value (zero).

Wilson coefficient	**Fully profiled fit**		**Individual fit**	
[TeV^{-2}]	68% CL interval	95% CL interval	68% CL interval	95% CL interval
C_{tW}/Λ^2	[−0.03, +0.17]	[−0.12, +0.26]	[+0.10, +0.26]	[+0.02, +0.34]
C^{I}_{tW}/Λ^2	[−0.04, +0.07]	[−0.10, +0.13]	[−0.03, +0.07]	[−0.08, +0.12]
$C_{\varphi tb}/\Lambda^2$	[−4.6, −2.3] ∪ [+0.5, +3.8]	[−5.8, +4.8]	[−3.6, +1.0]	[−4.6, +2.6]
C_{bW}/Λ^2	[−1.0, 0.0] ∪ [+0.2, +1.4]	[−1.4, +1.8]	[−0.2, +0.4]	[−0.5, +0.7]
C^{I}_{bW}/Λ^2	[−0.4, +0.5]	[−0.9, +0.9]	[−0.3, +0.3]	[−0.6, +0.6]
C_{Qq}/Λ^2	[+0.17, +0.37]	[+0.08, +0.50]	[+0.12, +0.24]	[+0.05, +0.29]
$C_{\varphi Q}/\Lambda^2$	[+0.17, +0.86]	[−0.19, +1.2]	[−0.45, +0.13]	[−0.75, +0.41]

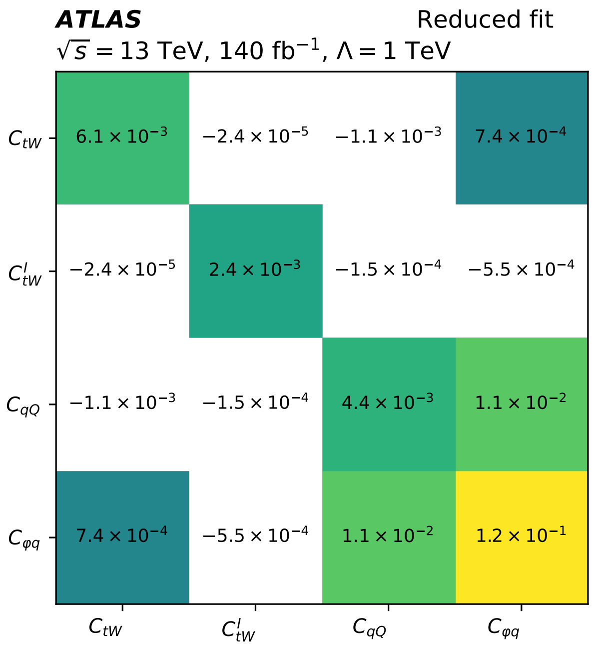

Figure 9: Covariance matrix for the reduced fit, assuming $\Lambda = 1$ TeV.

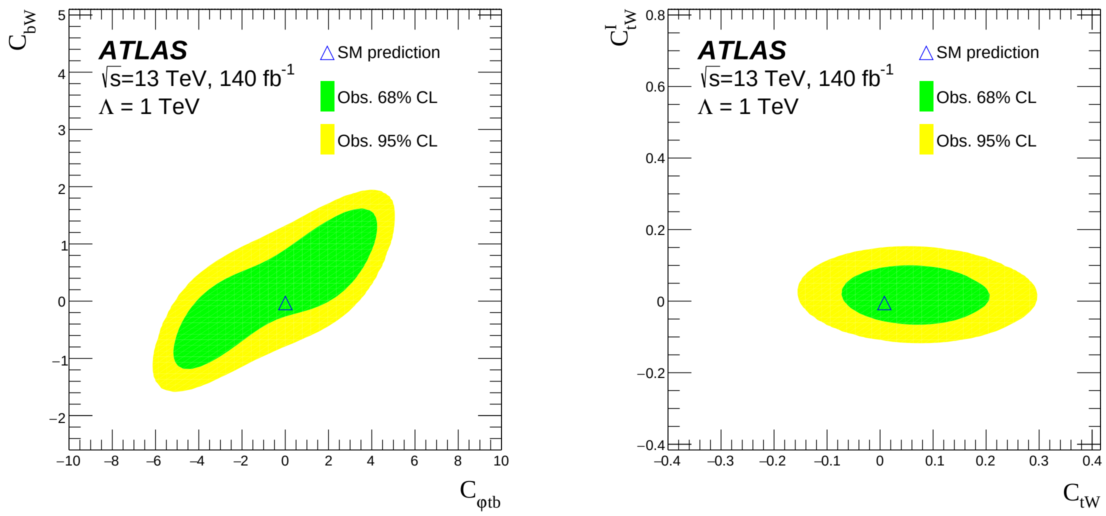

(a)

(b)

Figure 10: Likelihood scan of (a) $C_{\varphi tb}$ and C_{bW}, and (b) C_{tW} and C^{I}_{tW}, with all other parameters profiled. The expected SM point is marked with a blue triangle. The observed 68% and 95% CL regions are shown as inner green and outer yellow regions, respectively.

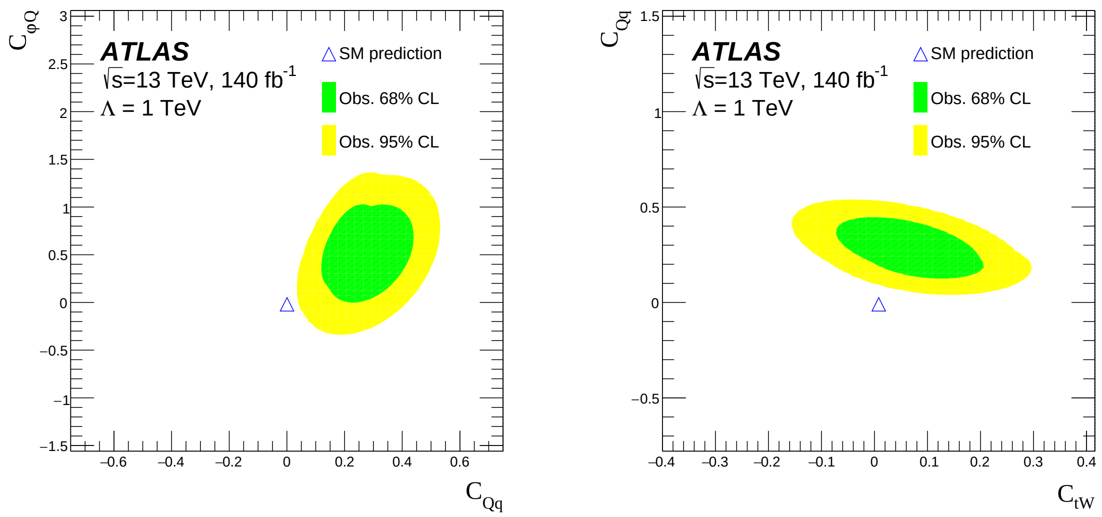

(a) (b)

Figure 11: Likelihood scan of (a) C_{Qq} and $C_{\varphi Q}$, and (b) C_{tW} and C_{Qq}, with all other parameters profiled. The expected SM point is marked with a blue triangle. The observed 68% and 95% CL regions are as inner green and outer yellow regions, respectively.

Two-dimensional (2-D) likelihood scans for the fully profiled fitting scheme are shown in Figure 10 and Figure 11. The 68% and 95% CL regions are obtained by using the conventional $-2\Delta\ln\mathcal{L}$ thresholds for two degrees of freedom [2]. It is known that one can construct a linear combination of $O_{\varphi tb}$ and O_{bW} that has no sensitivity to the fraction of top quarks that decay to right-handed W bosons [14]. Additional observables in this analysis somewhat break that degeneracy, but a strong correlation still remains. Negligible correlation between C_{tW} and C^{I}_{tW} is observed. There is, however, some correlation between the fitted results for C_{Qq} and $C_{\varphi Q}$ or C_{tW}.

The constraints on all seven WCs are summarised in Figure 12. Competitive constraints are placed on all of these parameters, the most restrictive being those on the real and imaginary parts of c_{tW}. The sensitivity to the various WCs arises from different aspects of the data:

- The imaginary components of c_{tW} and the product of $c_{\varphi tb}$ and c_{bW} are constrained by the imaginary parts of the M-function coefficients, while the constraints on the real parts of c_{tW}, c_{bW}, and $c_{\varphi tb}$ are determined by the real parts of the M-function coefficients. Since O_{bW} and $O_{\varphi tb}$ do not produce large interference with the SM amplitude, the corresponding WCs are less constrained.
- $C_{\varphi Q}$ and C_{Qq} are constrained by the event counts in the two p_{T} regions; $C_{\varphi Q}$ affects the overall rate, whereas C_{Qq} impacts the high-p_{T} region more than the low-p_{T} region. Having multiple p_{T} regions allows one to separate the effects of these two WCs. A non-zero C_{Qq} also predicts a slight reduction in the polarisation of the produced top quarks, with more of an effect in the high-p_{T} region [114]. The fitted result of C_{Qq}, which corresponds to a 2.8σ deviation from the SM, is attributed to the small difference between the number of events observed in the high-p_{T} signal region and the number predicted by the Powheg Box v2 simulation. More studies are needed to determine whether NNLO effects could provide better agreement with the data. Since both C_{Qq} and $C_{\varphi Q}$ affect the event

counts, two bins in p_T are the minimum required to separate their effects. In the future, it would be beneficial to use more p_T bins to better determine C_{Qq}.

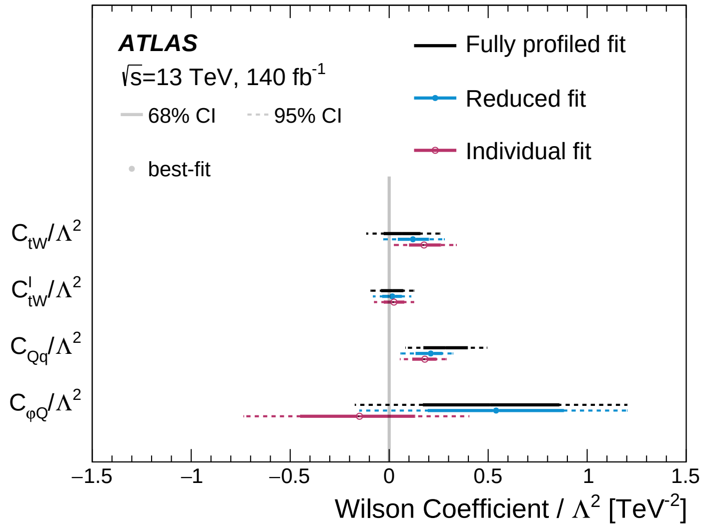

(a)

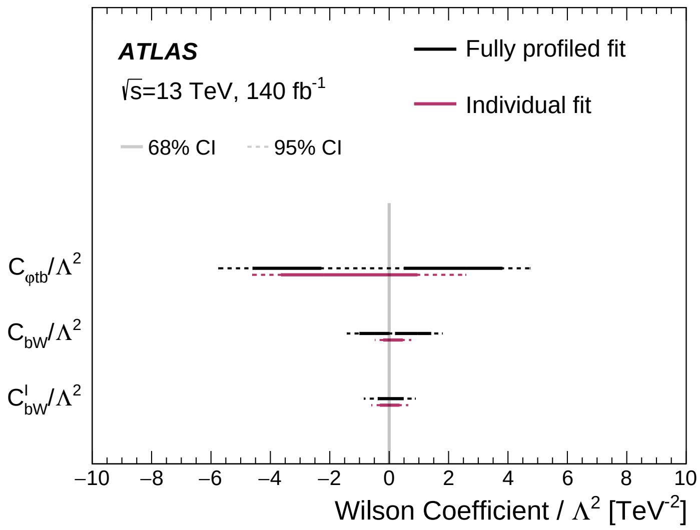

(b)

Figure 12: Summary of confidence intervals extracted from the likelihood fits described in Section 9 for (a) C_{tW}, C^I_{tW}, C_{Qq}, $C_{\varphi Q}$ and (b) $C_{\varphi tb}$, C_{bW}, C^I_{bW}. The WC 68% CL (thick line) and 95% CL (dotted line) intervals are shown for each of the different fitting schemes.

The best previously published constraint on C_{tW} comes from a measurement of the fraction of top-quark decays that produce each W-boson helicity state (F_0, F_L, F_R) in pp collisions at $\sqrt{s}$ =8 TeV, assuming that $C_{\varphi Q} = 0$ [27]. This analysis improves on that result by a factor of 2, while removing the assumption that the other WCs are zero. The 2-D limit contours for $C_{\varphi tb}$ and C_{bW} improve on the results from the measurement of F_R in Ref. [27] by providing constraints along the direction to which F_R is blind, while achieving comparable precision along the direction to which F_R is sensitive. This result also improves on the limits on C^I_{tW} from measurements of top-quark polarisation [16] by a factor of 3. More recent measurements from CMS [22] also yield constraints on the WCs investigated here. The precision of those constraints is a factor of 2 better in $C_{\varphi tb}$ and C_{bW}, and complementary to those presented here; however, they do not provide any information on the imaginary components of these WCs. Reference [22] also provides tighter constraints on C_{Qq} by a factor of 3. The constraints on C_{Qq} presented here are consistent within the uncertainties of those results. Reference [22] also reported the best previous constraints on $C_{\varphi Q}$. The measurement of the total t-channel single-top-quark cross-section [10] provides slightly better constraints on $C_{\varphi Q}$, but only when assuming that all other WCs are zero. This paper improves the result of $C_{\varphi Q}$ by a factor of 2.

10 Conclusion

In summary, constraints are placed on dimension-six Wilson coefficients at the tWb vertex, and on the four-quark coefficient C_{Qq}, using the 140 fb^{-1} dataset collected from $\sqrt{s}$ = 13 TeV pp collisions by the ATLAS detector during Run 2 of the LHC. The strategy used in this study offers an approach for probing EFT Wilson coefficients with high precision through Fourier-based angular analysis. The quadruple-differential decay spectrum of t-channel single-top-quark events is projected onto an orthonormal M-function basis, and the 23 leading normalised M-function coefficients for each of four different channels are fitted simultaneously with the event yields using a maximum-likelihood method. Although the systematic uncertainty is the dominant source of error overall, no individual source of systematic uncertainty significantly outweighs the total statistical uncertainty, which is primarily driven by the size of the data sample. All best-fit points are consistent with the SM expectation.

Acknowledgements

We thank CERN for the very successful operation of the LHC and its injectors, as well as the support staff at CERN and at our institutions worldwide without whom ATLAS could not be operated efficiently.

The crucial computing support from all WLCG partners is acknowledged gratefully, in particular from CERN, the ATLAS Tier-1 facilities at TRIUMF/SFU (Canada), NDGF (Denmark, Norway, Sweden), CC-IN2P3 (France), KIT/GridKA (Germany), INFN-CNAF (Italy), NL-T1 (Netherlands), PIC (Spain), RAL (UK) and BNL (USA), the Tier-2 facilities worldwide and large non-WLCG resource providers. Major contributors of computing resources are listed in Ref. [115].

We gratefully acknowledge the support of ANPCyT, Argentina; YerPhI, Armenia; ARC, Australia; BMWFW and FWF, Austria; ANAS, Azerbaijan; CNPq and FAPESP, Brazil; NSERC, NRC and CFI, Canada; CERN; ANID, Chile; CAS, MOST and NSFC, China; Minciencias, Colombia; MEYS CR, Czech Republic; DNRF and DNSRC, Denmark; IN2P3-CNRS and CEA-DRF/IRFU, France; SRNSFG, Georgia; BMFTR, HGF and MPG, Germany; GSRI, Greece; RGC and Hong Kong SAR, China; ICHEP and Academy of Sciences and Humanities, Israel; INFN, Italy; MEXT and JSPS, Japan; CNRST, Morocco; NWO, Netherlands; RCN, Norway; MNiSW, Poland; FCT, Portugal; MNE/IFA, Romania; MSTDI, Serbia; MSSR, Slovakia; ARIS and MVZI, Slovenia; DSI/NRF, South Africa; MICIU/AEI, Spain; SRC and Wallenberg Foundation, Sweden; SERI, SNSF and Cantons of Bern and Geneva, Switzerland; NSTC, Taipei; TENMAK, Türkiye; STFC/UKRI, United Kingdom; DOE and NSF, United States of America.

Individual groups and members have received support from BCKDF, CANARIE, CRC and DRAC, Canada; CERN-CZ, FORTE and PRIMUS, Czech Republic; COST, ERC, ERDF, Horizon 2020, ICSC-NextGenerationEU and Marie Skłodowska-Curie Actions, European Union; Investissements d'Avenir Labex, Investissements d'Avenir Idex and ANR, France; DFG and AvH Foundation, Germany; Herakleitos, Thales and Aristeia programmes co-financed by EU-ESF and the Greek NSRF, Greece; BSF-NSF and MINERVA, Israel; NCN and NAWA, Poland; La Caixa Banking Foundation, CERCA Programme Generalitat de Catalunya and PROMETEO and GenT Programmes Generalitat Valenciana, Spain; Göran Gustafssons Stiftelse, Sweden; The Royal Society and Leverhulme Trust, United Kingdom.

In addition, individual members wish to acknowledge support from CERN: European Organization for Nuclear Research (CERN DOCT); Chile: Agencia Nacional de Investigación y Desarrollo (FONDECYT 1230812, FONDECYT 1240864, Fondecyt 3240661, Fondecyt Regular 1240721); China: Chinese Ministry of Science and Technology (MOST-2023YFA1605700, MOST-2023YFA1609300), National Natural Science Foundation of China (NSFC - 12175119, NSFC 12275265); Czech Republic: Czech Science Foundation (GACR - 24-11373S), Ministry of Education Youth and Sports (ERC-CZ-LL2327, FORTE CZ.02.01.01/00/22_008/0004632), PRIMUS Research Programme (PRIMUS/21/SCI/017); EU: H2020 European Research Council (ERC - 101002463); European Union: European Research Council (BARD No. 101116429, ERC - 948254, ERC 101089007), European Regional Development Fund (SMASH COFUND 101081355, SLO ERDF), European Union, Future Artificial Intelligence Research (FAIR-NextGenerationEU PE00000013), Italian Center for High Performance Computing, Big Data and Quantum Computing (ICSC, NextGenerationEU); France: Agence Nationale de la Recherche (ANR-21-CE31-0022, ANR-22-EDIR-0002, ANR-24-CE31-0504-01); Germany: Deutsche Forschungsgemeinschaft (DFG - 469666862, DFG - CR 312/5-2); China: Research Grants Council (GRF); Italy: Istituto Nazionale di Fisica Nucleare (ICSC, NextGenerationEU), Ministero dell'Università e della Ricerca (NextGenEU 153D23001490006 M4C2.1.1, NextGenEU I53D23000820006 M4C2.1.1, NextGenEU I53D23001490006 M4C2.1.1, SOE2024_0000023); Japan: Japan Society for the Promotion of Science (JSPS KAKENHI JP22H01227, JSPS KAKENHI JP22H04944, JSPS KAKENHI JP22KK0227, JSPS KAKENHI JP24K23939, JSPS KAKENHI JP24KK0251, JSPS KAKENHI JP25H00650, JSPS KAKENHI JP25H01291, JSPS KAKENHI JP25K01023); Norway: Research Council of Norway (RCN-314472); Poland: Ministry of Science and Higher Education (IDUB AGH, POB8, D4 no 9722), Polish National Science Centre (NCN 2021/42/E/ST2/00350, NCN OPUS 2023/51/B/ST2/02507, NCN UMO-2019/34/E/ST2/00393, UMO-2022/47/O/ST2/00148, UMO-2023/49/B/ST2/04085, UMO-2023/51/B/ST2/00920, UMO-2024/53/N/ST2/00869); Portugal: Foundation for Science and Technology (FCT); Spain: Ministry of Science and Innovation (MCIN & NextGenEU PCI2022-135018-2, MICIN & FEDER PID2021-125273NB, RYC2019-028510-I, RYC2020-030254-I, RYC2021-031273-I, RYC2022-038164-I); Sweden: Carl Trygger Foundation (Carl Trygger Foundation CTS 22:2312), Swedish Research Council (Swedish Research Council 2023-04654, VR 2021-03651, VR 2022-03845, VR 2022-04683, VR 2023-03403, VR 2024-05451), Knut and Alice Wallenberg Foundation (KAW 2018.0458, KAW 2022.0358, KAW 2023.0366); Switzerland: Swiss National Science Foundation (SNSF - PCEFP2_194658); United Kingdom: Royal Society (NIF-R1-231091); United States of America: U.S. Department of Energy (ECA DE-AC02-76SF00515), Neubauer Family Foundation.

References

[1] ATLAS and CMS Collaborations, *Combination of Measurements of the Top Quark Mass from Data Collected by the ATLAS and CMS Experiments at $\sqrt{s} = 7$ and 8 TeV*, Phys. Rev. Lett. **132** (2024) 261902, arXiv: 2402.08713 [hep-ex].

[2] Particle Data Group Collaboration, *Review of Particle Physics*, Phys. Rev. D **110** (2024) 030001.

[3] I. Brivio and M. Trott, *The standard model as an effective field theory*, Phys. Rept. **793** (2019) 1, arXiv: 1706.08945 [hep-ph].

[4] K. G. Wilson and W. Zimmermann, *Operator product expansions and composite field operators in the general framework of quantum field theory*, Comm. Math. Phys. **24** (1972) 87.

[5] S. Willenbrock and C. Zhang, *Effective Field Theory Beyond the Standard Model*, Ann. Rev. Nucl. Part. Sci. **64** (2014) 83, arXiv: 1401.0470 [hep-ph].

[6] W. Buchmüller and D. Wyler, *Effective lagrangian analysis of new interactions and flavour conservation*, Nucl. Phys. B **268** (1986) 621.

[7] B. Grzadkowski, M. Iskrzyński, M. Misiak and J. Rosiek, *Dimension-Six Terms in the Standard Model Lagrangian*, JHEP **10** (2010) 085, arXiv: 1008.4884 [hep-ph].

[8] L. Evans and P. Bryant, *LHC Machine*, JINST **3** (2008) S08001.

[9] CMS Collaboration, *Measurement of the single top quark and antiquark production cross sections in the t channel and their ratio in proton–proton collisions at $\sqrt{s} = 13$ TeV*, Phys. Lett. B **800** (2020) 135042, arXiv: 1812.10514 [hep-ex].

[10] ATLAS Collaboration, *Measurement of t-channel production of single top quarks and antiquarks in pp collisions at 13 TeV using the full ATLAS Run 2 data sample*, JHEP **05** (2024) 305, arXiv: 2403.02126 [hep-ex].

[11] J. M. Campbell, R. Frederix, F. Maltoni and F. Tramontano, *Next-to-Leading-Order Predictions for t-Channel Single-Top Production at Hadron Colliders*, Phys. Rev. Lett. **102** (2009) 182003, arXiv: 0903.0005 [hep-ph].

[12] F. Maltoni, G. Ridolfi and M. Ubiali, *b-initiated processes at the LHC: a reappraisal*, JHEP **07** (2012) 022, arXiv: 1203.6393 [hep-ph].

[13] E. Bothmann, F. Krauss and M. Schönherr, *Single top-quark production with SHERPA*, Eur. Phys. J. C **78** (2018) 220, arXiv: 1711.02568 [hep-ph].

[14] J. A. Aguilar-Saavedra, J. Boudreau, C. Escobar and J. Mueller, *The fully differential top decay distribution*, Eur. Phys. J. C **77** (2017) 200, arXiv: 1702.03297 [hep-ph].

[15] J. A. Aguilar-Saavedra and S. Amor Dos Santos, *New directions for top quark polarization in the t-channel process*, Phys. Rev. D **89** (2014) 114009, arXiv: 1404.1585 [hep-ph].

[16] ATLAS Collaboration, *Measurement of the polarisation of single top quarks and antiquarks produced in the t-channel at $\sqrt{s} = 13$ TeV and bounds on the tWb dipole operator from the ATLAS experiment*, JHEP **11** (2022) 040, arXiv: 2202.11382 [hep-ex].

[17] ATLAS Collaboration, *Inclusive and differential cross-section measurements of $t\bar{t}Z$ production in pp collisions at $\sqrt{s} = 13$ TeV with the ATLAS detector, including EFT and spin-correlation interpretations*, JHEP **07** (2024) 163, arXiv: 2312.04450 [hep-ex].

[18] ATLAS Collaboration, *Measurements of inclusive and differential cross-sections of $t\bar{t}\gamma$ production in pp collisions at $\sqrt{s} = 13$ TeV with the ATLAS detector*, JHEP **10** (2024) 191, arXiv: 2403.09452 [hep-ex].

[19] CMS Collaboration, *Search for new physics in top quark production in dilepton final states in proton–proton collisions at $\sqrt{s} = 13$ TeV*, Eur. Phys. J. C **79** (2019) 886, arXiv: 1903.11144 [hep-ex].

[20] CMS Collaboration, *Search for new physics in top quark production with additional leptons in proton–proton collisions at $\sqrt{s} = 13$ TeV using effective field theory*, JHEP **03** (2021) 095, arXiv: 2012.04120 [hep-ex].

[21] CMS Collaboration, *Probing effective field theory operators in the associated production of top quarks with a Z boson in multilepton final states at $\sqrt{s} = 13$ TeV*, JHEP **12** (2021) 083, arXiv: 2107.13896 [hep-ex].

[22] CMS Collaboration, *Search for physics beyond the standard model in top quark production with additional leptons in the context of effective field theory*, JHEP **12** (2023) 068, arXiv: 2307.15761 [hep-ex].

[23] CMS Collaboration, *Search for new physics using effective field theory in 13 TeV pp collision events that contain a top quark pair and a boosted Z or Higgs boson*, Phys. Rev. D **108** (2023) 032008, arXiv: 2208.12837 [hep-ex].

[24] ATLAS Collaboration, *Search for anomalous couplings in the Wtb vertex from the measurement of double differential angular decay rates of single top quarks produced in the t-channel with the ATLAS detector*, JHEP **04** (2016) 023, arXiv: 1510.03764 [hep-ex].

[25] ATLAS Collaboration, *Probing the Wtb vertex structure in t-channel single-top-quark production and decay in pp collisions at $\sqrt{s} = 8$ TeV with the ATLAS detector*, JHEP **04** (2017) 124, arXiv: 1702.08309 [hep-ex].

[26] ATLAS Collaboration, *Measurements of top-quark pair differential cross-sections in the lepton+jets channel in pp collisions at $\sqrt{s} = 8$ TeV using the ATLAS detector*, Eur. Phys. J. C **76** (2016) 538, arXiv: 1511.04716 [hep-ex].

[27] ATLAS and CMS Collaborations, *Combination of the W boson polarization measurements in top quark decays using ATLAS and CMS data at $\sqrt{s} = 8$ TeV*, JHEP **08** (2020) 051, arXiv: 2005.03799 [hep-ex].

[28] B. Grzadkowski and M. Misiak, *Anomalous Wtb coupling effects in the weak radiative B-meson decay*, Phys. Rev. D **78** (2008) 077501, arXiv: 0802.1413 [hep-ph], Erratum: Phys. Rev. D **84** (2011) 059903.

[29] J. A. Aguilar-Saavedra and J. Bernabéu, *W polarisation beyond helicity fractions in top quark decays*, Nucl. Phys. B **840** (2010) 349, arXiv: 1005.5382 [hep-ph].

[30] ATLAS Collaboration, *Differential $t\bar{t}$ cross-section measurements using boosted top quarks in the all-hadronic final state with 139 fb^{-1} of ATLAS data*, JHEP **04** (2023) 080, arXiv: 2205.02817 [hep-ex].

[31] ATLAS Collaboration, *Evidence for the charge asymmetry in $pp \to t\bar{t}$ production at $\sqrt{s} = 13$ TeV with the ATLAS detector*, JHEP **08** (2023) 077, arXiv: 2208.12095 [hep-ex].

[32] ATLAS Collaboration, *The ATLAS Experiment at the CERN Large Hadron Collider*, JINST **3** (2008) S08003.

[33] G. Avoni et al., *The new LUCID-2 detector for luminosity measurement and monitoring in ATLAS*, JINST **13** (2018) P07017.

[34] ATLAS Collaboration, *Performance of the ATLAS trigger system in 2015*, Eur. Phys. J. C **77** (2017) 317, arXiv: 1611.09661 [hep-ex].

[35] ATLAS Collaboration, *Software and computing for Run 3 of the ATLAS experiment at the LHC*, Eur. Phys. J. C **85** (2025) 234, arXiv: 2404.06335 [hep-ex].

[36] ATLAS Collaboration, *ATLAS data quality operations and performance for 2015–2018 data-taking*, JINST **15** (2020) P04003, arXiv: 1911.04632 [physics.ins-det].

[37] ATLAS Collaboration, *Performance of electron and photon triggers in ATLAS during LHC Run 2*, Eur. Phys. J. C **80** (2020) 47, arXiv: 1909.00761 [hep-ex].

[38] ATLAS Collaboration, *Performance of the ATLAS muon triggers in Run 2*, JINST **15** (2020) P09015, arXiv: 2004.13447 [physics.ins-det].

[39] T. Sjöstrand, S. Mrenna and P. Skands, *A brief introduction to PYTHIA 8.1*, Comput. Phys. Commun. **178** (2008) 852, arXiv: 0710.3820 [hep-ph].

[40] NNPDF Collaboration, R. D. Ball et al., *Parton distributions with LHC data*, Nucl. Phys. B **867** (2013) 244, arXiv: 1207.1303 [hep-ph].

[41] ATLAS Collaboration, *The Pythia 8 A3 tune description of ATLAS minimum bias and inelastic measurements incorporating the Donnachie–Landshoff diffractive model*, ATL-PHYS-PUB-2016-017, 2016, URL: https://cds.cern.ch/record/2206965.

[42] J. Pumplin et al., *New Generation of Parton Distributions with Uncertainties from Global QCD Analysis*, JHEP **07** (2002) 012, arXiv: hep-ph/0201195.

[43] ATLAS Collaboration, *Measurement of the Z/γ^* boson transverse momentum distribution in pp collisions at $\sqrt{s} = 7$ TeV with the ATLAS detector*, JHEP **09** (2014) 145, arXiv: 1406.3660 [hep-ex].

[44] R. Frederix, E. Re and P. Torrielli, *Single-top t-channel hadroproduction in the four-flavour scheme with POWHEG and aMC@NLO*, JHEP **09** (2012) 130, arXiv: 1207.5391 [hep-ph].

[45] P. Nason, *A new method for combining NLO QCD with shower Monte Carlo algorithms*, JHEP **11** (2004) 040, arXiv: hep-ph/0409146.

[46] S. Frixione, P. Nason and C. Oleari, *Matching NLO QCD computations with parton shower simulations: the POWHEG method*, JHEP **11** (2007) 070, arXiv: 0709.2092 [hep-ph].

[47] S. Alioli, P. Nason, C. Oleari and E. Re, *A general framework for implementing NLO calculations in shower Monte Carlo programs: the POWHEG BOX*, JHEP **06** (2010) 043, arXiv: 1002.2581 [hep-ph].

[48] NNPDF Collaboration, R. D. Ball et al., *Parton distributions for the LHC run II*, JHEP **04** (2015) 040, arXiv: 1410.8849 [hep-ph].

[49] S. Alioli, P. Nason, C. Oleari and E. Re, *NLO single-top production matched with shower in POWHEG: s- and t-channel contributions*, JHEP **09** (2009) 111, arXiv: 0907.4076 [hep-ph], Erratum: JHEP **02** (2010) 011.

[50] S. Frixione, E. Laenen, P. Motylinski and B. R. Webber, *Angular correlations of lepton pairs from vector boson and top quark decays in Monte Carlo simulations*, JHEP **04** (2007) 081, arXiv: hep-ph/0702198.

[51] P. Artoisenet, R. Frederix, O. Mattelaer and R. Rietkerk, *Automatic spin-entangled decays of heavy resonances in Monte Carlo simulations*, JHEP **03** (2013) 015, arXiv: 1212.3460 [hep-ph].

[52] T. Sjöstrand et al., *An introduction to PYTHIA 8.2*, Comput. Phys. Commun. **191** (2015) 159, arXiv: 1410.3012 [hep-ph].

[53] ATLAS Collaboration, *ATLAS Pythia 8 tunes to 7 TeV data*, ATL-PHYS-PUB-2014-021, 2014, URL: https://cds.cern.ch/record/1966419.

[54] J. Campbell, T. Neumann and Z. Sullivan, *Single-top-quark production in the t-channel at NNLO*, JHEP **02** (2021) 040, arXiv: 2012.01574 [hep-ph].

[55] R. D. Ball et al., *The PDF4LHC21 combination of global PDF fits for the LHC Run III*, J. Phys. G **49** (2022) 080501, arXiv: 2203.05506 [hep-ph].

[56] S. Frixione, G. Ridolfi and P. Nason, *A positive-weight next-to-leading-order Monte Carlo for heavy flavour hadroproduction*, JHEP **09** (2007) 126, arXiv: 0707.3088 [hep-ph].

[57] ATLAS Collaboration, *Studies on top-quark Monte Carlo modelling for Top2016*, ATL-PHYS-PUB-2016-020, 2016, URL: https://cds.cern.ch/record/2216168.

[58] M. Beneke, P. Falgari, S. Klein and C. Schwinn, *Hadronic top-quark pair production with NNLL threshold resummation*, Nucl. Phys. B **855** (2012) 695, arXiv: 1109.1536 [hep-ph].

[59] M. Cacciari, M. Czakon, M. Mangano, A. Mitov and P. Nason, *Top-pair production at hadron colliders with next-to-next-to-leading logarithmic soft-gluon resummation*, Phys. Lett. B **710** (2012) 612, arXiv: 1111.5869 [hep-ph].

[60] P. Bärnreuther, M. Czakon and A. Mitov, *Percent-Level-Precision Physics at the Tevatron: Next-to-Next-to-Leading Order QCD Corrections to $q\bar{q} \to t\bar{t} + X$*, Phys. Rev. Lett. **109** (2012) 132001, arXiv: 1204.5201 [hep-ph].

[61] M. Czakon and A. Mitov, *NNLO corrections to top-pair production at hadron colliders: the all-fermionic scattering channels*, JHEP **12** (2012) 054, arXiv: 1207.0236 [hep-ph].

[62] M. Czakon and A. Mitov, *NNLO corrections to top pair production at hadron colliders: the quark-gluon reaction*, JHEP **01** (2013) 080, arXiv: 1210.6832 [hep-ph].

[63] M. Czakon, P. Fiedler and A. Mitov, *Total Top-Quark Pair-Production Cross Section at Hadron Colliders Through $O(\alpha_S^4)$*, Phys. Rev. Lett. **110** (2013) 252004, arXiv: 1303.6254 [hep-ph].

[64] M. Czakon and A. Mitov, *Top++: A program for the calculation of the top-pair cross-section at hadron colliders*, Comput. Phys. Commun. **185** (2014) 2930, arXiv: 1112.5675 [hep-ph].

[65] J. Alwall et al., *The automated computation of tree-level and next-to-leading order differential cross sections, and their matching to parton shower simulations*, JHEP **07** (2014) 079, arXiv: 1405.0301 [hep-ph].

[66] J. A. Aguilar Saavedra et al., *Interpreting top-quark LHC measurements in the standard-model effective field theory*, (2018), arXiv: 1802.07237 [hep-ph].

[67] ATLAS Collaboration, *Analysis of the Wtb vertex from the measurement of triple-differential angular decay rates of single top quarks produced in the t-channel at $\sqrt{s} = 8$ TeV with the ATLAS detector*, JHEP **12** (2017) 017, arXiv: 1707.05393 [hep-ex].

[68] M. de Beurs, E. Laenen, M. Vreeswijk and E. Vryonidou, *Effective operators in t-channel single top production and decay*, Eur. Phys. J. C **78** (2018) 919, arXiv: 1807.03576 [hep-ph].

[69] E. Bothmann et al., *Event generation with Sherpa 2.2*, SciPost Phys. **7** (2019) 034, arXiv: 1905.09127 [hep-ph].

[70] F. Buccioni et al., *OpenLoops 2*, Eur. Phys. J. C **79** (2019) 866, arXiv: 1907.13071 [hep-ph].

[71] F. Cascioli, P. Maierhöfer and S. Pozzorini, *Scattering Amplitudes with Open Loops*, Phys. Rev. Lett. **108** (2012) 111601, arXiv: 1111.5206 [hep-ph].

[72] A. Denner, S. Dittmaier and L. Hofer, *Collier: A fortran-based complex one-loop library in extended regularizations*, Comput. Phys. Commun. **212** (2017) 220, arXiv: 1604.06792 [hep-ph].

[73] S. Schumann and F. Krauss, *A parton shower algorithm based on Catani–Seymour dipole factorisation*, JHEP **03** (2008) 038, arXiv: 0709.1027 [hep-ph].

[74] J.-C. Winter, F. Krauss and G. Soff, *A modified cluster-hadronisation model*, Eur. Phys. J. C **36** (2004) 381, arXiv: hep-ph/0311085.

[75] T. Gleisberg and S. Höche, *Comix, a new matrix element generator*, JHEP **12** (2008) 039, arXiv: 0808.3674 [hep-ph].

[76] C. Anastasiou, L. Dixon, K. Melnikov and F. Petriello, *High-precision QCD at hadron colliders: Electroweak gauge boson rapidity distributions at next-to-next-to leading order*, Phys. Rev. D **69** (2004) 094008, arXiv: hep-ph/0312266.

[77] E. Re, *Single-top Wt-channel production matched with parton showers using the POWHEG method*, Eur. Phys. J. C **71** (2011) 1547, arXiv: 1009.2450 [hep-ph].

[78] S. Höche, F. Krauss, M. Schönherr and F. Siegert, *A critical appraisal of NLO+PS matching methods*, JHEP **09** (2012) 049, arXiv: 1111.1220 [hep-ph].

[79] S. Höche, F. Krauss, M. Schönherr and F. Siegert, *QCD matrix elements + parton showers. The NLO case*, JHEP **04** (2013) 027, arXiv: 1207.5030 [hep-ph].

[80] S. Catani, F. Krauss, B. R. Webber and R. Kuhn, *QCD Matrix Elements + Parton Showers*, JHEP **11** (2001) 063, arXiv: hep-ph/0109231.

[81] S. Höche, F. Krauss, S. Schumann and F. Siegert, *QCD matrix elements and truncated showers*, JHEP **05** (2009) 053, arXiv: 0903.1219 [hep-ph].

[82] D. J. Lange, *The EvtGen particle decay simulation package*, Nucl. Instrum. Meth. A **462** (2001) 152.

[83] ATLAS Collaboration, *Vertex Reconstruction Performance of the ATLAS Detector at $\sqrt{s}$ = 13 TeV*, ATL-PHYS-PUB-2015-026, 2015, URL: https://cds.cern.ch/record/2037717.

[84] ATLAS Collaboration, *Electron and photon performance measurements with the ATLAS detector using the 2015–2017 LHC proton–proton collision data*, JINST **14** (2019) P12006, arXiv: 1908.00005 [hep-ex].

[85] ATLAS Collaboration, *Muon reconstruction and identification efficiency in ATLAS using the full Run 2 pp collision data set at $\sqrt{s}$ = 13 TeV*, Eur. Phys. J. C **81** (2021) 578, arXiv: 2012.00578 [hep-ex].

[86] ATLAS Collaboration, *Studies of the muon momentum calibration and performance of the ATLAS detector with pp collisions at $\sqrt{s}$ = 13 TeV*, Eur. Phys. J. C **83** (2023) 686, arXiv: 2212.07338 [hep-ex].

[87] ATLAS Collaboration, *Tools for estimating fake/non-prompt lepton backgrounds with the ATLAS detector at the LHC*, JINST **18** (2023) T11004, arXiv: 2211.16178 [hep-ex].

[88] ATLAS Collaboration, *Jet reconstruction and performance using particle flow with the ATLAS Detector*, Eur. Phys. J. C **77** (2017) 466, arXiv: 1703.10485 [hep-ex].

[89] M. Cacciari, G. P. Salam and G. Soyez, *The anti-k_t jet clustering algorithm*, JHEP **04** (2008) 063, arXiv: 0802.1189 [hep-ph].

[90] M. Cacciari, G. P. Salam and G. Soyez, *FastJet user manual*, Eur. Phys. J. C **72** (2012) 1896, arXiv: 1111.6097 [hep-ph].

[91] ATLAS Collaboration, *Jet energy scale and resolution measured in proton–proton collisions at $\sqrt{s} = 13$ TeV with the ATLAS detector*, Eur. Phys. J. C **81** (2021) 689, arXiv: 2007.02645 [hep-ex].

[92] ATLAS Collaboration, *Performance of pile-up mitigation techniques for jets in pp collisions at $\sqrt{s} = 8$ TeV using the ATLAS detector*, Eur. Phys. J. C **76** (2016) 581, arXiv: 1510.03823 [hep-ex].

[93] ATLAS Collaboration, *Identification and rejection of pile-up jets at high pseudorapidity with the ATLAS detector*, Eur. Phys. J. C **77** (2017) 580, arXiv: 1705.02211 [hep-ex], Erratum: Eur. Phys. J. C **77** (2017) 712.

[94] ATLAS Collaboration, *Selection of jets produced in 13 TeV proton–proton collisions with the ATLAS detector*, ATLAS-CONF-2015-029, 2015, URL: https://cds.cern.ch/record/2037702.

[95] ATLAS Collaboration, *ATLAS flavour-tagging algorithms for the LHC Run 2 pp collision dataset*, Eur. Phys. J. C **83** (2023) 681, arXiv: 2211.16345 [physics.data-an].

[96] ATLAS Collaboration, *ATLAS b-jet identification performance and efficiency measurement with $t\bar{t}$ events in pp collisions at $\sqrt{s} = 13$ TeV*, Eur. Phys. J. C **79** (2019) 970, arXiv: 1907.05120 [hep-ex].

[97] ATLAS Collaboration, *Measurement of the c-jet mistagging efficiency in $t\bar{t}$ events using pp collision data at $\sqrt{s} = 13$ TeV collected with the ATLAS detector*, Eur. Phys. J. C **82** (2022) 95, arXiv: 2109.10627 [hep-ex].

[98] ATLAS Collaboration, *Calibration of the light-flavour jet mistagging efficiency of the b-tagging algorithms with Z+jets events using 139 fb^{-1} of ATLAS proton–proton collision data at $\sqrt{s} = 13$ TeV*, Eur. Phys. J. C **83** (2023) 728, arXiv: 2301.06319 [hep-ex].

[99] ATLAS Collaboration, *Measurement of the tau lepton reconstruction and identification performance in the ATLAS experiment using pp collisions at $\sqrt{s} = 13$ TeV*, ATLAS-CONF-2017-029, 2017, URL: https://cds.cern.ch/record/2261772.

[100] ATLAS Collaboration, *Identification of hadronic tau lepton decays using neural networks in the ATLAS experiment*, ATL-PHYS-PUB-2019-033, 2019, URL: https://cds.cern.ch/record/2688062.

[101] ATLAS Collaboration, *Reconstruction, Identification, and Calibration of hadronically decaying tau leptons with the ATLAS detector for the LHC Run 3 and reprocessed Run 2 data*, ATL-PHYS-PUB-2022-044, 2022, URL: https://cds.cern.ch/record/2827111.

[102] ATLAS Collaboration, *The performance of missing transverse momentum reconstruction and its significance with the ATLAS detector using 140 fb^{-1} of $\sqrt{s} = 13$ TeV pp collisions*, Eur. Phys. J. C **85** (2025) 606, arXiv: 2402.05858 [hep-ex].

[103] J. Erdmann et al., *A likelihood-based reconstruction algorithm for top-quark pairs and the KLFitter framework*, Nucl. Instrum. Meth. A **748** (2014) 18, arXiv: 1312.5595 [hep-ex].

[104] ATLAS Collaboration, *Luminosity determination in pp collisions at $\sqrt{s} = 13$ TeV using the ATLAS detector at the LHC*, Eur. Phys. J. C **83** (2023) 982, arXiv: 2212.09379 [hep-ex].

[105] ATLAS Collaboration, *Measurement of the Inelastic Proton–Proton Cross Section at $\sqrt{s} = 13$ TeV with the ATLAS Detector at the LHC*, Phys. Rev. Lett. **117** (2016) 182002, arXiv: 1606.02625 [hep-ex].

[106] ATLAS Collaboration, *Performance of missing transverse momentum reconstruction with the ATLAS detector using proton–proton collisions at $\sqrt{s} = 13$ TeV*, Eur. Phys. J. C **78** (2018) 903, arXiv: 1802.08168 [hep-ex].

[107] S. Höche, S. Mrenna, S. Payne, C. T. Preuss and P. Skands, *A Study of QCD Radiation in VBF Higgs Production with Vincia and Pythia*, SciPost Phys. **12** (2022) 010, arXiv: 2106.10987 [hep-ph].

[108] ATLAS Collaboration, *Studies on top-quark Monte Carlo modelling with Sherpa and MG5_aMC@NLO*, ATL-PHYS-PUB-2017-007, 2017, URL: https://cds.cern.ch/record/2261938.

[109] J. Butterworth et al., *PDF4LHC recommendations for LHC Run II*, J. Phys. G **43** (2016) 023001, arXiv: 1510.03865 [hep-ph].

[110] M. Czakon et al., *Top-pair production at the LHC through NNLO QCD and NLO EW*, JHEP **10** (2017) 186, arXiv: 1705.04105 [hep-ph].

[111] E. P. Wigner, *Group Theory and its Application to the Quantum Mechanics of Atomic Spectra*, Proc. Edinb. Math. Soc. **12** (1960) 67.

[112] J. A. Aguilar-Saavedra, N. F. Castro and A. Onofre, *Constraints on the Wtb vertex from early LHC data*, Phys. Rev. D **83** (2011) 117301, arXiv: 1105.0117 [hep-ph].

[113] M. Jacob and G. C. Wick, *On the General Theory of Collisions for Particles with Spin*, Annals Phys. **7** (1959) 404.

[114] I. Brivio et al., *O new physics, where art thou? A global search in the top sector*, JHEP **02** (2020) 131, arXiv: 1910.03606 [hep-ph].

[115] ATLAS Collaboration, *ATLAS Computing Acknowledgements*, ATL-SOFT-PUB-2025-001, 2025, URL: https://cds.cern.ch/record/2922210.

The ATLAS Collaboration

G. Aad[103], E. Aakvaag[17], B. Abbott[122], S. Abdelhameed[118a], K. Abeling[55], N.J. Abicht[49], S.H. Abidi[30], M. Aboelela[45], A. Aboulhorma[36e], H. Abramowicz[156], Y. Abulaiti[119], B.S. Acharya[69a,69b,m], A. Ackermann[63a], C. Adam Bourdarios[4], L. Adamczyk[86a], S.V. Addepalli[148], M.J. Addison[102], J. Adelman[117], A. Adiguzel[22c], T. Adye[136], A.A. Affolder[138], Y. Afik[40], M.N. Agaras[13], A. Aggarwal[101], C. Agheorghiesei[28c], F. Ahmadov[39,ad], S. Ahuja[96], S. Ahuja[168], X. Ai[142b], G. Aielli[76a,76b], A. Aikot[168], M. Ait Tamlihat[36e], B. Aitbenchikh[36a], T.P.A. Åkesson[99], A.V. Akimov[150], D. Akiyama[173], N.N. Akolkar[25], S. Aktas[171], G.L. Alberghi[24b], J. Albert[170], U. Alberti[20], P. Albicocco[53], G.L. Albouy[60], S. Alderweireldt[52], Z.L. Alegria[123], M. Aleksa[37], I.N. Aleksandrov[39], C. Alexa[28b], T. Alexopoulos[10], F. Alfonsi[24b], M. Algren[56], M. Alhroob[172], B. Ali[134], H.M.J. Ali[92,w], S. Ali[32], S.W. Alibocus[93], M. Aliev[34c], G. Alimonti[71a], W. Alkakhi[55], C. Allaire[66], B.M.M. Allbrooke[151], D.R. Allen[123], J.S. Allen[102], J.F. Allen[52], P.P. Allport[21], A. Aloisio[72a,72b], F. Alonso[91], C. Alpigiani[141], Z.M.K. Alsolami[92], A. Alvarez Fernandez[101], M. Alves Cardoso[56], M.G. Alviggi[72a,72b], M. Aly[102], Y. Amaral Coutinho[82b], A. Ambler[105], C. Amelung[37], M. Amerl[102], C.G. Ames[110], T. Amezza[129], D. Amidei[107], B. Amini[54], K. Amirie[160], A. Amirkhanov[39], S.P. Amor Dos Santos[132a], K.R. Amos[168], D. Amperiadou[157], S. An[83], C. Anastopoulos[144], T. Andeen[11], J.K. Anders[93], A.C. Anderson[59], A. Andreazza[71a,71b], S. Angelidakis[9], A. Angerami[42], A.V. Anisenkov[39], A. Annovi[74a], C. Antel[37], E. Antipov[150], M. Antonelli[53], F. Anulli[75a], M. Aoki[83], T. Aoki[158], M.A. Aparo[151], L. Aperio Bella[48], M. Apicella[31], C. Appelt[156], A. Apyan[27], M. Arampatzi[10], S.J. Arbiol Val[87], C. Arcangeletti[53], A.T.H. Arce[51], J-F. Arguin[109], S. Argyropoulos[157], J.-H. Arling[48], O. Arnaez[4], H. Arnold[150], G. Artoni[75a,75b], H. Asada[112], K. Asai[120], S. Asatryan[178], N.A. Asbah[37], R.A. Ashby Pickering[172], A.M. Aslam[96], K. Assamagan[30], R. Astalos[29a], K.S.V. Astrand[99], S. Atashi[164], R.J. Atkin[34a], H. Atmani[36f], P.A. Atmasiddha[130], K. Augsten[134], A.D. Auriol[41], V.A. Austrup[102], A.S. Avad[95], G. Avolio[37], K. Axiotis[56], A. Azzam[13], D. Babal[29b], H. Bachacou[137], K. Bachas[157,q], A. Bachiu[35], E. Bachmann[50], M.J. Backes[63a], A. Badea[40], T.M. Baer[107], P. Bagnaia[75a,75b], M. Bahmani[19], D. Bahner[54], K. Bai[125], J.T. Baines[136], L. Baines[95], O.K. Baker[177], E. Bakos[16], D. Bakshi Gupta[8], L.E. Balabram Filho[82b], V. Balakrishnan[122], R. Balasubramanian[4], E.M. Baldin[38], P. Balek[86a], E. Ballabene[24b,24a], F. Balli[137], L.M. Baltes[63a], W.K. Balunas[33], J. Balz[101], I. Bamwidhi[118b], E. Banas[87], M. Bandieramonte[131], A. Bandyopadhyay[25], S. Bansal[25], L. Barak[156], M. Barakat[48], E.L. Barberio[106], D. Barberis[18b], M. Barbero[103], M.Z. Barel[116], T. Barillari[111], M-S. Barisits[37], T. Barklow[148], P. Baron[135], D.A. Baron Moreno[102], A. Baroncelli[62], A.J. Barr[128], J.D. Barr[97], F. Barreiro[100], J. Barreiro Guimarães da Costa[14], M.G. Barros Teixeira[132a], S. Barsov[38], F. Bartels[63a], R. Bartoldus[148], A.E. Barton[92], P. Bartos[29a], M. Baselga[49], S. Bashiri[87], A. Bassalat[66,b], M.J. Basso[161a], S. Bataju[45], R. Bate[169], R.L. Bates[59], S. Batlamous[100], M. Battaglia[138], D. Battulga[19], M. Bauce[75a,75b], M. Bauer[79], P. Bauer[25], L.T. Bayer[48], L.T. Bazzano Hurrell[31], J.B. Beacham[111], T. Beau[129], J.Y. Beaucamp[91], P.H. Beauchemin[163], P. Bechtle[25], H.P. Beck[20,p], K. Becker[172], A.J. Beddall[81], V.A. Bednyakov[39], C.P. Bee[150], L.J. Beemster[16], M. Begalli[82d], M. Begel[30], J.K. Behr[48], J.F. Beirer[37], F. Beisiegel[25], M. Belfkir[118b], G. Bella[156], L. Bellagamba[24b], A. Bellerive[35], C.D. Bellgraph[68], P. Bellos[21], K. Beloborodov[38], I. Benaoumeur[21], D. Benchekroun[36a], F. Bendebba[36a], Y. Benhammou[156], K.C. Benkendorfer[61], L. Beresford[48],

M. Beretta [53], E. Bergeaas Kuutmann [166], N. Berger [4], B. Bergmann [134], J. Beringer [18a], G. Bernardi [5], C. Bernius [148], F.U. Bernlochner [25], A. Berrocal Guardia [13], T. Berry [96], P. Berta [135], A. Berti [132a], R. Bertrand [103], S. Bethke [111], A. Betti [75a,75b], A.J. Bevan [95], L. Bezio [56], N.K. Bhalla [54], S. Bharthuar [111], S. Bhatta [150], P. Bhattarai [148], Z.M. Bhatti [119], K.D. Bhide [54], V.S. Bhopatkar [123], R.M. Bianchi [131], G. Bianco [24b,24a], O. Biebel [110], M. Biglietti [77a], C.S. Billingsley [45], Y. Bimgdi [36f], M. Bindi [55], A. Bingham [176], A. Bingul [22b], C. Bini [75a,75b], G.A. Bird [33], M. Birman [174], M. Biros [135], S. Biryukov [151], T. Bisanz [49], E. Bisceglie [24b,24a], J.P. Biswal [136], D. Biswas [146], I. Bloch [48], A. Blue [59], U. Blumenschein [95], V.S. Bobrovnikov [39], L. Boccardo [57b,57a], M. Boehler [54], B. Boehm [171], D. Bogavac [13], A.G. Bogdanchikov [38], L.S. Boggia [129], V. Boisvert [96], P. Bokan [37], T. Bold [86a], M. Bomben [5], M. Bona [95], M. Boonekamp [137], A.G. Borbély [59], I.S. Bordulev [38], G. Borissov [92], D. Bortoletto [128], D. Boscherini [24b], M. Bosman [13], K. Bouaouda [36a], N. Bouchhar [168], L. Boudet [4], J. Boudreau [131], E.V. Bouhova-Thacker [92], D. Boumediene [41], R. Bouquet [57b,57a], A. Boveia [121], J. Boyd [37], D. Boye [30], I.R. Boyko [39], L. Bozianu [56], J. Bracinik [21], N. Brahimi [4], G. Brandt [176], O. Brandt [33], B. Brau [104], J.E. Brau [125], R. Brener [174], L. Brenner [116], R. Brenner [166], S. Bressler [174], G. Brianti [78a,78b], D. Britton [59], D. Britzger [111], I. Brock [25], R. Brock [108], G. Brooijmans [42], A.J. Brooks [68], E.M. Brooks [161b], E. Brost [30], L.M. Brown [170,161a], L.E. Bruce [61], T.L. Bruckler [128], P.A. Bruckman de Renstrom [87], B. Brüers [48], A. Bruni [24b], G. Bruni [24b], D. Brunner [47a,47b], M. Bruschi [24b], N. Bruscino [75a,75b], T. Buanes [17], Q. Buat [141], D. Buchin [111], A.G. Buckley [59], O. Bulekov [81], B.A. Bullard [148], S. Burdin [93], C.D. Burgard [49], A.M. Burger [90], B. Burghgrave [8], O. Burlayenko [54], J. Burleson [167], J.C. Burzynski [147], E.L. Busch [42], V. Büscher [101], P.J. Bussey [59], O. But [25], J.M. Butler [26], C.M. Buttar [59], J.M. Butterworth [97], P. Butti [37], W. Buttinger [136], C.J. Buxo Vazquez [108], A.R. Buzykaev [39], S. Cabrera Urbán [168], L. Cadamuro [66], H. Cai [37], Y. Cai [24b,113c,24a], Y. Cai [113a], V.M.M. Cairo [37], O. Cakir [3a], N. Calace [37], P. Calafiura [18a], G. Calderini [129], P. Calfayan [35], L. Calic [99], G. Callea [59], L.P. Caloba [82b], D. Calvet [41], S. Calvet [41], R. Camacho Toro [129], S. Camarda [37], D. Camarero Munoz [27], P. Camarri [76a,76b], C. Camincher [170], M. Campanelli [97], A. Camplani [43], V. Canale [72a,72b], A.C. Canbay [3a], E. Canonero [96], J. Cantero [168], Y. Cao [167], F. Capocasa [27], M. Capua [44b,44a], A. Carbone [71a,71b], R. Cardarelli [76a], J.C.J. Cardenas [8], M.P. Cardiff [27], G. Carducci [44b,44a], T. Carli [37], G. Carlino [72a], J.I. Carlotto [13], B.T. Carlson [131,r], E.M. Carlson [170], J. Carmignani [93], L. Carminati [71a,71b], A. Carnelli [4], M. Carnesale [37], S. Caron [115], E. Carquin [139g], I.B. Carr [106], S. Carrá [73a,73b], G. Carratta [24b,24a], C. Carrion Martinez [168], A.M. Carroll [125], M.P. Casado [13,h], P. Casolaro [72a,72b], M. Caspar [48], W.R. Castiglioni [40], F.L. Castillo [4], L. Castillo Garcia [13], V. Castillo Gimenez [168], N.F. Castro [132a,132e], A. Catinaccio [37], J.R. Catmore [127], T. Cavaliere [4], V. Cavaliere [30], L.J. Caviedes Betancourt [23b], E. Celebi [81], S. Cella [37], V. Cepaitis [56], K. Cerny [124], A.S. Cerqueira [82a], A. Cerri [74a,74b,am], L. Cerrito [76a,76b], F. Cerutti [18a], B. Cervato [71a,71b], A. Cervelli [24b], G. Cesarini [53], S.A. Cetin [81], P.M. Chabrillat [129], R. Chakkappai [66], S. Chakraborty [172], A. Chambers [61], J. Chan [18a], W.Y. Chan [158], J.D. Chapman [33], E. Chapon [137], B. Chargeishvili [154b], D.G. Charlton [21], C. Chauhan [135], Y. Che [113a], S. Chekanov [6], G.A. Chelkov [39,a], B. Chen [156], B. Chen [170], H. Chen [30], J. Chen [143a], J. Chen [147], M. Chen [128], S. Chen [88], S.J. Chen [113a], X. Chen [143a], X. Chen [15,ah], Z. Chen [62], C.L. Cheng [175], H.C. Cheng [64a], S. Cheong [148], A. Cheplakov [39], E. Cherepanova [116], R. Cherkaoui El Moursli [36e], E. Cheu [7], K. Cheung [65], L. Chevalier [137], V. Chiarella [53], G. Chiarelli [74a], G. Chiodini [70a], A.S. Chisholm [21], A. Chitan [28b], M. Chitishvili [168], M.V. Chizhov [39,s], K. Choi [11], Y. Chou [141], E.Y.S. Chow [115], K.L. Chu [174], M.C. Chu [64a], X. Chu [14,113c], Z. Chubinidze [53], J. Chudoba [133], J.J. Chwastowski [87],

D. Cieri[111], K.M. Ciesla[86a], V. Cindro[94], A. Ciocio[18a], F. Cirotto[72a,72b], Z.H. Citron[174], M. Citterio[71a], D.A. Ciubotaru[28b], A. Clark[56], P.J. Clark[52], N. Clarke Hall[97], C. Clarry[160], S.E. Clawson[48], C. Clement[47a,47b], L. Clissa[24b,24a], Y. Coadou[103], M. Cobal[69a,69c], A. Coccaro[57b], R.F. Coelho Barrue[132a], R. Coelho Lopes De Sa[104], S. Coelli[71a], M.M. Cohen[130], L.S. Colangeli[160], B. Cole[42], P. Collado Soto[100], J. Collot[60], R. Coluccia[70a,70b], P. Conde Muiño[132a,132g], M.P. Connell[34c], S.H. Connell[34c], E.I. Conroy[128], M. Contreras Cossio[11], F. Conventi[72a,aj], A.M. Cooper-Sarkar[128], L. Corazzina[75a,75b], F.A. Corchia[24b,24a], A. Cordeiro Oudot Choi[141], L.D. Corpe[41], M. Corradi[75a,75b], F. Corriveau[105,ab], A. Cortes-Gonzalez[158], M.J. Costa[168], F. Costanza[4], D. Costanzo[144], J. Couthures[4], G. Cowan[96], K. Cranmer[175], L. Cremer[49], D. Cremonini[24b,24a], S. Crépé-Renaudin[60], F. Crescioli[129], T. Cresta[73a,73b], M. Cristinziani[146], M. Cristoforetti[78a,78b], E. Critelli[97], V. Croft[116], G. Crosetti[44b,44a], A. Cueto[100], H. Cui[97], Z. Cui[7], B.M. Cunnett[151], W.R. Cunningham[59], F. Curcio[168], J.R. Curran[52], M.J. Da Cunha Sargedas De Sousa[57b,57a], J.V. Da Fonseca Pinto[82b], C. Da Via[102], W. Dabrowski[86a], T. Dado[37], S. Dahbi[153], T. Dai[107], D. Dal Santo[20], C. Dallapiccola[104], M. Dam[43], G. D'amen[30], V. D'Amico[110], J.R. Dandoy[35], M. D'Andrea[57b,57a], D. Dannheim[37], G. D'anniballe[74a,74b], M. Danninger[147], V. Dao[150], G. Darbo[57b], S.J. Das[30], F. Dattola[48], S. D'Auria[71a,71b], A. D'Avanzo[72a,72b], T. Davidek[135], J. Davidson[172], I. Dawson[95], K. De[8], C. De Almeida Rossi[160], R. De Asmundis[72a], N. De Biase[48], S. De Castro[24b,24a], N. De Groot[115], P. de Jong[116], H. De la Torre[117], A. De Maria[113a], A. De Salvo[75a], U. De Sanctis[76a,76b], F. De Santis[70a,70b], A. De Santo[151], J.B. De Vivie De Regie[60], J. Debevc[94], D.V. Dedovich[39], J. Degens[93], A.M. Deiana[45], J. Del Peso[100], L. Delagrange[129], F. Deliot[137], C.M. Delitzsch[49], M. Della Pietra[72a,72b], D. Della Volpe[56], A. Dell'Acqua[37], L. Dell'Asta[71a,71b], M. Delmastro[4], C.C. Delogu[57b,57a], P.A. Delsart[60], S. Demers[177], M. Demichev[39], S.P. Denisov[38], H. Denizli[22a,l], M.G. Depala[93], L. D'Eramo[41], D. Derendarz[87], F. Derue[129], P. Dervan[93,*], A.M. Desai[1], K. Desch[25], F.A. Di Bello[74a,74b], A. Di Ciaccio[76a,76b], L. Di Ciaccio[4], A. Di Domenico[75a,75b], C. Di Donato[72a,72b], A. Di Girolamo[37], G. Di Gregorio[66], A. Di Luca[78a,78b], B. Di Micco[77a,77b], R. Di Nardo[77a,77b], K.F. Di Petrillo[40], M. Diamantopoulou[35], F.A. Dias[116], M.A. Diaz[139a,139b], A.R. Didenko[39], M. Didenko[168], S.D. Diefenbacher[18a], E.B. Diehl[107], S. Díez Cornell[48], C. Diez Pardos[146], C. Dimitriadi[149], A. Dimitrievska[21], A. Dimri[150], Y. Ding[62], J. Dingfelder[25], T. Dingley[128], I-M. Dinu[28b], S.J. Dittmeier[63b], F. Dittus[37], M. Divisek[135], B. Dixit[93], F. Djama[103], T. Djobava[154b], C. Doglioni[102,99], A. Dohnalova[29a], Z. Dolezal[135], K. Domijan[86a], K.M. Dona[40], M. Donadelli[82d], B. Dong[108], J. Donini[41], A. D'Onofrio[72a,72b], M. D'Onofrio[93], J. Dopke[136], A. Doria[72a], N. Dos Santos Fernandes[132a], I.A. Dos Santos Luz[82e], P. Dougan[102], M.T. Dova[91], A.T. Doyle[59], M.P. Drescher[55], E. Dreyer[174], I. Drivas-koulouris[10], M. Drnevich[119], D. Du[62], T.A. du Pree[116], Z. Duan[113a], M. Dubau[4], F. Dubinin[39], M. Dubovsky[29a], E. Duchovni[174], G. Duckeck[110], P.K. Duckett[97], O.A. Ducu[28b], D. Duda[52], A. Dudarev[37], M.M. Dudek[87], E.R. Duden[27], M. D'uffizi[102], L. Duflot[66], M. Dührssen[37], I. Duminica[28g], A.E. Dumitriu[28b], M. Dunford[63a], K. Dunne[47a,47b], A. Duperrin[103], H. Duran Yildiz[3a], A. Durglishvili[154b], G.I. Dyckes[18a], M. Dyndal[86a], B.S. Dziedzic[37], Z.O. Earnshaw[151], G.H. Eberwein[128], B. Eckerova[29a], S. Eggebrecht[55], E. Egidio Purcino De Souza[82e], G. Eigen[17], K. Einsweiler[18a], T. Ekelof[166], P.A. Ekman[99], S. El Farkh[36b], Y. El Ghazali[62], H. El Jarrari[105], A. El Moussaouy[36a], D. Elitez[37], M. Ellert[166], F. Ellinghaus[176], T.A. Elliot[96], N. Ellis[37], J. Elmsheuser[30], M. Elsawy[118a], M. Elsing[37], D. Emeliyanov[136], Y. Enari[83], S. Epari[109], D. Ernani Martins Neto[87], F. Ernst[37], M. Escalier[66], C. Escobar[168], E. Etzion[156],

G. Evans[132a,132b], H. Evans[68], L.S. Evans[48], A. Ezhilov[38], S. Ezzarqtouni[36a], F. Fabbri[24b,24a], L. Fabbri[24b,24a], G. Facini[97], V. Fadeyev[138], R.M. Fakhrutdinov[38], D. Fakoudis[101], S. Falciano[75a], L.F. Falda Ulhoa Coelho[27], F. Fallavollita[111], G. Falsetti[44b,44a], J. Faltova[135], C. Fan[167], K.Y. Fan[64b], Y. Fan[14], Y. Fang[14,113c], M. Fanti[71a,71b], M. Faraj[69a,69b], Z. Farazpay[98], A. Farbin[8], A. Farilla[77a], K. Farman[153], T. Farooque[108], J.N. Farr[177], M.S. Farrington[61], S.M. Farrington[136,52], F. Fassi[36e], D. Fassouliotis[9], L. Fayard[66], P. Federic[135], P. Federicova[133], O.L. Fedin[38,a], M. Feickert[175], L. Feligioni[103], D.E. Fellers[18a], C. Feng[142a], Y. Feng[14], Z. Feng[116], M.J. Fenton[164], L. Ferencz[48], B. Fernandez Barbadillo[92], P. Fernandez Martinez[67], M.J.V. Fernoux[103], J. Ferrando[92], A. Ferrari[166], P. Ferrari[116,115], R. Ferrari[73a], D. Ferrere[56], C. Ferretti[107], M.P. Fewell[1], D. Fiacco[75a,75b], F. Fiedler[101], P. Fiedler[134], S. Filimonov[39], M.S. Filip[28b,t], A. Filipčič[94], E.K. Filmer[161a], F. Filthaut[115], M.C.N. Fiolhais[132a,132c,c], L. Fiorini[168], W.C. Fisher[108], T. Fitschen[102], P.M. Fitzhugh[137], I. Fleck[146], P. Fleischmann[107], T. Flick[176], M. Flores[34d,ag], L.R. Flores Castillo[64a], M. Foll[127], F.M. Follega[78a,78b], N. Fomin[33], J.H. Foo[160], A. Formica[137], A.C. Forti[102], E. Fortin[37], A.W. Fortman[18a], L. Foster[18a], L. Fountas[9,i], D. Fournier[66], H. Fox[92], P. Francavilla[74a,74b], S. Francescato[61], S. Franchellucci[56], M. Franchini[24b,24a], S. Franchino[63a], D. Francis[37], L. Franco[48], L. Franconi[48], M. Franklin[61], G. Frattari[27], Y.Y. Frid[156], J. Friend[59], N. Fritzsche[37], A. Froch[56], D. Froidevaux[37], J.A. Frost[136], Y. Fu[108], S. Fuenzalida Garrido[139g], M. Fujimoto[150], K.Y. Fung[64a], E. Furtado De Simas Filho[82e], M. Furukawa[158], M. Fuste Costa[48], J. Fuster[168], A. Gaa[55], A. Gabrielli[24b,24a], A. Gabrielli[160], P. Gadow[37], G. Gagliardi[57b,57a], L.G. Gagnon[18a], S. Gaid[84b], S. Galantzan[156], J. Gallagher[1], E.J. Gallas[128], A.L. Gallen[166], B.J. Gallop[136], K.K. Gan[121], S. Ganguly[158], Y. Gao[52], A. Garabaglu[141], F.M. Garay Walls[139a,139b], C. García[168], A. Garcia Alonso[116], A.G. Garcia Caffaro[177], J.E. García Navarro[168], M.A. Garcia Ruiz[23b], M. Garcia-Sciveres[18a], G.L. Gardner[130], R.W. Gardner[40], N. Garelli[163], R.B. Garg[148], J.M. Gargan[33], C.A. Garner[160], C.M. Garvey[34a], V.K. Gassmann[163], G. Gaudio[73a], V. Gautam[13], P. Gauzzi[75a,75b], J. Gavranovic[94], I.L. Gavrilenko[132a], A. Gavrilyuk[38], C. Gay[169], G. Gaycken[125], E.N. Gazis[10], A. Gekow[121], C. Gemme[57b], M.H. Genest[60], A.D. Gentry[114], S. George[96], T. Geralis[46], A.A. Gerwin[122], P. Gessinger-Befurt[37], M. Ghani[172], K. Ghorbanian[95], A. Ghosal[146], A. Ghosh[164], A. Ghosh[7], B. Giacobbe[24b], S. Giagu[75a,75b], T. Giani[116], A. Giannini[62], S.M. Gibson[96], M. Gignac[138], D.T. Gil[86b], A.K. Gilbert[86a], B.J. Gilbert[42], D. Gillberg[35], G. Gilles[116], D.M. Gingrich[2,ai], M.P. Giordani[69a,69c], P.F. Giraud[137], G. Giugliarelli[69a,69c], D. Giugni[71a], F. Giuli[76a,76b], I. Gkialas[9,i], L.K. Gladilin[38], C. Glasman[100], M. Glazewska[20], R.M. Gleason[164], G. Glemža[48], M. Glisic[125], I. Gnesi[44b], Y. Go[30], M. Goblirsch-Kolb[37], B. Gocke[49], D. Godin[109], B. Gokturk[22a], S. Goldfarb[106], T. Golling[56], M.G.D. Gololo[34c], A. Golub[141], D. Golubkov[38], J.P. Gombas[108], A. Gomes[132a,132b], G. Gomes Da Silva[146], A.J. Gomez Delegido[37], R. Gonçalo[132a], L. Gonella[21], A. Gongadze[154c], F. Gonnella[21], J.L. Gonski[148], R.Y. González Andana[52], S. González de la Hoz[168], M.V. Gonzalez Rodrigues[48], R. Gonzalez Suarez[166], S. Gonzalez-Sevilla[56], L. Goossens[37], B. Gorini[37], E. Gorini[70a,70b], A. Gorišek[94], T.C. Gosart[130], A.T. Goshaw[51], M.I. Gostkin[39], S. Goswami[123], C.A. Gottardo[37], S.A. Gotz[110], M. Gouighri[36b], A.G. Goussiou[141], N. Govender[34c], R.P. Grabarczyk[128], I. Grabowska-Bold[86a], K. Graham[35], E. Gramstad[127], S. Grancagnolo[70a,70b], C.M. Grant[1], P.M. Gravila[28f], F.G. Gravili[70a,70b], H.M. Gray[18a], M. Greco[111], M.J. Green[1], C. Grefe[25], A.S. Grefsrud[17], I.M. Gregor[48], K.T. Greif[164], P. Grenier[148], S.G. Grewe[111], A.A. Grillo[138], K. Grimm[32], S. Grinstein[13,x], J.-F. Grivaz[66], E. Gross[174], J. Grosse-Knetter[55], L.H. Grossman[18b], L. Guan[107], G. Guerrieri[37],

R. Guevara[127], R. Gugel[101], J.A.M. Guhit[107], A. Guida[19], E. Guilloton[172], S. Guindon[37], F. Guo[14,113c], J. Guo[143a], L. Guo[48], L. Guo[113b,v], Y. Guo[107], Y. Guo[42], A. Gupta[49], R. Gupta[131], S. Gupta[27], S. Gurbuz[25], S.S. Gurdasani[48], G. Gustavino[75a,75b], P. Gutierrez[122], L.F. Gutierrez Zagazeta[130], M. Gutsche[50], C. Gutschow[97], C. Gwenlan[128], C.B. Gwilliam[93], E.S. Haaland[127], A. Haas[119], M. Habedank[59], C. Haber[18a], H.K. Hadavand[8], A. Haddad[41], A. Hadef[50], A.I. Hagan[92], J.J. Hahn[146], E.H. Haines[97], M. Haleem[171], J. Haley[123], G.D. Hallewell[103], J.A. Hallford[48], K. Hamano[170], H. Hamdaoui[166], M. Hamer[25], S.E.D. Hammoud[66], E.J. Hampshire[96], J. Han[142a], L. Han[113a], L. Han[62], S. Han[14], K. Hanagaki[83], M. Hance[138], D.A. Hangal[42], H. Hanif[147], M.D. Hank[130], J.B. Hansen[43], P.H. Hansen[43], T. Harenberg[176], S. Harkusha[178], M.L. Harris[104], Y.T. Harris[25], J. Harrison[13], P.F. Harrison[172], M.L.E. Hart[97], N.M. Hartman[111], N.M. Hartmann[110], R.Z. Hasan[96,136], Y. Hasegawa[145], F. Haslbeck[128], S. Hassan[17], R. Hauser[108], M. Haviernik[135], C.M. Hawkes[21], R.J. Hawkings[37], Y. Hayashi[158], D. Hayden[108], C. Hayes[107], R.L. Hayes[116], C.P. Hays[128], J.M. Hays[95], H.S. Hayward[93], M. He[14,113c], Y. He[48], Y. He[97], N.B. Heatley[95], V. Hedberg[99], J. Heilman[35], S. Heim[48], T. Heim[18a], J.J. Heinrich[125], L. Heinrich[111], J. Hejbal[133], M. Helbig[50], A. Held[175], S. Hellesund[17], C.M. Helling[169], S. Hellman[47a,47b], A.M. Henriques Correia[37], H. Herde[99], Y. Hernández Jiménez[150], L.M. Herrmann[25], T. Herrmann[50], G. Herten[54], R. Hertenberger[110], L. Hervas[37], M.E. Hesping[101], N.P. Hessey[161a], J. Hessler[111], M. Hidaoui[36b], N. Hidic[135], E. Hill[160], T.S. Hillersoy[17], S.J. Hillier[21], J.R. Hinds[108], F. Hinterkeuser[25], M. Hirose[126], S. Hirose[162], D. Hirschbuehl[176], T.G. Hitchings[102], B. Hiti[94], J. Hobbs[150], R. Hobincu[28e], N. Hod[174], A.M. Hodges[167], M.C. Hodgkinson[144], B.H. Hodkinson[128], A. Hoecker[37], D.D. Hofer[107], J. Hofer[168], J. Hofner[101], M. Holzbock[37], L.B.A.H. Hommels[33], V. Homsak[128], J.J. Hong[68], T.M. Hong[131], B.H. Hooberman[167], W.H. Hopkins[6], M.C. Hoppesch[167], Y. Horii[112], M.E. Horstmann[111], S. Hou[153], M.R. Housenga[167], J. Howarth[59], J. Hoya[6], M. Hrabovsky[124], T. Hryn'ova[4], P.J. Hsu[65], S.-C. Hsu[141], T. Hsu[66], M. Hu[18a], Q. Hu[62], S. Huang[33], X. Huang[14,113c], Y. Huang[135], Y. Huang[113b], Y. Huang[14], Z. Huang[66], Z. Hubacek[134], F. Huegging[25], T.B. Huffman[128], M. Hufnagel Maranha De Faria[82a], C.A. Hugli[48], M. Huhtinen[37], S.K. Huiberts[127], R. Hulsken[105], C.E. Hultquist[18a], D.L. Humphreys[104], N. Huseynov[12], J. Huston[108], J. Huth[61], L. Huth[48], R. Hyneman[7], G. Iacobucci[56], G. Iakovidis[30], L. Iconomidou-Fayard[66], J.P. Iddon[37], P. Iengo[72a,72b], Y. Iiyama[158], T. Iizawa[158], Y. Ikegami[83], D. Iliadis[157], N. Ilic[160], H. Imam[36a], G. Inacio Goncalves[82d], S.A. Infante Cabanas[139c], T. Ingebretsen Carlson[47a,47b], J.M. Inglis[95], G. Introzzi[73a,73b], M. Iodice[77a], V. Ippolito[75a,75b], R.K. Irwin[93], M. Ishino[158], W. Islam[175], C. Issever[19], S. Istin[22a,ao], K. Itabashi[126], H. Ito[173], R. Iuppa[78a,78b], A. Ivina[174], S. Izumiyama[112], V. Izzo[72a], P. Jacka[134], P. Jackson[1], P. Jain[48], K. Jakobs[54], T. Jakoubek[174], J. Jamieson[59], W. Jang[158], S. Jankovych[135], M. Javurkova[104], P. Jawahar[102], L. Jeanty[125], J. Jejelava[154a,ae], P. Jenni[54,f], C.E. Jessiman[35], C. Jia[142a], H. Jia[169], J. Jia[150], X. Jia[111,113c], Z. Jia[113a], C. Jiang[52], Q. Jiang[64b], S. Jiggins[48], M. Jimenez Ortega[168], J. Jimenez Pena[13], S. Jin[113a], A. Jinaru[28b], O. Jinnouchi[140], P. Johansson[144], K.A. Johns[7], J.W. Johnson[138], F.A. Jolly[48], D.M. Jones[151], E. Jones[48], K.S. Jones[8], P. Jones[33], R.W.L. Jones[92], T.J. Jones[93], H.L. Joos[55], R. Joshi[121], J. Jovicevic[16], X. Ju[18a], J.J. Junggeburth[37], T. Junkermann[63a], A. Juste Rozas[13,x], M.K. Juzek[87], S. Kabana[139f], A. Kaczmarska[87], S.A. Kadir[148], M. Kado[111], H. Kagan[121], M. Kagan[148], A. Kahn[130], C. Kahra[101], T. Kaji[158], E. Kajomovitz[155], N. Kakati[174], N. Kakoty[13], I. Kalaitzidou[54], S. Kandel[8], N. Kanellos[10], N.J. Kang[138], D. Kar[34j], E. Karentzos[25], K. Karki[8],

O. Karkout[116], S.N. Karpov[39], Z.M. Karpova[39], V. Kartvelishvili[92,154b], A.N. Karyukhin[38], E. Kasimi[157], J. Katzy[48], S. Kaur[35], K. Kawade[145], M.P. Kawale[122], C. Kawamoto[88], T. Kawamoto[62], E.F. Kay[37], S. Kazakos[108], V.F. Kazanin[38], J.M. Keaveney[34a], R. Keeler[170], G.V. Kehris[61], J.S. Keller[35], J.M. Kelly[170], J.J. Kempster[151], O. Kepka[133], J. Kerr[161b], B.P. Kerridge[136], B.P. Kerševan[94], L. Keszeghova[29a], R.A. Khan[131], A. Khanov[123], A.G. Kharlamov[38], T. Kharlamova[38], E.E. Khoda[141], M. Kholodenko[132a], T.J. Khoo[19], G. Khoriauli[171], Y. Khoulaki[36a], Y.A.R. Khwaira[129], B. Kibirige[34j], D. Kim[6], D.W. Kim[18b], Y.K. Kim[40], N. Kimura[97], M.K. Kingston[55], A. Kirchhoff[55], C. Kirfel[25], F. Kirfel[25], J. Kirk[136], A.E. Kiryunin[111], S. Kita[162], O. Kivernyk[25], M. Klassen[163], C. Klein[35], L. Klein[171], M.H. Klein[45], S.B. Klein[56], U. Klein[93], A. Klimentov[30], T. Klioutchnikova[37], P. Kluit[116], S. Kluth[111], E. Kneringer[79], T.M. Knight[160], A. Knue[49], M. Kobel[50], D. Kobylianskii[174], S.F. Koch[128], M. Kocian[148], P. Kodyš[135], D.M. Koeck[125], T. Koffas[35], O. Kolay[50], I. Koletsou[4], T. Komarek[87], K. Köneke[55], A.X.Y. Kong[1], T. Kono[120], N. Konstantinidis[97], P. Kontaxakis[56], B. Konya[99], R. Kopeliansky[42], S. Koperny[86a], R. Koppenhofer[54], K. Korcyl[87], K. Kordas[157,d], A. Korn[97], S. Korn[55], I. Korolkov[13], N. Korotkova[38], B. Kortman[116], O. Kortner[111], S. Kortner[111], W.H. Kostecka[117], M. Kostov[29a], V.V. Kostyukhin[146], A. Kotsokechagia[37], A. Kotwal[51], A. Koulouris[37], A. Kourkoumeli-Charalampidi[73a,73b], C. Kourkoumelis[9], E. Kourlitis[111], O. Kovanda[125], R. Kowalewski[170], W. Kozanecki[125], A.S. Kozhin[38], V.A. Kramarenko[38], G. Kramberger[94], P. Kramer[25], M.W. Krasny[129], A. Krasznahorkay[104], A.C. Kraus[117], J.W. Kraus[176], J.A. Kremer[48], N.B. Krengel[146], T. Kresse[50], L. Kretschmann[176], J. Kretzschmar[93], P. Krieger[160], K. Krizka[21], K. Kroeninger[49], H. Kroha[111], J. Kroll[133], J. Kroll[130], K.S. Krowpman[108], U. Kruchonak[39], H. Krüger[25], N. Krumnack[80], M.C. Kruse[51], O. Kuchinskaia[39], S. Kuday[3a], S. Kuehn[37], R. Kuesters[54], T. Kuhl[48], V. Kukhtin[39], Y. Kulchitsky[39], S. Kuleshov[139d,139b], J. Kull[1], E.V. Kumar[110], M. Kumar[34j], N. Kumari[48], P. Kumari[161b], A. Kupco[133], A. Kupich[38], O. Kuprash[54], H. Kurashige[85], L.L. Kurchaninov[161a], O. Kurdysh[4], A. Kurova[38], M. Kuze[140], A.K. Kvam[104], J. Kvita[124], N.G. Kyriacou[141], M. Laassiri[30], C. Lacasta[168], F. Lacava[75a,75b], H. Lacker[19], D. Lacour[129], N.N. Lad[97], E. Ladygin[39], A. Lafarge[41], B. Laforge[129], T. Lagouri[177], F.Z. Lahbabi[36a], S. Lai[55,37], W.S. Lai[97], I.K. Lakomiec[55], J.E. Lambert[170], S. Lammers[68], W. Lampl[7], C. Lampoudis[157,d], G. Lamprinoudis[171], A.N. Lancaster[117], E. Lançon[30], U. Landgraf[54], M.P.J. Landon[95], V.S. Lang[54], A.J. Lankford[164], F. Lanni[37], C.S. Lantz[167], K. Lantzsch[25], A. Lanza[73a], M. Lanzac Berrocal[168], J.F. Laporte[137], T. Lari[71a], D. Larsen[17], L. Larson[11], F. Lasagni Manghi[24b], M. Lassnig[37], S.D. Lawlor[144], R. Lazaridou[164], M. Lazzaroni[71a,71b], E.T.T. Le[164], H.D.M. Le[108], E.M. Le Boulicaut[177], L.T. Le Pottier[18a], B. Leban[24b,24a], F. Ledroit-Guillon[60], T.F. Lee[161b], L.L. Leeuw[34c], M. Lefebvre[170], C. Leggett[18a], G. Lehmann Miotto[37], M. Leigh[56], W.A. Leight[104], W. Leinonen[115], A. Leisos[157,u], M.A.L. Leite[82c], C.E. Leitgeb[19], R. Leitner[135], K.J.C. Leney[45], T. Lenz[25], S. Leone[74a], C. Leonidopoulos[52], A. Leopold[149], J.H. Lepage Bourbonnais[35], R. Les[108], C.G. Lester[33], M. Levchenko[38], J. Levêque[4], L.J. Levinson[174], G. Levrini[24b,24a], M.P. Lewicki[87], C. Lewis[141], D.J. Lewis[4], L. Lewitt[144], A. Li[30], B. Li[142a], C. Li[107], C-Q. Li[111], H. Li[142a], H. Li[102], H. Li[15], H. Li[62], H. Li[142a], J. Li[143a], K. Li[14], L. Li[143a], R. Li[177], S. Li[14,113c], S. Li[143b,143a], T. Li[5], X. Li[105], Y. Li[14], Z. Li[158], Z. Li[14,113c], Z. Li[62], S. Liang[14,113c], Z. Liang[14], M. Liberatore[137], B. Liberti[76a], G.B. Libotte[82d], K. Lie[64c], J. Lieber Marin[82e], H. Lien[68], H. Lin[107], S.F. Lin[150], L. Linden[110], R.E. Lindley[7], J.H. Lindon[37], J. Ling[61], E. Lipeles[130], A. Lipniacka[17], A. Lister[169], J.D. Little[68], B. Liu[14], B.X. Liu[113b], D. Liu[155], D. Liu[138], E.H.L. Liu[21], J.K.K. Liu[119], K. Liu[143b], K. Liu[143b,143a], M. Liu[62], M.Y. Liu[62], P. Liu[14], Q. Liu[148], S. Liu[150], X. Liu[142a], Y. Liu[113b,113c], Y. Liu[167], Y.L. Liu[142a], Y.W. Liu[62], Z. Liu[66,k], S.L. Lloyd[95], E.M. Lobodzinska[48], P. Loch[7], E. Lodhi[160], K. Lohwasser[144], E. Loiacono[48], J.D. Lomas[21], J.D. Long[42], I. Longarini[164], R. Longo[167], A. Lopez Solis[13], N.A. Lopez-canelas[7], N. Lorenzo Martinez[4], A.M. Lory[110], M. Losada[118a], G. Löschcke Centeno[4], X. Lou[47a,47b], X. Lou[14,113c], A. Lounis[66], P.A. Love[92], M. Lu[66], S. Lu[130], Y.J. Lu[153], H.J. Lubatti[141], C. Luci[75a,75b], F.L. Lucio Alves[113a], F. Luehring[68], B.S. Lunday[130], O. Lundberg[149], J. Lunde[37], N.A. Luongo[6], M.S. Lutz[37], A.B. Lux[26], D. Lynn[30], R. Lysak[133], V. Lysenko[134], E. Lytken[99], V. Lyubushkin[39], T. Lyubushkina[39], M.M. Lyukova[150], H. Ma[30], K. Ma[62], L.L. Ma[142a], W. Ma[62], Y. Ma[123], J.C. MacDonald[101], P.C. Machado De Abreu Farias[82e], D. Macina[37], R. Madar[41], T. Madula[97], J. Maeda[85], T. Maeno[30], P.T. Mafa[34c,j], H. Maguire[144], M. Maheshwari[33], V. Maiboroda[66], A. Maio[132a,132b,132d], K. Maj[86a], O. Majersky[48], S. Majewski[125], R. Makhmanazarov[38], N. Makovec[66], V. Maksimovic[16], B. Malaescu[129], J. Malamant[127], Pa. Malecki[87], V.P. Maleev[38], F. Malek[60,o], M. Mali[94], D. Malito[96], A. Maloizel[5], S. Maltezos[10], A. Malvezzi Lopes[82d], S. Malyukov[39], J. Mamuzic[94], G. Mancini[53], M.N. Mancini[27], G. Manco[73a,73b], J.P. Mandalia[95], S.S. Mandarry[151], I. Mandić[94], L. Manhaes de Andrade Filho[82a], I.M. Maniatis[174], J. Manjarres Ramos[90], D.C. Mankad[174], A. Mann[110], T. Manoussos[37], M.N. Mantinan[40], S. Manzoni[37], L. Mao[143a], X. Mapekula[34c], A. Marantis[157], R.R. Marcelo Gregorio[95], G. Marchiori[5], C. Marcon[71a], E. Maricic[16], M. Marinescu[48], S. Marium[48], M. Marjanovic[122], A. Markhoos[54], M. Markovitch[66], M.K. Maroun[104], M.C. Marr[147], G.T. Marsden[102], E.J. Marshall[92], Z. Marshall[18a], S. Marti-Garcia[168], J. Martin[97], T.A. Martin[136], V.J. Martin[52], B. Martin dit Latour[17], L. Martinelli[75a,75b], M. Martinez[13,x], P. Martinez Agullo[168], V.I. Martinez Outschoorn[104], P. Martinez Suarez[37], S. Martin-Haugh[136], G. Martinovicova[135], V.S. Martoiu[28b], A.C. Martyniuk[97], A. Marzin[37], D. Mascione[78a,78b], L. Masetti[101], J. Masik[102], A.L. Maslennikov[39], S.L. Mason[42], P. Massarotti[72a,72b], P. Mastrandrea[74a,74b], A. Mastroberardino[44b,44a], T. Masubuchi[126], T.T. Mathew[125], J. Matousek[135], D.M. Mattern[49], K. Mauer[48], J. Maurer[28b], T. Maurin[59], A.J. Maury[66], B. Maček[94], C. Mavungu Tsava[103], D.A. Maximov[38], A.E. May[102], E. Mayer[41], R. Mazini[34j], I. Maznas[117], S.M. Mazza[138], E. Mazzeo[37], J.P. Mc Gowan[170], S.P. Mc Kee[107], C.A. Mc Lean[6], C.C. McCracken[169], E.F. McDonald[106], A.E. McDougall[116], L.F. Mcelhinney[92], J.A. Mcfayden[151], R.P. McGovern[130], R.P. Mckenzie[34j], T.C. Mclachlan[48], D.J. Mclaughlin[97], S.J. McMahon[136], C.M. Mcpartland[93], R.A. McPherson[170,ab], S. Mehlhase[110], A. Mehta[93], D. Melini[168], B.R. Mellado Garcia[34j], A.H. Melo[55], F. Meloni[48], A.M. Mendes Jacques Da Costa[102], L. Meng[92], S. Menke[111], M. Mentink[37], E. Meoni[44b,44a], G. Mercado[117], S. Merianos[157], C. Merlassino[69a,69c], C. Meroni[71a,71b], J. Metcalfe[6], A.S. Mete[6], E. Meuser[101], C. Meyer[68], J-P. Meyer[137], Y. Miao[113a], R.P. Middleton[136], M. Mihovilovic[66], L. Mijović[52], G. Mikenberg[174], M. Mikestikova[133], M. Mikuž[94], H. Mildner[101], A. Milic[37], D.W. Miller[40], E.H. Miller[148], A. Milov[174], D.A. Milstead[47a,47b], T. Min[113a], A.A. Minaenko[38], I.A. Minashvili[154b], A.I. Mincer[119], B. Mindur[86a], M. Mineev[39], Y. Mino[88], L.M. Mir[13], M. Miralles Lopez[59], M. Mironova[18a], M. Missio[41], A. Mitra[172], V.A. Mitsou[168], Y. Mitsumori[112], O. Miu[160], P.S. Miyagawa[95], T. Mkrtchyan[37], M. Mlinarevic[97], T. Mlinarevic[97], M. Mlynarikova[135], L. Mlynarska[86a], C. Mo[143a], S. Mobius[20], M.H. Mohamed Farook[114], S. Mohapatra[42], M.F. Mohd Soberi[52], S. Mohiuddin[123], G. Mokgatitswane[34j], L. Moleri[174], U. Molinatti[128], L.G. Mollier[20], B. Mondal[133], S. Mondal[134], K. Mönig[48], E. Monnier[103], L. Monsonis Romero[168], J. Montejo Berlingen[13], A. Montella[47a,47b], M. Montella[121], F. Montereali[77a,77b],

F. Monticelli[91], S. Monzani[69a,69c], A. Morancho Tarda[43], N. Morange[66], A.L. Moreira De Carvalho[48], M. Moreno Llácer[168], C. Moreno Martinez[56], J.M. Moreno Perez[23b], P. Morettini[57b], S. Morgenstern[37], M. Morii[61], M. Morinaga[158], M. Moritsu[89], F. Morodei[75a,75b], P. Moschovakos[37], B. Moser[54], M. Mosidze[154b], T. Moskalets[45], P. Moskvitina[115], J. Moss[32], P. Moszkowicz[86a], T. Motta Quirino[82d], A. Moussa[36d], Y. Moyal[174], H. Moyano Gomez[13], E.J.W. Moyse[104], T.G. Mroz[87], S. Muanza[103], M. Mucha[25], J. Mueller[131], R. Müller[37], G.A. Mullier[166], A.J. Mullin[33], J.J. Mullin[51], A.C. Mullins[45], A.E. Mulski[61], D.P. Mungo[160], D. Munoz Perez[168], F.J. Munoz Sanchez[102], W.J. Murray[172,136], M. Muškinja[94], C. Mwewa[48], A.G. Myagkov[38,a], A.J. Myers[8], G. Myers[107], M. Myska[134], B.P. Nachman[148], K. Nagai[128], K. Nagano[83], R. Nagasaka[158], J.L. Nagle[30,al], E. Nagy[103], A.M. Nairz[37], Y. Nakahama[83], K. Nakamura[83], K. Nakkalil[5], A. Nandi[63b], H. Nanjo[126], E.A. Narayanan[45], Y. Narukawa[158], I. Naryshkin[38], L. Nasella[71a,71b], S. Nasri[118b], C. Nass[25], G. Navarro[23a], A. Nayaz[19], P.Y. Nechaeva[38], S. Nechaeva[24b,24a], F. Nechansky[133], L. Nedic[128], T.J. Neep[21], A. Negri[73a,73b], M. Negrini[24b], C. Nellist[116], C. Nelson[105], K. Nelson[107], S. Nemecek[133], M. Nessi[37,g], M.S. Neubauer[167], J. Newell[93], P.R. Newman[21], C.W. Ng[131], Y.W.Y. Ng[167], B. Ngair[118a], H.D.N. Nguyen[109], J.D. Nichols[122], R.B. Nickerson[128], R. Nicolaidou[137], J. Nielsen[138], M. Niemeyer[55], J. Niermann[37], N. Nikiforou[37], V. Nikolaenko[38,a], I. Nikolic-Audit[129], P. Nilsson[30], I. Ninca[48], G. Ninio[156], A. Nisati[75a], R. Nisius[111], N. Nitika[174], E.K. Nkadimeng[34b], T. Nobe[158], D. Noll[148], T. Nommensen[152], M.B. Norfolk[144], B.J. Norman[35], L.C. Nosler[18a], M. Noury[36a], J. Novak[94], T. Novak[94], P. Novotny[174], R. Novotny[134], L. Nozka[124], K. Ntekas[164], D. Ntounis[148], N.M.J. Nunes De Moura Junior[82b], J. Ocariz[129], I. Ochoa[132a], A. Odella Rodriguez[13], S. Oerdek[48,y], J.T. Offermann[40], A. Ogrodnik[87], A. Oh[102], C.C. Ohm[149], H. Oide[83], M.L. Ojeda[37], Y. Okumura[158], L.F. Oleiro Seabra[132a], I. Oleksiyuk[56], G. Oliveira Correa[13], D. Oliveira Damazio[30], J.L. Oliver[1], R. Omar[68], Ö.O. Öncel[54], A.P. O'Neill[20], A. Onofre[132a,132e,e], P.U.E. Onyisi[11], M.J. Oreglia[40], D. Orestano[77a,77b], R. Orlandini[77a,77b], R.S. Orr[160], L.M. Osojnak[42], Y. Osumi[112], G. Otero y Garzon[31], H. Otono[89], M. Ouchrif[36d], F. Ould-Saada[127], T. Ovsiannikova[141], M. Owen[59], R.E. Owen[136], V.E. Ozcan[22a], F. Ozturk[87], N. Ozturk[8], S. Ozturk[81], H.A. Pacey[128], K. Pachal[161a], A. Pacheco Pages[13], C. Padilla Aranda[13], G. Padovano[75a,75b], S. Pagan Griso[18a], J. Pampel[25], J. Pan[177], D.K. Panchal[11], C.E. Pandini[60], J.G. Panduro Vazquez[136], H.D. Pandya[1], H. Pang[137], P. Pani[48], G. Panizzo[69a,69c], L. Panwar[129], L. Paolozzi[56], S. Parajuli[167], A. Paramonov[6], C. Paraskevopoulos[53], D. Paredes Hernandez[64b], S.R. Paredes Saenz[52], A. Pareti[73a,73b], K.R. Park[42], T.H. Park[111], F. Parodi[57b,57a], J.A. Parsons[42], U. Parzefall[54], B. Pascual Dias[41], L. Pascual Dominguez[100], E. Pasqualucci[75a], S. Passaggio[57b], F. Pastore[96], P. Patel[87], U.M. Patel[51], J.R. Pater[102], T. Pauly[37], F. Pauwels[135], C.I. Pazos[163], M. Pedersen[127], R. Pedro[132a], S.V. Peleganchuk[38], O. Penc[133], S. Peng[15], G.D. Penn[177], K.E. Penski[110], M. Penzin[38], B.S. Peralva[82d], A.P. Pereira Peixoto[141], L. Pereira Sanchez[148], D.V. Perepelitsa[30,al], G. Perera[104], E. Perez Codina[37], M. Perganti[10], H. Pernegger[37], S. Perrella[75a,75b], K. Peters[48], R.F.Y. Peters[102], B.A. Petersen[37], T.C. Petersen[43], E. Petit[103], V. Petousis[134], A.R. Petri[71a,71b], C. Petridou[157,d], T. Petru[135], M. Pettee[18a], A. Petukhov[81], K. Petukhova[37], R. Pezoa[139g], L. Pezzotti[24b,24a], G. Pezzullo[177], L. Pfaffenbichler[37], A.J. Pfleger[79], T.M. Pham[175], T. Pham[106], P.W. Phillips[136], G. Piacquadio[150], E. Pianori[18a], F. Piazza[125], R. Piegaia[31], D. Pietreanu[28b], A.D. Pilkington[102], M. Pinamonti[69a,69c], J.L. Pinfold[2], G. Pinheiro Matos[42], B.C. Pinheiro Pereira[132a], J. Pinol Bel[13], A.E. Pinto Pinoargote[129], L. Pintucci[69a,69c], K.M. Piper[151], A. Pirttikoski[56], D.A. Pizzi[35],

L. Pizzimento[64b], A. Plebani[33], M.-A. Pleier[30], V. Pleskot[135], E. Plotnikova[39], G. Poddar[95], R. Poettgen[99], L. Poggioli[129], S. Polacek[135], G. Polesello[73a], A. Poley[147], A. Polini[24b], C.S. Pollard[172], Z.B. Pollock[121], E. Pompa Pacchi[122], N.I. Pond[97], D. Ponomarenko[68], L. Pontecorvo[37], S. Popa[28a], G.A. Popeneciu[28d], A. Poreba[37], D.M. Portillo Quintero[161a], S. Pospisil[134], M.A. Postill[144], P. Postolache[28c], K. Potamianos[172], P.A. Potepa[86a], I.N. Potrap[39], C.J. Potter[33], H. Potti[152], J. Poveda[168], M.E. Pozo Astigarraga[37], R. Pozzi[37], A. Prades Ibanez[76a,76b], S.R. Pradhan[144], J. Pretel[170], D. Price[102], M. Primavera[70a], L. Primomo[69a,69c], M.A. Principe Martin[100], R. Privara[124], T. Procter[86b], M.L. Proffitt[141], N. Proklova[130], K. Prokofiev[64c], G. Proto[111], J. Proudfoot[6], M. Przybycien[86a], W.W. Przygoda[86b], A. Psallidas[46], J.E. Puddefoot[144], D. Pudzha[53], H.I. Purnell[1], D. Pyatiizbyantseva[115], J. Qian[107], R. Qian[108], D. Qichen[128], Y. Qin[13], T. Qiu[52], A. Quadt[55], M. Queitsch-Maitland[102], G. Quetant[56], R.P. Quinn[169], G. Rabanal Bolanos[61], D. Rafanoharana[111], F. Raffaeli[76a,76b], F. Ragusa[71a,71b], J.L. Rainbolt[40], S. Rajagopalan[30], E. Ramakoti[39], L. Rambelli[57b,57a], I.A. Ramirez-Berend[35], K. Ran[107,113c], D.S. Rankin[130], N.P. Rapheeha[34j], H. Rasheed[28b], A. Rastogi[18a], S. Rave[101], S. Ravera[57b,57a], B. Ravina[37], I. Ravinovich[174], M. Raymond[37], A.L. Read[127], N.P. Readioff[144], D.M. Rebuzzi[73a,73b], A.S. Reed[59], K. Reeves[27], D. Reikher[37], A. Rej[49], C. Rembser[37], H. Ren[62], M. Renda[28b], F. Renner[48], A.G. Rennie[59], M. Repik[56], A.L. Rescia[57b,57a], S. Resconi[71a], M. Ressegotti[57b,57a], S. Rettie[116], W.F. Rettie[35], M.M. Revering[33], E. Reynolds[18a], O.L. Rezanova[39], P. Reznicek[135], H. Riani[36d], N. Ribaric[51], B. Ricci[69a,69c], E. Ricci[78a,78b], R. Richter[111], S. Richter[47a,47b], E. Richter-Was[86b], M. Ridel[129], S. Ridouani[36d], P. Rieck[119], P. Riedler[37], E.M. Riefel[47a,47b], J.O. Rieger[116], M. Rijssenbeek[150], M. Rimoldi[34c], L. Rinaldi[24b,24a], P. Rincke[166,55], G. Ripellino[166], I. Riu[13], J.C. Rivera Vergara[170], F. Rizatdinova[123], E. Rizvi[95], B.R. Roberts[40], S.S. Roberts[138], D. Robinson[33], A. Robson[59], A. Rocchi[76a,76b], C. Roda[74a,74b], F.A. Rodriguez[117], S. Rodriguez Bosca[37], Y. Rodriguez Garcia[23a], A.M. Rodríguez Vera[117], S. Roe[37], J.T. Roemer[37], O. Røhne[127], R.A. Rojas[37], C.P.A. Roland[129], A. Romaniouk[79], E. Romano[73a,73b], M. Romano[24b], A.C. Romero Hernandez[167], N. Rompotis[93], L. Roos[129], S. Rosati[75a], B.J. Rosser[40], E. Rossi[128], E. Rossi[72a,72b], L.P. Rossi[61], L. Rossini[54], R. Rosten[121], M. Rotaru[28b], D. Rousseau[66], D. Rousso[48], S. Roy-Garand[160], A. Rozanov[103], Z.M.A. Rozario[59], Y. Rozen[155], A. Rubio Jimenez[168], V.H. Ruelas Rivera[19], T.A. Ruggeri[1], A. Ruggiero[128], A. Ruiz-Martinez[168], A. Rummler[37], G.B. Rupnik Boero[37], Z. Rurikova[54], N.A. Rusakovich[39], S. Ruscelli[49], H.L. Russell[170], G. Russo[75a,75b], J.P. Rutherfoord[7], S. Rutherford Colmenares[33], M. Rybar[135], P. Rybczynski[86a], A. Ryzhov[45], H.F-W. Sadrozinski[138], F. Safai Tehrani[75a], S. Saha[1], M. Sahinsoy[81], B. Sahoo[174], A. Saibel[168], B.T. Saifuddin[122], M. Saimpert[137], G.T. Saito[82c], M. Saito[158], T. Saito[158], A. Sala[71a,71b], A. Salnikov[148], J. Salt[168], A. Salvador Salas[156], F. Salvatore[151], A. Salzburger[37], D. Sammel[54], E. Sampson[92], D. Sampsonidis[157,d], D. Sampsonidou[125], M.A.A. Samy[59], J. Sánchez[168], V. Sanchez Sebastian[168], H. Sandaker[127], C.O. Sander[48], J.A. Sandesara[175], M. Sandhoff[176], C. Sandoval[23b], L. Sanfilippo[63a], D.P.C. Sankey[136], T. Sano[88], A. Sansoni[53], M. Santana Queiroz[18b], L. Santi[37], C. Santoni[41], H. Santos[132a,132b], A. Santra[174], E. Sanzani[24b,24a], K.A. Saoucha[84b], J.G. Saraiva[132a,132d], J. Sardain[7], O. Sasaki[83], K. Sato[162], C. Sauer[37], E. Sauvan[4], P. Savard[160,ai], R. Sawada[158], C. Sawyer[136], L. Sawyer[98], A.M. Sayed[27], C. Sbarra[24b], A. Sbrizzi[24b,24a], T. Scanlon[97], J. Schaarschmidt[141], U. Schäfer[101], A.C. Schaffer[66,45], D. Schaile[110], R.D. Schamberger[150], C. Scharf[19], M.M. Schefer[20], V.A. Schegelsky[38], D. Scheirich[135], M. Schernau[139f], C. Scheulen[56], C. Schiavi[57b,57a], M. Schioppa[44b,44a], B. Schlag[148], S. Schlenker[37],

J. Schmeing[176], E. Schmidt[111], M.A. Schmidt[176], K. Schmieden[25], C. Schmitt[101], N. Schmitt[101], S. Schmitt[48], N.A. Schneider[110], L. Schoeffel[137], A. Schoening[63b], P.G. Scholer[35], E. Schopf[146], M. Schott[25], S. Schramm[56], T. Schroer[56], H-C. Schultz-Coulon[63a], M. Schumacher[54], B.A. Schumm[138], Ph. Schune[137], H.R. Schwartz[7], A. Schwartzman[148], T.A. Schwarz[107], Ph. Schwemling[137], R. Schwienhorst[108], F.G. Sciacca[20], A. Sciandra[30], G. Sciolla[27], F. Scuri[74a], C.D. Sebastiani[37], K. Sedlaczek[117], S.C. Seidel[114], A. Seiden[138], B.D. Seidlitz[42], C. Seitz[48], J.M. Seixas[82b], G. Sekhniaidze[72a], L. Selem[60], N. Semprini-Cesari[24b,24a], A. Semushin[178], D. Sengupta[56], V. Senthilkumar[168], L. Serin[66], M. Sessa[72a,72b], H. Severini[122], F. Sforza[57b,57a], A. Sfyrla[56], Q. Sha[14], H. Shaddix[117], A.H. Shah[33], R. Shaheen[149], J.D. Shahinian[130], M. Shamim[37], L.Y. Shan[14], M. Shapiro[18a], A. Sharma[37], A.S. Sharma[169], P. Sharma[30], P.B. Shatalov[38], K. Shaw[151], S.M. Shaw[102], Q. Shen[14], D.J. Sheppard[147], P. Sherwood[97], L. Shi[97], X. Shi[14], S. Shimizu[83], I.P.J. Shipsey[128,*], S. Shirabe[89], M. Shiyakova[39,z], M.J. Shochet[40], D.R. Shope[127], B. Shrestha[122], S. Shrestha[121,an], I. Shreyber[39], M.J. Shroff[170], P. Sicho[133], A.M. Sickles[167], E. Sideras Haddad[34j,165], A.C. Sidley[116], A. Sidoti[24b], F. Siegert[50], Dj. Sijacki[16], F. Sili[62], J.M. Silva[52], I. Silva Ferreira[82b], M.V. Silva Oliveira[30], S.B. Silverstein[47a], S. Simion[66], R. Simoniello[37], E.L. Simpson[102], H. Simpson[151], L.R. Simpson[6], S. Simsek[81], S. Sindhu[55], P. Sinervo[160], S.N. Singh[27], S. Singh[30], S. Sinha[48], S. Sinha[102], M. Sioli[24b,24a], K. Sioulas[9], I. Siral[37], E. Sitnikova[48], J. Sjölin[47a,47b], A. Skaf[55], E. Skorda[21], P. Skubic[122], M. Slawinska[87], I. Slazyk[17], I. Sliusar[127], V. Smakhtin[174], B.H. Smart[136], S.Yu. Smirnov[139b], Y. Smirnov[34c], L.N. Smirnova[38,a], O. Smirnova[99], A.C. Smith[42], D.R. Smith[164], J.L. Smith[102], M.B. Smith[35], R. Smith[148], H. Smitmanns[101], M. Smizanska[92], K. Smolek[134], P. Smolyanskiy[134], A.A. Snesarev[39], H.L. Snoek[116], R.M. Snyder[51], S. Snyder[30], R. Sobie[170,ab], A. Soffer[156], C.A. Solans Sanchez[37], E.Yu. Soldatov[39], U. Soldevila[168], A.A. Solodkov[34j], S. Solomon[27], A. Soloshenko[39], K. Solovieva[54], O.V. Solovyanov[41], P. Sommer[50], A. Sonay[13], A. Sopczak[134], A.L. Sopio[52], F. Sopkova[29b], J.D. Sorenson[114], I.R. Sotarriva Alvarez[140], V. Sothilingam[63a], O.J. Soto Sandoval[139c,139b], S. Sottocornola[68], R. Soualah[84a], Z. Soumaimi[36e], D. South[48], N. Soybelman[174], S. Spagnolo[70a,70b], D. Sperlich[54], B. Spisso[72a,72b], D.P. Spiteri[59], L. Splendori[103], M. Spousta[135], E.J. Staats[35], R. Stamen[63a], E. Stanecka[87], W. Stanek-Maslouska[48], M.V. Stange[50], B. Stanislaus[18a], M.M. Stanitzki[48], E.A. Starchenko[38], G.H. Stark[138], J. Stark[90], P. Staroba[133], P. Starovoitov[84b], R. Staszewski[87], C. Stauch[110], G. Stavropoulos[46], A. Stefl[37], A. Stein[101], P. Steinberg[30], B. Stelzer[147,161a], H.J. Stelzer[131], O. Stelzer[161a], H. Stenzel[58], T.J. Stevenson[151], G.A. Stewart[37], J.R. Stewart[123], G. Stoicea[28b], M. Stolarski[132a], S. Stonjek[111], A. Straessner[50], J. Strandberg[149], S. Strandberg[47a,47b], M. Stratmann[176], M. Strauss[122], T. Strebler[103], P. Strizenec[29b], R. Ströhmer[171], D.M. Strom[125], R. Stroynowski[45], A. Strubig[47a,47b], S.A. Stucci[30], B. Stugu[17], J. Stupak[122], N.A. Styles[48], D. Su[148], S. Su[62], X. Su[62], D. Suchy[29a], A.D. Sudhakar Ponnu[55], L. Sudit[174], K. Sugizaki[130], V.V. Sulin[38], D.M.S. Sultan[128], L. Sultanaliyeva[25], S. Sultansoy[3b], S. Sun[175], W. Sun[14], N. Sur[99], N. Suri Jr[177], M.R. Sutton[151], M. Svatos[133], P.N. Swallow[33], M. Swiatlowski[161a], A. Swoboda[37], I. Sykora[29a], M. Sykora[135], T. Sykora[135], D. Ta[101], K. Tackmann[48,y], A. Taffard[164], R. Tafirout[161a], Y. Takubo[83], M. Talby[103], A.A. Talyshev[38], K.C. Tam[64b], N.M. Tamir[156], A. Tanaka[158], J. Tanaka[158], R. Tanaka[66], M. Tanasini[150], Z. Tao[169], S. Tapia Araya[139g], S. Tapprogge[101], A. Tarek Abouelfadl Mohamed[37], S. Tarem[155], K. Tariq[14], G. Tarna[37], G.F. Tartarelli[71a], M.J. Tartarin[90], P. Tas[135], M. Tasevsky[133], E. Tassi[44b,44a], A.C. Tate[167], Y. Tayalati[36e,aa], G.N. Taylor[106], W. Taylor[161b], R.J. Taylor Vara[168], A.S. Tegetmeier[90],

P. Teixeira-Dias[96], J.J. Teoh[160], K. Terashi[158], J. Terron[100], S. Terzo[13], M. Testa[53], R.J. Teuscher[160,ab], A. Thaler[79], O. Theiner[56], T. Theveneaux-Pelzer[103], D.W. Thomas[96], J.P. Thomas[21], E.A. Thompson[18a], P.D. Thompson[21], E. Thomson[130], R.E. Thornberry[45], C. Tian[62], Y. Tian[56], V. Tikhomirov[81], Yu.A. Tikhonov[39], S. Timoshenko[38], D. Timoshyn[135], E.X.L. Ting[1], P. Tipton[177], A. Tishelman-Charny[30], K. Todome[140], S. Todorova-Nova[135], L. Toffolin[69a,69c], M. Togawa[83], J. Tojo[89], S. Tokár[29a], O. Toldaiev[68], G. Tolkachev[103], M. Tomoto[83], L. Tompkins[148,n], E. Torrence[125], H. Torres[90], D.I. Torres Arza[139g], E. Torró Pastor[168], M. Toscani[31], C. Tosciri[40], M. Tost[11], D.R. Tovey[144], T. Trefzger[171], P.M. Tricarico[13], A. Tricoli[30], I.M. Trigger[161a], S. Trincaz-Duvoid[129], D.A. Trischuk[170], A. Tropina[39], D. Truncali[76a,76b], L. Truong[34c], M. Trzebinski[87], A. Trzupek[87], F. Tsai[150], M. Tsai[107], A. Tsiamis[157], P.V. Tsiareshka[39], S. Tsigaridas[161a], A. Tsirigotis[157,u], V. Tsiskaridze[154a], E.G. Tskhadadze[154a], Y. Tsujikawa[88], I.I. Tsukerman[38], V. Tsulaia[18a], S. Tsuno[83], K. Tsuri[120], D. Tsybychev[150], Y. Tu[64b], A. Tudorache[28b], V. Tudorache[28b], S.B. Tuncay[128], S. Turchikhin[57b,57a], I. Turk Cakir[3a], R. Turra[71a], T. Turtuvshin[39,ac], P.M. Tuts[42], S. Tzamarias[157,d], Y. Uematsu[83], F. Ukegawa[162], P.A. Ulloa Poblete[139c,139b], E.N. Umaka[30], G. Unal[37], A. Undrus[30], G. Unel[164], J. Urban[29b], P. Urrejola[139e], G. Usai[8], R. Ushioda[159], M. Usman[109], F. Ustuner[52], Z. Uysal[81], V. Vacek[134], B. Vachon[105], T. Vafeiadis[37], A. Vaitkus[97], C. Valderanis[110], E. Valdes Santurio[47a,47b], M. Valente[37], S. Valentinetti[24b,24a], A. Valero[168], E. Valiente Moreno[168], A. Vallier[90], J.A. Valls Ferrer[168], D.R. Van Arneman[116], A. Van Der Graaf[49], H.Z. Van Der Schyf[34j], P. Van Gemmeren[6], M. Van Rijnbach[37], S. Van Stroud[97], I. Van Vulpen[116], P. Vana[135], M. Vanadia[76a,76b], U.M. Vande Voorde[149], W. Vandelli[37], E.R. Vandewall[148], D. Vannicola[156], L. Vannoli[53], R. Vari[75a], M. Varma[177], E.W. Varnes[7], C. Varni[79], D. Varouchas[66], L. Varriale[168], K.E. Varvell[152], M.E. Vasile[28b], L. Vaslin[83], M.D. Vassilev[148], A. Vasyukov[39], L.M. Vaughan[123], R. Vavricka[135], T. Vazquez Schroeder[13], J. Veatch[32], V. Vecchio[102], M.J. Veen[104], I. Veliscek[30], I. Velkovska[94], L.M. Veloce[160], F. Veloso[132a,132c], A.G. Veltman[52], S. Veneziano[75a], A. Ventura[70a,70b], A. Verbytskyi[111], M. Verducci[74a,74b], C. Vergis[95], M. Verissimo De Araujo[82b], W. Verkerke[116], J.C. Vermeulen[116], C. Vernieri[148], M. Vessella[164], M.C. Vetterli[147,ai], A. Vgenopoulos[101], N. Viaux Maira[139g,af], T. Vickey[144], O.E. Vickey Boeriu[144], G.H.A. Viehhauser[128], L. Vigani[63b], M. Vigl[111], M. Villa[24b,24a], M. Villaplana Perez[168], E.M. Villhauer[40], E. Vilucchi[53], M. Vincent[168], M.G. Vincter[35], A. Visibile[116], A. Visive[116], C. Vittori[37], I. Vivarelli[24b,24a], M.I. Vivas Albornoz[48], E. Voevodina[111], F. Vogel[110], J.C. Voigt[50], P. Vokac[134], Yu. Volkotrub[86b], L. Vomberg[25], E. Von Toerne[25], B. Vormwald[37], K. Vorobev[51], M. Vos[168], K. Voss[146], M. Vozak[37], L. Vozdecky[122], N. Vranjes[16], M. Vranjes Milosavljevic[16], M. Vreeswijk[116], N.K. Vu[143b,143a], R. Vuillermet[37], O. Vujinovic[101], I. Vukotic[40], I.K. Vyas[35], J.F. Wack[33], S. Wada[162], C. Wagner[148], J.M. Wagner[18a], W. Wagner[176], S. Wahdan[176], H. Wahlberg[91], C.H. Waits[122], J. Walder[136], R. Walker[110], K. Walkingshaw Pass[59], W. Walkowiak[146], A. Wall[130], E.J. Wallin[99], T. Wamorkar[18a], K. Wandall-Christensen[168], A. Wang[62], A.Z. Wang[138], C. Wang[48], C. Wang[11], H. Wang[18a], J. Wang[64c], P. Wang[102], P. Wang[97], R. Wang[61], R. Wang[6], S.M. Wang[153], S. Wang[14], T. Wang[115], T. Wang[62], W.T. Wang[128], W. Wang[14], X. Wang[167], X. Wang[143a], X. Wang[48], Y. Wang[150], Y. Wang[62], Z. Wang[107], Z. Wang[143b], Z. Wang[107], C. Wanotayaroj[83], A. Warburton[105], A.L. Warnerbring[146], S. Waterhouse[96], A.T. Watson[21], H. Watson[52], M.F. Watson[21], E. Watton[37], G. Watts[141], B.M. Waugh[97], J.M. Webb[54], C. Weber[30], M.S. Weber[20], S.M. Weber[63a], C. Wei[62], Y. Wei[54], A.R. Weidberg[128], E.J. Weik[119], J. Weingarten[49], C. Weiser[54], C.J. Wells[48], T. Wenaus[30], T. Wengler[37], N.S. Wenke[111], N. Wermes[25], M. Wessels[63a], A.M. Wharton[92], A.S. White[61],

A. White [8], M.J. White [1], D. Whiteson [164], L. Wickremasinghe [126], W. Wiedenmann [175], M. Wielers [136], R. Wierda [149], C. Wiglesworth [43], H.G. Wilkens [37], J.J.H. Wilkinson [33], D.M. Williams [42], H.H. Williams [130], S. Williams [33], S. Willocq [104], B.J. Wilson [102], D.J. Wilson [102], P.J. Windischhofer [40], F.I. Winkel [31], F. Winklmeier [125], B.T. Winter [54], M. Wittgen [148], M. Wobisch [98], T. Wojtkowski [60], Z. Wolffs [116], J. Wollrath [37], M.W. Wolter [87], H. Wolters [132a,132c], M.C. Wong [138], E.L. Woodward [42], S.D. Worm [48], B.K. Wosiek [87], K.W. Woźniak [87], S. Wozniewski [55], K. Wraight [59], C. Wu [160], C. Wu [21], J. Wu [158], M. Wu [113b], M. Wu [115], S.L. Wu [175], S. Wu [14,ak], X. Wu [62], Y.Q. Wu [160], Y. Wu [62], Z. Wu [4], Z. Wu [113a], J. Wuerzinger [111], T.R. Wyatt [102], B.M. Wynne [52], S. Xella [43], L. Xia [113a], M. Xie [62], A. Xiong [125], D. Xu [14], H. Xu [62], L. Xu [62], R. Xu [130], T. Xu [107], W. Xu [113a], Y. Xu [141], Z. Xu [52], R. Xue [131], B. Yabsley [152], S. Yacoob [34a], Y. Yamaguchi [83], E. Yamashita [158], H. Yamauchi [162], T. Yamazaki [18a], Y. Yamazaki [85], S. Yan [59], Z. Yan [104], H.J. Yang [143a,143b], H.T. Yang [62], S. Yang [62], T. Yang [64c], X. Yang [37], X. Yang [14], Y. Yang [158], Y. Yang [62], W-M. Yao [18a], C.L. Yardley [151], J. Ye [14], S. Ye [30], X. Ye [62], Y. Yeh [97], I. Yeletskikh [39], B. Yeo [18b], M.R. Yexley [97], T.P. Yildirim [128], K. Yorita [173], C.J.S. Young [37], C. Young [148], I.N.L. Young [59], N.D. Young [125], Y. Yu [62], J. Yuan [14,113c], M. Yuan [107], R. Yuan [143b], L. Yue [97], M. Zaazoua [62], B. Zabinski [87], I. Zahir [36a], A. Zaio [57b,57a], Z.K. Zak [87], T. Zakareishvili [168], S. Zambito [56], J.A. Zamora Saa [139d], J. Zang [158], R. Zanzottera [71a,71b], O. Zaplatilek [134], C. Zeitnitz [176], H. Zeng [14], D.T. Zenger Jr [27], O. Zenin [38], T. Ženiš [29a], S. Zenz [95], D. Zerwas [66], D.F. Zhang [144], G. Zhang [14,ak], J. Zhang [142a], J. Zhang [6], L. Zhang [62], L. Zhang [113a], P. Zhang [14,113c], R. Zhang [113a], S. Zhang [90], T. Zhang [158], Y. Zhang [141], Y. Zhang [97], Y. Zhang [62], Y. Zhang [113a], Z. Zhang [18a], Z. Zhang [142a], Z. Zhang [66], H. Zhao [141], T. Zhao [142a], Y. Zhao [35], Z. Zhao [62], Z. Zhao [62], A. Zhemchugov [39], J. Zheng [113a], K. Zheng [167], X. Zheng [62], Z. Zheng [148], D. Zhong [167], B. Zhou [107], B. Zhou [143b], H. Zhou [7], N. Zhou [143a], Y. Zhou [15], Y. Zhou [113a], Y. Zhou [7], J. Zhu [107], X. Zhu [143b], Y. Zhu [143a], Y. Zhu [62], X. Zhuang [14], K. Zhukov [68], N.I. Zimine [39], J. Zinsser [63b], M. Ziolkowski [146], L. Živković [16], A. Zoccoli [24b,24a], K. Zoch [61], A. Zografos [37], T.G. Zorbas [144], O. Zormpa [46], L. Zwalinski [37].

[1]Department of Physics, University of Adelaide, Adelaide; Australia.
[2]Department of Physics, University of Alberta, Edmonton AB; Canada.
[3(a)]Department of Physics, Ankara University, Ankara;[(b)]Division of Physics, TOBB University of Economics and Technology, Ankara; Türkiye.
[4]LAPP, Université Savoie Mont Blanc, CNRS/IN2P3, Annecy; France.
[5]APC, Université Paris Cité, CNRS/IN2P3, Paris; France.
[6]High Energy Physics Division, Argonne National Laboratory, Argonne IL; United States of America.
[7]Department of Physics, University of Arizona, Tucson AZ; United States of America.
[8]Department of Physics, University of Texas at Arlington, Arlington TX; United States of America.
[9]Physics Department, National and Kapodistrian University of Athens, Athens; Greece.
[10]Physics Department, National Technical University of Athens, Zografou; Greece.
[11]Department of Physics, University of Texas at Austin, Austin TX; United States of America.
[12]Institute of Physics, Azerbaijan Academy of Sciences, Baku; Azerbaijan.
[13]Institut de Física d'Altes Energies (IFAE), Barcelona Institute of Science and Technology, Barcelona; Spain.
[14]Institute of High Energy Physics, Chinese Academy of Sciences, Beijing; China.
[15]Physics Department, Tsinghua University, Beijing; China.
[16]Institute of Physics, University of Belgrade, Belgrade; Serbia.

[17]Department for Physics and Technology, University of Bergen, Bergen; Norway.
[18(a)]Physics Division, Lawrence Berkeley National Laboratory, Berkeley CA;[(b)]University of California, Berkeley CA; United States of America.
[19]Institut für Physik, Humboldt Universität zu Berlin, Berlin; Germany.
[20]Albert Einstein Center for Fundamental Physics and Laboratory for High Energy Physics, University of Bern, Bern; Switzerland.
[21]School of Physics and Astronomy, University of Birmingham, Birmingham; United Kingdom.
[22(a)]Department of Physics, Bogazici University, Istanbul;[(b)]Department of Physics Engineering, Gaziantep University, Gaziantep;[(c)]Department of Physics, Istanbul University, Istanbul; Türkiye.
[23(a)]Facultad de Ciencias y Centro de Investigaciónes, Universidad Antonio Nariño, Bogotá;[(b)]Departamento de Física, Universidad Nacional de Colombia, Bogotá; Colombia.
[24(a)]Dipartimento di Fisica e Astronomia A. Righi, Università di Bologna, Bologna;[(b)]INFN Sezione di Bologna; Italy.
[25]Physikalisches Institut, Universität Bonn, Bonn; Germany.
[26]Department of Physics, Boston University, Boston MA; United States of America.
[27]Department of Physics, Brandeis University, Waltham MA; United States of America.
[28(a)]Transilvania University of Brasov, Brasov;[(b)]Horia Hulubei National Institute of Physics and Nuclear Engineering, Bucharest;[(c)]Department of Physics, Alexandru Ioan Cuza University of Iasi, Iasi;[(d)]National Institute for Research and Development of Isotopic and Molecular Technologies, Physics Department, Cluj-Napoca;[(e)]National University of Science and Technology Politechnica, Bucharest;[(f)]West University in Timisoara, Timisoara;[(g)]Faculty of Physics, University of Bucharest, Bucharest; Romania.
[29(a)]Faculty of Mathematics, Physics and Informatics, Comenius University, Bratislava;[(b)]Department of Subnuclear Physics, Institute of Experimental Physics of the Slovak Academy of Sciences, Kosice; Slovak Republic.
[30]Physics Department, Brookhaven National Laboratory, Upton NY; United States of America.
[31]Universidad de Buenos Aires, Facultad de Ciencias Exactas y Naturales, Departamento de Física, y CONICET, Instituto de Física de Buenos Aires (IFIBA), Buenos Aires; Argentina.
[32]California State University, CA; United States of America.
[33]Cavendish Laboratory, University of Cambridge, Cambridge; United Kingdom.
[34(a)]Department of Physics, University of Cape Town, Cape Town;[(b)]iThemba Labs, Western Cape;[(c)]Department of Mechanical Engineering Science, University of Johannesburg, Johannesburg;[(d)]National Institute of Physics, University of the Philippines Diliman (Philippines);[(e)]Department of Physics, Stellenbosch University, Matieland;[(f)]University of KwaZulu-Natal, School of Agriculture and Science, Mathematics, Westville;[(g)]University of South Africa, Department of Physics, Pretoria;[(h)]University of Pretoria, Department of Mechanical and Aeronautical Engineering, Pretoria;[(i)]University of Zululand, KwaDlangezwa;[(j)]School of Physics, University of the Witwatersrand, Johannesburg; South Africa.
[35]Department of Physics, Carleton University, Ottawa ON; Canada.
[36(a)]Faculté des Sciences Ain Chock, Université Hassan II de Casablanca;[(b)]Faculté des Sciences, Université Ibn-Tofail, Kénitra;[(c)]Faculté des Sciences Semlalia, Université Cadi Ayyad, LPHEA-Marrakech;[(d)]LPMR, Faculté des Sciences, Université Mohamed Premier, Oujda;[(e)]Faculté des sciences, Université Mohammed V, Rabat;[(f)]Institute of Applied Physics, Mohammed VI Polytechnic University, Ben Guerir; Morocco.
[37]CERN, Geneva; Switzerland.
[38]Affiliated with an institute formerly covered by a cooperation agreement with CERN.
[39]Affiliated with an international laboratory covered by a cooperation agreement with CERN.
[40]Enrico Fermi Institute, University of Chicago, Chicago IL; United States of America.

[41]LPC, Université Clermont Auvergne, CNRS/IN2P3, Clermont-Ferrand; France.
[42]Nevis Laboratory, Columbia University, Irvington NY; United States of America.
[43]Niels Bohr Institute, University of Copenhagen, Copenhagen; Denmark.
[44][(a)]Dipartimento di Fisica, Università della Calabria, Rende;[(b)]INFN Gruppo Collegato di Cosenza, Laboratori Nazionali di Frascati; Italy.
[45]Physics Department, Southern Methodist University, Dallas TX; United States of America.
[46]National Centre for Scientific Research "Demokritos", Agia Paraskevi; Greece.
[47][(a)]Department of Physics, Stockholm University;[(b)]Oskar Klein Centre, Stockholm; Sweden.
[48]Deutsches Elektronen-Synchrotron DESY, Hamburg and Zeuthen; Germany.
[49]Fakultät Physik , Technische Universität Dortmund, Dortmund; Germany.
[50]Institut für Kern- und Teilchenphysik, Technische Universität Dresden, Dresden; Germany.
[51]Department of Physics, Duke University, Durham NC; United States of America.
[52]SUPA - School of Physics and Astronomy, University of Edinburgh, Edinburgh; United Kingdom.
[53]INFN e Laboratori Nazionali di Frascati, Frascati; Italy.
[54]Physikalisches Institut, Albert-Ludwigs-Universität Freiburg, Freiburg; Germany.
[55]II. Physikalisches Institut, Georg-August-Universität Göttingen, Göttingen; Germany.
[56]Département de Physique Nucléaire et Corpusculaire, Université de Genève, Genève; Switzerland.
[57][(a)]Dipartimento di Fisica, Università di Genova, Genova;[(b)]INFN Sezione di Genova; Italy.
[58]II. Physikalisches Institut, Justus-Liebig-Universität Giessen, Giessen; Germany.
[59]SUPA - School of Physics and Astronomy, University of Glasgow, Glasgow; United Kingdom.
[60]LPSC, Université Grenoble Alpes, CNRS/IN2P3, Grenoble INP, Grenoble; France.
[61]Laboratory for Particle Physics and Cosmology, Harvard University, Cambridge MA; United States of America.
[62]Department of Modern Physics and State Key Laboratory of Particle Detection and Electronics, University of Science and Technology of China, Hefei; China.
[63][(a)]Kirchhoff-Institut für Physik, Ruprecht-Karls-Universität Heidelberg, Heidelberg;[(b)]Physikalisches Institut, Ruprecht-Karls-Universität Heidelberg, Heidelberg; Germany.
[64][(a)]Department of Physics, Chinese University of Hong Kong, Shatin, N.T., Hong Kong;[(b)]Department of Physics, University of Hong Kong, Hong Kong;[(c)]Department of Physics and Institute for Advanced Study, Hong Kong University of Science and Technology, Clear Water Bay, Kowloon, Hong Kong; China.
[65]Department of Physics, National Tsing Hua University, Hsinchu; Taiwan.
[66]IJCLab, Université Paris-Saclay, CNRS/IN2P3, 91405, Orsay; France.
[67]Centro Nacional de Microelectrónica (IMB-CNM-CSIC), Barcelona; Spain.
[68]Department of Physics, Indiana University, Bloomington IN; United States of America.
[69][(a)]INFN Gruppo Collegato di Udine, Sezione di Trieste, Udine;[(b)]ICTP, Trieste;[(c)]Dipartimento Politecnico di Ingegneria e Architettura, Università di Udine, Udine; Italy.
[70][(a)]INFN Sezione di Lecce;[(b)]Dipartimento di Matematica e Fisica, Università del Salento, Lecce; Italy.
[71][(a)]INFN Sezione di Milano;[(b)]Dipartimento di Fisica, Università di Milano, Milano; Italy.
[72][(a)]INFN Sezione di Napoli;[(b)]Dipartimento di Fisica, Università di Napoli, Napoli; Italy.
[73][(a)]INFN Sezione di Pavia;[(b)]Dipartimento di Fisica, Università di Pavia, Pavia; Italy.
[74][(a)]INFN Sezione di Pisa;[(b)]Dipartimento di Fisica E. Fermi, Università di Pisa, Pisa; Italy.
[75][(a)]INFN Sezione di Roma;[(b)]Dipartimento di Fisica, Sapienza Università di Roma, Roma; Italy.
[76][(a)]INFN Sezione di Roma Tor Vergata;[(b)]Dipartimento di Fisica, Università di Roma Tor Vergata, Roma; Italy.
[77][(a)]INFN Sezione di Roma Tre;[(b)]Dipartimento di Matematica e Fisica, Università Roma Tre, Roma; Italy.
[78][(a)]INFN-TIFPA;[(b)]Università degli Studi di Trento, Trento; Italy.

[79]Universität Innsbruck, Department of Astro and Particle Physics, Innsbruck; Austria.
[80]Department of Physics and Astronomy, Iowa State University, Ames IA; United States of America.
[81]Istinye University, Sariyer, Istanbul; Türkiye.
[82(a)]Departamento de Engenharia Elétrica, Universidade Federal de Juiz de Fora (UFJF), Juiz de Fora;[(b)]Universidade Federal do Rio De Janeiro COPPE/EE/IF, Rio de Janeiro;[(c)]Instituto de Física, Universidade de São Paulo, São Paulo;[(d)]Rio de Janeiro State University, Rio de Janeiro;[(e)]Federal University of Bahia, Bahia; Brazil.
[83]KEK, High Energy Accelerator Research Organization, Tsukuba; Japan.
[84(a)]Khalifa University of Science and Technology, Abu Dhabi;[(b)]University of Sharjah, Sharjah; United Arab Emirates.
[85]Graduate School of Science, Kobe University, Kobe; Japan.
[86(a)]AGH University of Krakow, Faculty of Physics and Applied Computer Science, Krakow;[(b)]Marian Smoluchowski Institute of Physics, Jagiellonian University, Krakow; Poland.
[87]Institute of Nuclear Physics Polish Academy of Sciences, Krakow; Poland.
[88]Faculty of Science, Kyoto University, Kyoto; Japan.
[89]Research Center for Advanced Particle Physics and Department of Physics, Kyushu University, Fukuoka ; Japan.
[90]L2IT, Université de Toulouse, CNRS/IN2P3, UPS, Toulouse; France.
[91]Instituto de Física La Plata, Universidad Nacional de La Plata and CONICET, La Plata; Argentina.
[92]Physics Department, Lancaster University, Lancaster; United Kingdom.
[93]Oliver Lodge Laboratory, University of Liverpool, Liverpool; United Kingdom.
[94]Department of Experimental Particle Physics, Jožef Stefan Institute and Department of Physics, University of Ljubljana, Ljubljana; Slovenia.
[95]Department of Physics and Astronomy, Queen Mary University of London, London; United Kingdom.
[96]Department of Physics, Royal Holloway University of London, Egham; United Kingdom.
[97]Department of Physics and Astronomy, University College London, London; United Kingdom.
[98]Louisiana Tech University, Ruston LA; United States of America.
[99]Fysiska institutionen, Lunds universitet, Lund; Sweden.
[100]Departamento de Física Teorica C-15 and CIAFF, Universidad Autónoma de Madrid, Madrid; Spain.
[101]Institut für Physik, Universität Mainz, Mainz; Germany.
[102]School of Physics and Astronomy, University of Manchester, Manchester; United Kingdom.
[103]CPPM, Aix-Marseille Université, CNRS/IN2P3, Marseille; France.
[104]Department of Physics, University of Massachusetts, Amherst MA; United States of America.
[105]Department of Physics, McGill University, Montreal QC; Canada.
[106]School of Physics, University of Melbourne, Victoria; Australia.
[107]Department of Physics, University of Michigan, Ann Arbor MI; United States of America.
[108]Department of Physics and Astronomy, Michigan State University, East Lansing MI; United States of America.
[109]Group of Particle Physics, University of Montreal, Montreal QC; Canada.
[110]Fakultät für Physik, Ludwig-Maximilians-Universität München, München; Germany.
[111]Max-Planck-Institut für Physik (Werner-Heisenberg-Institut), München; Germany.
[112]Graduate School of Science and Kobayashi-Maskawa Institute, Nagoya University, Nagoya; Japan.
[113(a)]Department of Physics, Nanjing University, Nanjing;[(b)]School of Science, Shenzhen Campus of Sun Yat-sen University;[(c)]University of Chinese Academy of Science (UCAS), Beijing; China.
[114]Department of Physics and Astronomy, University of New Mexico, Albuquerque NM; United States of America.
[115]Institute for Mathematics, Astrophysics and Particle Physics, Radboud University/Nikhef, Nijmegen;

Netherlands.
[116]Nikhef National Institute for Subatomic Physics and University of Amsterdam, Amsterdam; Netherlands.
[117]Department of Physics, Northern Illinois University, DeKalb IL; United States of America.
[118(a)]New York University Abu Dhabi, Abu Dhabi;[(b)]United Arab Emirates University, Al Ain; United Arab Emirates.
[119]Department of Physics, New York University, New York NY; United States of America.
[120]Ochanomizu University, Otsuka, Bunkyo-ku, Tokyo; Japan.
[121]Ohio State University, Columbus OH; United States of America.
[122]Homer L. Dodge Department of Physics and Astronomy, University of Oklahoma, Norman OK; United States of America.
[123]Department of Physics, Oklahoma State University, Stillwater OK; United States of America.
[124]Palacký University, Joint Laboratory of Optics, Olomouc; Czech Republic.
[125]Institute for Fundamental Science, University of Oregon, Eugene, OR; United States of America.
[126]Graduate School of Science, University of Osaka, Osaka; Japan.
[127]Department of Physics, University of Oslo, Oslo; Norway.
[128]Department of Physics, Oxford University, Oxford; United Kingdom.
[129]LPNHE, Sorbonne Université, Université Paris Cité, CNRS/IN2P3, Paris; France.
[130]Department of Physics, University of Pennsylvania, Philadelphia PA; United States of America.
[131]Department of Physics and Astronomy, University of Pittsburgh, Pittsburgh PA; United States of America.
[132(a)]Laboratório de Instrumentação e Física Experimental de Partículas - LIP, Lisboa;[(b)]Departamento de Física, Faculdade de Ciências, Universidade de Lisboa, Lisboa;[(c)]Departamento de Física, Universidade de Coimbra, Coimbra;[(d)]Centro de Física Nuclear da Universidade de Lisboa, Lisboa;[(e)]Departamento de Física, Escola de Ciências, Universidade do Minho, Braga;[(f)]Departamento de Física Teórica y del Cosmos, Universidad de Granada, Granada (Spain);[(g)]Departamento de Física, Instituto Superior Técnico, Universidade de Lisboa, Lisboa; Portugal.
[133]Institute of Physics of the Czech Academy of Sciences, Prague; Czech Republic.
[134]Czech Technical University in Prague, Prague; Czech Republic.
[135]Charles University, Faculty of Mathematics and Physics, Prague; Czech Republic.
[136]Particle Physics Department, Rutherford Appleton Laboratory, Didcot; United Kingdom.
[137]IRFU, CEA, Université Paris-Saclay, Gif-sur-Yvette; France.
[138]Santa Cruz Institute for Particle Physics, University of California Santa Cruz, Santa Cruz CA; United States of America.
[139(a)]Departamento de Física, Pontificia Universidad Católica de Chile, Santiago;[(b)]Millennium Institute for Subatomic physics at high energy frontier (SAPHIR), Santiago;[(c)]Instituto de Investigación Multidisciplinario en Ciencia y Tecnología, y Departamento de Física, Universidad de La Serena;[(d)]Universidad Andres Bello, Department of Physics, Santiago;[(e)]Universidad San Sebastian, Recoleta;[(f)]Instituto de Alta Investigación, Universidad de Tarapacá, Arica;[(g)]Departamento de Física, Universidad Técnica Federico Santa María, Valparaíso; Chile.
[140]Department of Physics, Institute of Science, Tokyo; Japan.
[141]Department of Physics, University of Washington, Seattle WA; United States of America.
[142(a)]Institute of Frontier and Interdisciplinary Science and Key Laboratory of Particle Physics and Particle Irradiation (MOE), Shandong University, Qingdao;[(b)]School of Physics, Zhengzhou University; China.
[143(a)]State Key Laboratory of Dark Matter Physics, School of Physics and Astronomy, Shanghai Jiao Tong University, Key Laboratory for Particle Astrophysics and Cosmology (MOE), SKLPPC, Shanghai;[(b)]State Key Laboratory of Dark Matter Physics, Tsung-Dao Lee Institute, Shanghai Jiao Tong University,

Shanghai; China.
[144]Department of Physics and Astronomy, University of Sheffield, Sheffield; United Kingdom.
[145]Department of Physics, Shinshu University, Nagano; Japan.
[146]Department Physik, Universität Siegen, Siegen; Germany.
[147]Department of Physics, Simon Fraser University, Burnaby BC; Canada.
[148]SLAC National Accelerator Laboratory, Stanford CA; United States of America.
[149]Department of Physics, Royal Institute of Technology, Stockholm; Sweden.
[150]Departments of Physics and Astronomy, Stony Brook University, Stony Brook NY; United States of America.
[151]Department of Physics and Astronomy, University of Sussex, Brighton; United Kingdom.
[152]School of Physics, University of Sydney, Sydney; Australia.
[153]Institute of Physics, Academia Sinica, Taipei; Taiwan.
[154][(a)]E. Andronikashvili Institute of Physics, Iv. Javakhishvili Tbilisi State University, Tbilisi;[(b)]High Energy Physics Institute, Tbilisi State University, Tbilisi;[(c)]University of Georgia, Tbilisi; Georgia.
[155]Department of Physics, Technion, Israel Institute of Technology, Haifa; Israel.
[156]Raymond and Beverly Sackler School of Physics and Astronomy, Tel Aviv University, Tel Aviv; Israel.
[157]Department of Physics, Aristotle University of Thessaloniki, Thessaloniki; Greece.
[158]International Center for Elementary Particle Physics and Department of Physics, University of Tokyo, Tokyo; Japan.
[159]Graduate School of Science and Technology, Tokyo Metropolitan University, Tokyo; Japan.
[160]Department of Physics, University of Toronto, Toronto ON; Canada.
[161][(a)]TRIUMF, Vancouver BC;[(b)]Department of Physics and Astronomy, York University, Toronto ON; Canada.
[162]Division of Physics and Tomonaga Center for the History of the Universe, Faculty of Pure and Applied Sciences, University of Tsukuba, Tsukuba; Japan.
[163]Department of Physics and Astronomy, Tufts University, Medford MA; United States of America.
[164]Department of Physics and Astronomy, University of California Irvine, Irvine CA; United States of America.
[165]University of West Attica, Athens; Greece.
[166]Department of Physics and Astronomy, University of Uppsala, Uppsala; Sweden.
[167]Department of Physics, University of Illinois, Urbana IL; United States of America.
[168]Instituto de Física Corpuscular (IFIC), Centro Mixto Universidad de Valencia - CSIC, Valencia; Spain.
[169]Department of Physics, University of British Columbia, Vancouver BC; Canada.
[170]Department of Physics and Astronomy, University of Victoria, Victoria BC; Canada.
[171]Fakultät für Physik und Astronomie, Julius-Maximilians-Universität Würzburg, Würzburg; Germany.
[172]Department of Physics, University of Warwick, Coventry; United Kingdom.
[173]Waseda University, Tokyo; Japan.
[174]Department of Particle Physics and Astrophysics, Weizmann Institute of Science, Rehovot; Israel.
[175]Department of Physics, University of Wisconsin, Madison WI; United States of America.
[176]Fakultät für Mathematik und Naturwissenschaften, Fachgruppe Physik, Bergische Universität Wuppertal, Wuppertal; Germany.
[177]Department of Physics, Yale University, New Haven CT; United States of America.
[178]Yerevan Physics Institute, Yerevan; Armenia.
[a] Also at Affiliated with an institute formerly covered by a cooperation agreement with CERN.
[b] Also at An-Najah National University, Nablus; Palestine.
[c] Also at Borough of Manhattan Community College, City University of New York, New York NY; United States of America.

[d] Also at Center for Interdisciplinary Research and Innovation (CIRI-AUTH), Thessaloniki; Greece.
[e] Also at Centre of Physics of the Universities of Minho and Porto (CF-UM-UP); Portugal.
[f] Also at CERN, Geneva; Switzerland.
[g] Also at Département de Physique Nucléaire et Corpusculaire, Université de Genève, Genève; Switzerland.
[h] Also at Departament de Fisica de la Universitat Autonoma de Barcelona, Barcelona; Spain.
[i] Also at Department of Financial and Management Engineering, University of the Aegean, Chios; Greece.
[j] Also at Department of Mathematical Sciences, University of South Africa, Johannesburg; South Africa.
[k] Also at Department of Modern Physics and State Key Laboratory of Particle Detection and Electronics, University of Science and Technology of China, Hefei; China.
[l] Also at Department of Physics, Bolu Abant Izzet Baysal University, Bolu; Türkiye.
[m] Also at Department of Physics, King's College London, London; United Kingdom.
[n] Also at Department of Physics, Stanford University, Stanford CA; United States of America.
[o] Also at Department of Physics, Stellenbosch University; South Africa.
[p] Also at Department of Physics, University of Fribourg, Fribourg; Switzerland.
[q] Also at Department of Physics, University of Thessaly; Greece.
[r] Also at Department of Physics, Westmont College, Santa Barbara; United States of America.
[s] Also at Faculty of Physics, Sofia University, 'St. Kliment Ohridski', Sofia; Bulgaria.
[t] Also at Faculty of Physics, University of Bucharest ; Romania.
[u] Also at Hellenic Open University, Patras; Greece.
[v] Also at Henan University; China.
[w] Also at Imam Mohammad Ibn Saud Islamic University; Saudi Arabia.
[x] Also at Institucio Catalana de Recerca i Estudis Avancats, ICREA, Barcelona; Spain.
[y] Also at Institut für Experimentalphysik, Universität Hamburg, Hamburg; Germany.
[z] Also at Institute for Nuclear Research and Nuclear Energy (INRNE) of the Bulgarian Academy of Sciences, Sofia; Bulgaria.
[aa] Also at Institute of Applied Physics, Mohammed VI Polytechnic University, Ben Guerir; Morocco.
[ab] Also at Institute of Particle Physics (IPP); Canada.
[ac] Also at Institute of Physics and Technology, Mongolian Academy of Sciences, Ulaanbaatar; Mongolia.
[ad] Also at Institute of Physics, Azerbaijan Academy of Sciences, Baku; Azerbaijan.
[ae] Also at Institute of Theoretical Physics, Ilia State University, Tbilisi; Georgia.
[af] Also at Millennium Institute for Subatomic physics at high energy frontier (SAPHIR), Santiago; Chile.
[ag] Also at National Institute of Physics, University of the Philippines Diliman (Philippines); Philippines.
[ah] Also at The Collaborative Innovation Center of Quantum Matter (CICQM), Beijing; China.
[ai] Also at TRIUMF, Vancouver BC; Canada.
[aj] Also at Università di Napoli Parthenope, Napoli; Italy.
[ak] Also at University of Chinese Academy of Sciences (UCAS), Beijing; China.
[al] Also at University of Colorado Boulder, Department of Physics, Colorado; United States of America.
[am] Also at University of Sienna; Italy.
[an] Also at Washington College, Chestertown, MD; United States of America.
[ao] Also at Yeditepe University, Physics Department, Istanbul; Türkiye.
[*] Deceased